

POLITECNICO DI TORINO

Corso di Laurea in Ingegneria Biomedica

Tesi di Laurea Magistrale

Surface Functionalization And Structuring By Electron Beam For Enhanced Biological Response



Relatori:

Prof.ssa Silvia Spriano

Dott.ssa Sara Ferraris

Tutor:

Dr.techn. Fernando Gustavo Warchomicka

*Institute of Materials Science, Joining and Forming
Graz University of Technology*

Candidata:

Nunzia Balsebre

Ottobre 2019

CONTENTS

INTRODUCTION	5
BIOMATERIALS	6
METALS IN MEDICAL IMPLANTS	8
TITANIUM MICROSTRUCTURE AND ITS ALLOYS	10
THE ROLE OF HEAT TREATMENTS ON TITANIUM ALLOYS MICROSTRUCTURE.....	15
INFLUENCE OF MICRO AND NANO TOPOGRAPHY ON THE BEHAVIOR OF CELLS AND BACTERIA	20
CELL RESPONSE.....	20
BACTERIA RESPONSE	28
MATERIALS AND METHODS	36
SAMPLES POLISHING.....	36
ELECTRON BEAM STRUCTURING.....	40
CUTTING SAMPLES	44
HEAT TREATMENTS	46
METALLOGRAPHY	53
ETCHING	54
FINAL POLISHING	55
SAMPLE PREPARATION FOR BIOLOGICAL TESTS	56
MATERIAL'S CHARACTERIZATION METHODS	58
Scanning Electron Microscope (SEM).....	58
Field Emission Scanning Electron Microscope (FESEM).....	59
Light Optical Microscope (LOM).....	59
WETTABILITY TEST	60
SURFACE ROUGHNESS	62
X-RAY DIFFRACTION (XRD)	64
BIOLOGICAL CHARACTERIZATION	65
BACTERIAL CHARACTERIZATION	65
RESULTS AND DISCUSSION	66
Ti-6Al-4V	66
Ti-15Mo.....	80

SURFACE ROUGHNESS84
WETTABILITY TESTS.....85
XRD87
BIOLOGICAL RESULTS.....90
CONCLUSION.....94
BIBLIOGRAPHY95

INTRODUCTION

The aim of this master thesis is evaluating how micro and nano-topography could influence bacterial behavior, as requested in transmucosal dental implants or orthopedic implants, that are the main application fields of Titanium and Ti-alloys. Micro and nano-topographies were realized on different Titanium alloys substrates, Ti-6Al-4V, Ti-15Mo and CP Titanium (Grade 2) by means of Electron Beam Welding machine.

The first part of the work took place at the Institute of Materials Science, Joining and Forming (IMAT-TUGraz) in Graz, where were realized the different Titanium alloys surfaces. There were used several techniques to modify the materials, such as Polishing Machine to polish samples in order to obtain a mirror shape polishing, Electron Beam Welding machine in order to create microtopography on the surface of the material through oriented micro grooves, Dilatometer in order to carry out some heat treatments on the specimens and modify micro and nanostructure of the material, Etching Treatments, using Hydrofluoric acid (HF), to create nano-topography on the samples.

Some characterizations of the material were carried out in Graz, by means of Field Emission Scanning Electron Microscope (FESEM), by Light Optical Microscope (LOM) and by 3D Microscope in order to observe the surface of the samples and the cross section of them.

The second part of the materials characterization was carried out at Dipartimento di Scienza Applicata e Tecnologia (DISAT) at Politecnico of Turin, in Turin, where surface wettability was tested by contact angle measurements (water), crystallographic structure was investigated by means of XRD, surface profile measurements and roughness were investigated by means of a profilometer.

Finally, biological tests were performed at Eastern Piedmont University in Novara, using *Staphylococcus aureus* (SA, commercial, multi-drug resistant, ATCC 43300). Bacterial viability was evaluated through AlamarBlue test and CFU count method.

BIOMATERIALS

“A biomaterial is a non-viable material used in a medical device, intended to interact with biological systems” (Williams, 1986)[1] was the first definition of a biomaterial. After this one there was an evolution of this word for over 30 years and the final definition is: “Materials intended to interface with biological systems to evaluate, treat, argument or replace any tissue or function of the body” (O'Brien, 2011) [2].

We can split out biomaterials in different classes, focusing on their evolution:

1. First generation: 1950-1975; inert biomaterials, that ones with a minimal interaction/reaction with the surrounding tissues. They are still biocompatible materials;
2. Second generation: 1975-2000; bioactive materials and resorbable. They interact actively with surrounding tissues and they have a controlled reaction with physiological environment. Mostly used in drug release devices;
3. Third generation: from 2000 onward; their main goal is regeneration of functional tissue, stimulating a specific cell response at molecular level (for instance they could activate proliferation GF or differentiation ones in order to have different effects on tissue regeneration);

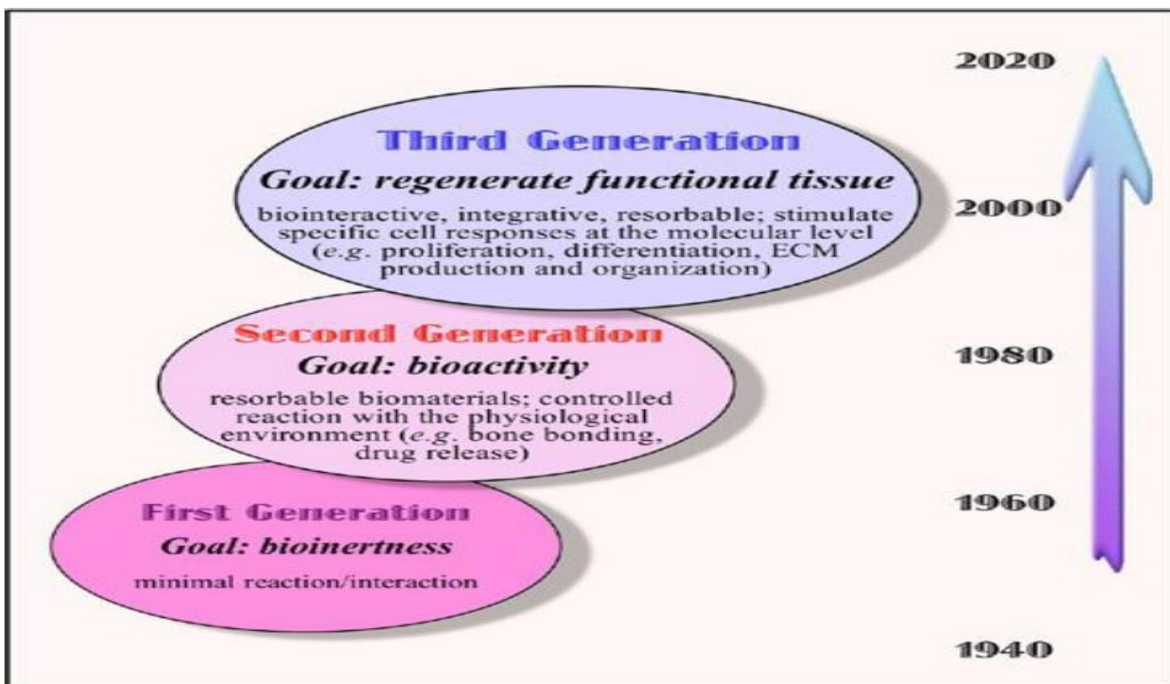


Figure 1.1 The three generations of biomaterials (Ratner, Hoffman, Schoen, & Lemons, 2013a) [3].

Materials for biomedical applications could be divided as shown in the figure below:

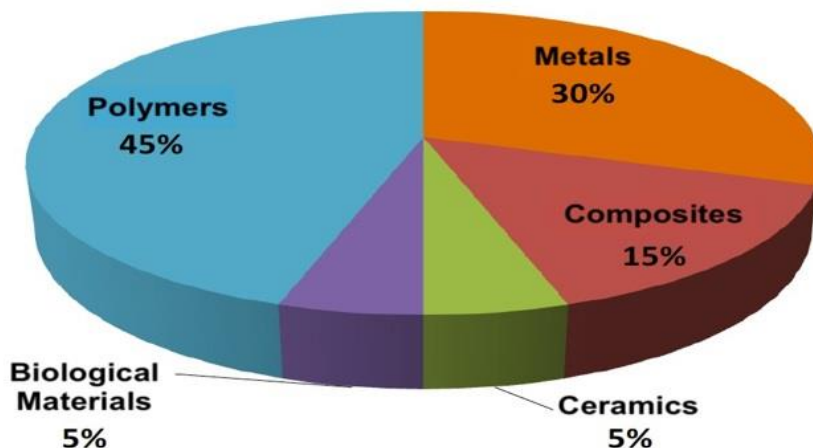


Figure 1.2 Different materials for biomedical applications and their percentage of use (ASM International, 2003) [4].

1. Polymers: in particular UHMWPE (Ultra High Molecular Weight Poly-Ethylene) for liner in hip prosthetic and PMMA (Poly Methyl-Methacrylate) for contact lenses;
2. Metals: in particular stainless steel, Titanium and its alloys and cobalt alloys;
3. Composites: Alumina (Al_2O_3), Zirconia (ZrO_2) and alumina-zirconia composites;
4. Biological materials;

TABLE 1 Key Applications of Synthetic Materials and Modified Natural Materials in Medicine*		
Application	Biomaterials Used	Number/Year – World (or World Market in US\$)
Skeletal system		
Joint replacements (hip, knee, shoulder)	Titanium, stainless steel, polyethylene	2,500,000
Bone fixation plates and screws	Metals, poly(lactic acid) (PLA)	1,500,000
Spine disks and fusion hardware		800,000
Bone cement	Poly(methyl methacrylate)	(\$600M)
Bone defect repair	Calcium phosphates	–
Artificial tendon or ligament	Polyester fibers	–
Dental implant-tooth fixation	Titanium	(\$4B)
Cardiovascular system		
Blood vessel prosthesis	Dacron, expanded Teflon	200,000
Heart valve	Dacron, carbon, metal, treated natural tissue	400,000
Pacemaker	Titanium, polyurethane	600,000
Implantable defibrillator	Titanium, polyurethane	300,000
Stent	Stainless steel, other metals, PLA	1,500,000
Catheter	Teflon, silicone, polyurethane	1B (\$20B)
Organs		
Heart assist device	Polyurethane, titanium, stainless steel	4000
Hemodialysis	Polysulfone, silicone	1,800,000 patients (\$70B)
Blood oxygenator	silicone	1,000,000
Skin substitute	Collagen, cadaver skin, nylon, silicone	(\$1B)
Ophthalmologic		
Contact lens	Acrylate/methacrylate/silicone polymers	150,000,000
Intraocular lens	Acrylate/methacrylate polymers	7,000,000
Corneal bandage lens	hydrogel	–
Glaucoma drain	Silicone, polypropylene	(\$200M)
Other		
Cochlear prosthesis	Platinum, platinum-iridium, silicone	250,000 total users
Breast implant	Silicone	700,000
Hernia mesh	Silicone, polypropylene, Teflon	200,000 (\$4B)
Sutures	PLA, polydioxanone, polypropylene, stainless steel	(\$2B)
Blood bags	Poly(vinyl chloride)	–
Ear tubes (Tympanostomy)	Silicone, Teflon	1,500,000
Intrauterine device (IUD)	Silicone, copper	1,000,000

Figure 1.3 Different applications of different biomaterials (Ratner et al., 2013b) [5].

In the table above we can see the biomaterials used and their different applications depending on mechanical properties and different characteristics of each one. For example, metals (such as stainless steel, titanium...) are mostly used in joint replacement for their high mechanical properties, while polymers are used for bone cements or soft tissue because of their low mechanical properties.

Another important classification in biomaterial field can be done dividing biomaterials on their interaction with the surrounding tissues:

Classification	Response	Examples	Effect
Biotolerant materials	Formation of thin connective tissue capsules (0.1–10 μm) and the capsule does not adhere to the implant surface	Polymer-poly tetra fluorethylene (PTFE), polymethyl metha acrylate (PMMA), Ti, Co–Cr, etc.	Rejection of the implant leading to failure of the implant
Bioactive materials	Formation of bony tissue around the implant material and strongly integrates with the implant surface	Bioglass, synthetic calcium phosphate including hydroxyl apatite (HAP)	Acceptance of the implant leading to success of implantation
Bioreabsorbable materials	Replaced by the autologous tissue	Poly-lactic acid and polyglycolic polymers and processed bone grafts, composites of all tissue extracts or proteins and structural support system	Acceptance of the implant leading to success of implantation

Tab. 1.1 Classification of biomaterials based on its interaction with its surrounding tissue (Geetha, Singh, Asokamani, & Gogia, 2009) [6].

METALS IN MEDICAL IMPLANTS

Metals are very important in medical applications and are widely used, but they have some drawbacks, like corrosion, wear debris, especially for metal-on-metal interface, as CoCr prosthesis and toxicity, due to prolonged release of metal ions (Posada, Tate, & Grant, 2015) [7]. Therefore, we must seek the right compromise between excellent biocompatibility (stainless steel, Titanium alloys), wear resistance (Co alloys), corrosion resistance and a Young’s modulus as close as possible to that one of the bone (Titanium alloys) and in the meantime avoid the ion release and low mechanical properties (C. Ramskogler, 2018) [8].

It’s very important, also, to consider the Young’s modulus because most of the metals for biomedical implants has a very high modulus and this aspect could lead to the so-called “stress shielding effect”(Asgharzadeh Shirazi, Ayatollahi, & Asnafi, 2017) [9]. As in healthy persons the bones will remodel in response to the loads they are placed under, then this effect is due to bone’s density reduction, as a result of removal of typical stress from the bone by an implant. Hence the bone will become weaker because it has no stimulus, required to maintain bone mass.

In conclusion we need a material with a Young's modulus close enough to bone Young's modulus in order to avoid this phenomenon and one of the best candidates, in comparison with stainless steel, Co-Cr alloys (Lutjering & Williams, 2007) [10], is Titanium and in particular its alloys (Young's modulus =110GPa) (M. Niinomi & Nakai, 2011) [11]. This value is still higher than that one of the bones (Young's modulus=10-30GPa), but for sure is lower than all other metal materials.

Has been shown the first and the main important reason why Titanium alloys could be the better choice in medical applications and implants. It's a very good material for its biocompatibility, corrosion resistance, stiffness and strength (Long & Rack, 1998) [12].

TITANIUM MICROSTRUCTURE AND ITS ALLOYS

Titanium is a chemical element, located among transition metals with atomic number 22. It presents different characteristics, such as low density, high corrosion resistance and the highest strength-to-density ratio of any other metallic element. Titanium is present in the earth's crust at a level of about 0.6% and is therefore the fourth most abundant structural metal after aluminum, iron, and magnesium. (Lutjering & Williams, 2007) [10].

It was discovered in 1791 by William Gregor and was named Titanium in honor of Titans in Greek mythology. Titanium is widely used in medical applications, in particular in dental implants (Oshida, 2007) [13] because of its good biocompatibility, corrosion resistance in comparison with other metals and last it has some properties to avoid bacterial adhesion, that is one of the most important issue in prosthesis applications (Ribeiro, Monteiro, & Ferraz, 2012) [14]. This is why one of the most important characteristic of Titanium is its osseous integration with the bone of the jaw (Ratner, Hoffman, Schoen, & Lemons, 2013b) [5].

Titanium can have two different crystal structure, depending on temperature: at low temperatures (room temperature) commercially pure Titanium and most of its alloys crystallizes in a hexagonal close packed structure (hcp), while at higher temperature (more than 882°C) it crystallizes in a body centered cubic structure (bcc). The first structure is called α -titanium and the second one is known as β -titanium. (Oshida, 2007) [13]. The allotropic transformation's temperature is called β transus temperature and it varies for every kind of titanium alloy, but for pure titanium is 882 ± 2 °C.

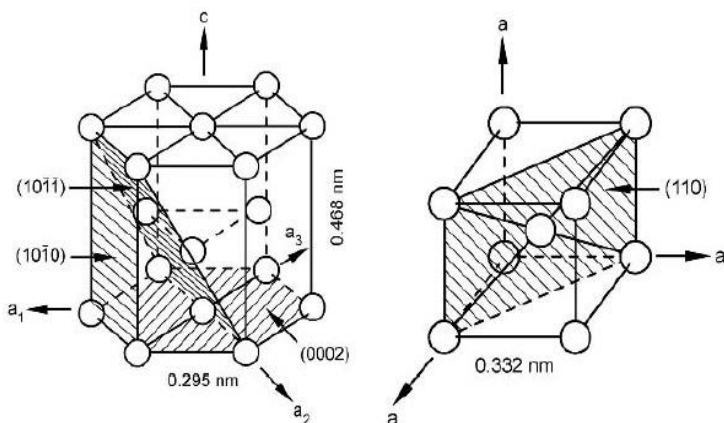


Figure 2.1 On the right side hcp structure and on the left side the bcc structure (Lutjering & Williams, 2007) [10].

There are different types of Titanium alloys:

- α : hexagonal close packed and commercially pure;
- $\alpha+\beta$: including Ti-6Al-4V (Ti-6%Al-4%V), that have about 5% to 40% of beta volume fraction at room temperature;
- β metastable: including Ti-15Mo (Ti-15%Mo), where β doesn't transform anymore to martensite even after quenching;
- β : they have higher density in comparison with other alloys and they are rich in beta-stabilizers in order to avoid the transformation of beta in alpha phase; also we can say that they show a better biocompatibility with human tissues because of their lower Young's modulus (between 55 and 85GPa, closer to the bone's one) (Mitsuo Niinomi, 1998) [15];

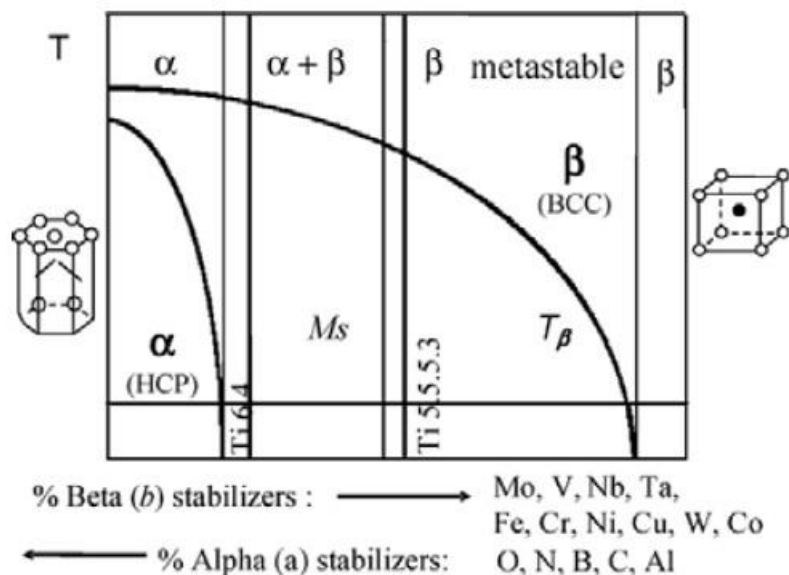


Figure 2.2 Phase diagram of titanium alloys (Abdul Md Mazid 2012) [16].

As we can see in Fig. 2.2 there are different elements that can influence β transus temperature: (Peters & Leyens, 2003) [17]

- α -stabilizers: aluminum; they lead to the formation of two phase (alpha and beta), that coexist together;
- β -stabilizers: there are β -isomorphous elements (Mo, V and Ta), that have higher solubility in Titanium and β -eutectoid elements (Fe, Cr, Ni, Si, Cu, Mn, H and Co) that can lead to the formation of intermetallic compounds;
- neutral elements: they don't influence so much β transus temperature;

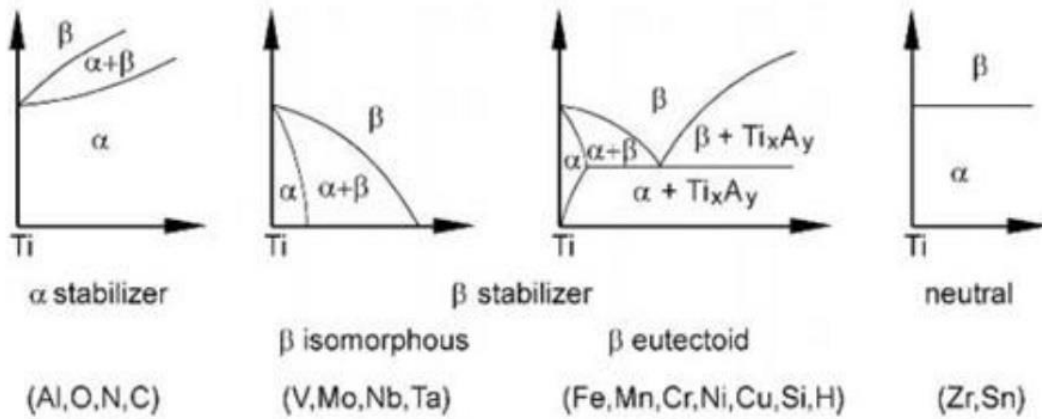


Figure 2.3 Effect of alloying elements on phase diagrams of titanium alloys (Yang Yang 2015) [18].

About mechanical properties we can say that every Titanium alloy has different features and every feature could influence the behavior of the alloy. We can see the different features in the table below: about density, α alloys have a lower density than β alloys due to the lower specific weight of aluminum compared to β alloying elements (Mo, V...). $\alpha + \beta$ alloys and β alloys can be respectively hardened to very high strength levels in comparison with α alloys; about fracture toughness, this is strongly dependent on the microstructure, in fact coarse and lamellar microstructures show higher values of fracture toughness than fine and equiaxed ones. It happens because coarse and lamellar microstructures can deflect the propagation of cracks along differently oriented lamella packets, consuming energy for this propagation.

It's also important to emphasize the high value of corrosion resistance in Titanium alloys, which makes it one of the best choices in biomedical field, due to the formation of a thin dense oxide layer (TiO_2) on the surface when there is the presence of oxygen in the atmosphere because there is a high affinity between the two elements. Because α alloy is more stable to oxidation than β , then β alloys are more susceptible to embrittlement; and this is the explanation of why welding treatments or heat treatments should be performed in vacuum or in an inert gas (Argon, for instance) in order to avoid oxidation on the Titanium surface.

	α	$\alpha+\beta$	β
Density	+	+	-
Strength	-	+	++
Ductility	-/+	+	+/-
Fracture toughness	+	-/+	+/-
Creep strength	+	+/-	-
Corrosion behavior	++	+	+/-
Oxidation behavior	++	+/-	-
Weldability	+	+/-	-
Cold formability	--	-	-/+

Tab. 2.1 Properties of α , $\alpha+\beta$ and β Ti alloys (Peters, M., & Leyens, C 2003) [17].

The more important Titanium alloys in biomedical field, currently used, are:

1. ASTM F67: commercially pure Titanium (98.9-99.6% Titanium), used mostly in dental applications or as coating for its low mechanical properties. It presents a monophasic α structure and it exists in four different types, Titanium grade 1, grade 2, grade 3 and grade 4, depending on the percentage of oxygen in the structure. Titanium grade 2 is the more used in biomedical applications and the oxygen is about 0.25%. Yield strength is 70MPa for Titanium grade 1 and 485MPa for Titanium grade 4; fatigue limit can change from 88.2MPa (Titanium grade 1) up to 216MPa (Titanium grade 4); Young's modulus is about 100-110GPa; (Rack & Qazi, 2006) [19] (Mitsuo Niinomi, 1998) [15]; main applications could be: cardiovascular stents and dental field for its low ductility and high strength;
2. ASTM F136: Ti-6Al-4V, that is one of the more common alloy, used in biomedical field. It's an $\alpha+\beta$ alloy and between 700 and 950°C the microstructure presents α grains (3-10 μ m) and β phase at grain boundaries. If I increase the temperature over 975°C and then I cool down up to room temperature, there will be α phase in β matrix in form of lamellae; finally, if the cooling rate is very fast (quenching) it will be possible to observe martensite. This alloy presents high mechanical strength, corrosion resistance and a good biocompatibility; main application: total joint replacement. One issue could be the release of ions, that is potentially cytotoxic, (Chen & Thouas, 2015) [20] therefore recently it has been introduced a new alloy with a very low release, Ti-6Al-7Nb, with similar characteristics in comparison with Ti64.
3. Timetal 367: Ti-6Al-7Nb, that presents a globular biphasic microstructure (β -phase=10-12%); high corrosion resistance and lower costs.

4. Ti-15Mo: is a beta titanium alloy capable of a wide variety of properties depending on the metallurgical condition. The achievable properties include low modulus of elasticity, high strength, excellent fatigue strength, good ductility, exceptional corrosion resistance, and well-documented biocompatibility. This alloy has different applications in biomedical field: orthopedic, trauma, spinal, dental, orthodontic, and cardiovascular applications. Physical properties:

- Beta Transus Temperature: 774°C ($\pm 14\text{C}^{\circ}$);
- Elastic Modulus: 78 GPa in the beta annealed condition, 106 GPa in the alpha plus beta annealed condition, 114 GPa in the micrograined alpha plus beta aged condition;

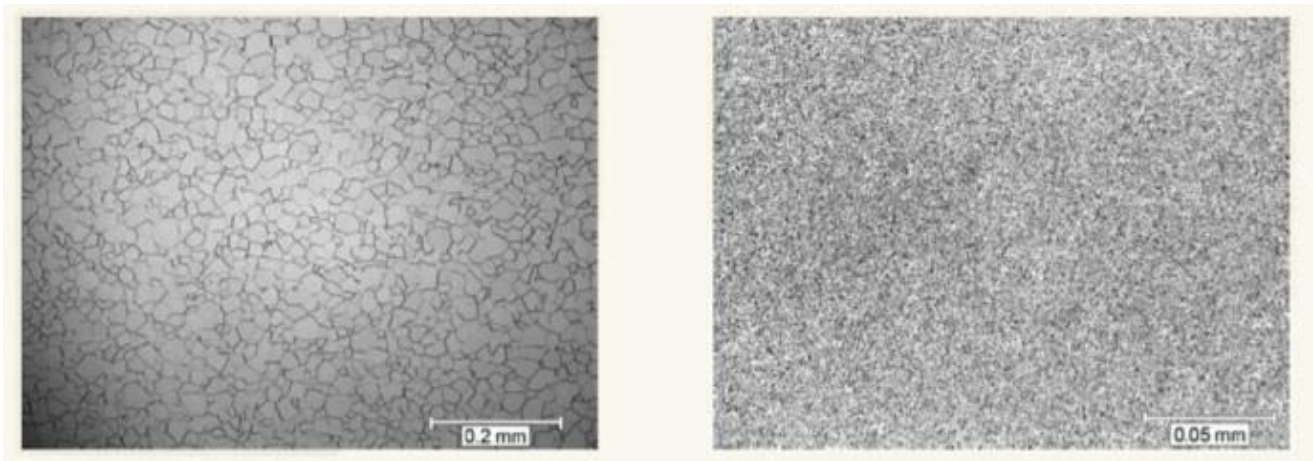


Figure 2.4 On the left Ti-15Mo β -Titanium Alloy; on the right side Ti-15Mo micro grained $\alpha+\beta$ alloy.

THE ROLE OF HEAT TREATMENTS ON TITANIUM ALLOYS MICROSTRUCTURE

First of all it's important to mention how microstructure of titanium alloys influences mechanical properties, such as Young's modulus, strength, ductility, fatigue crack...) (Peters & Leyens, 2003) [17].

<i>fine</i>	<i>coarse</i>	<i>Property</i>	<i>lamellar</i>	<i>equiaxed</i>
○	○	Elastic modulus	○	+/- (texture)
+	-	Strength	-	+
+	-	Ductility	-	+
-	+	Fracture toughness	+	-
+	-	Fatigue crack initiation	-	+
-	+	Fatigue crack propagation	+	-
-	+	Creep strength	+	-
+	-	Superplasticity	-	+
+	-	Oxidation behavior	+	-

Tab. 2.2 Influence of microstructure on selected properties of titanium alloys. (Peters, M., & Leyens, C 2003) [17]. + = high influence; - = less influence; O = not influence;

Microstructure can be modified by means of thermomechanical treatments (heat treatments, deformation, recrystallization, aging and annealing).

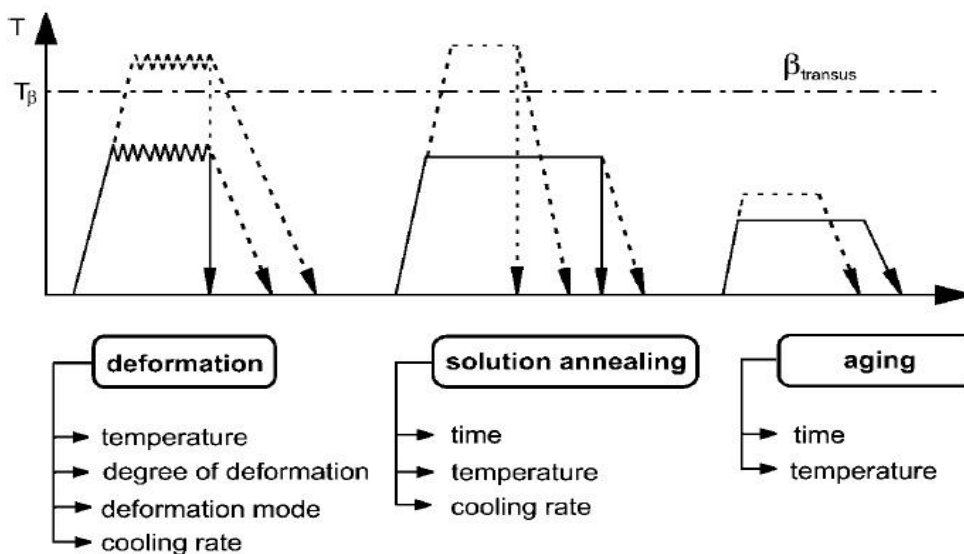


Figure 2.5 Thermomechanical treatment of titanium alloys (Peters, M., & Leyens, C 2003) [17].

The lamellar microstructure is generated upon cooling from the β phase field, while the equiaxed microstructure is a result of recrystallization process and both can have coarse or fine arrangement.

- Lamellar microstructure: it's possible to obtain lamellae by cool down from β transus temperature up to room temperature because below beta transus temperature α starts to nucleate at grain boundaries and grows in form of lamellae into beta grain. Changing the cooling rate, it's possible to change the morphology of lamellae, for instance a slow cooling rate leads to have pure lamellar microstructures with coarser lamellae if the cooling rate is reduced; so α lamellae derived by slow cooling rates are thicker than those ones obtained by faster cooling rates;

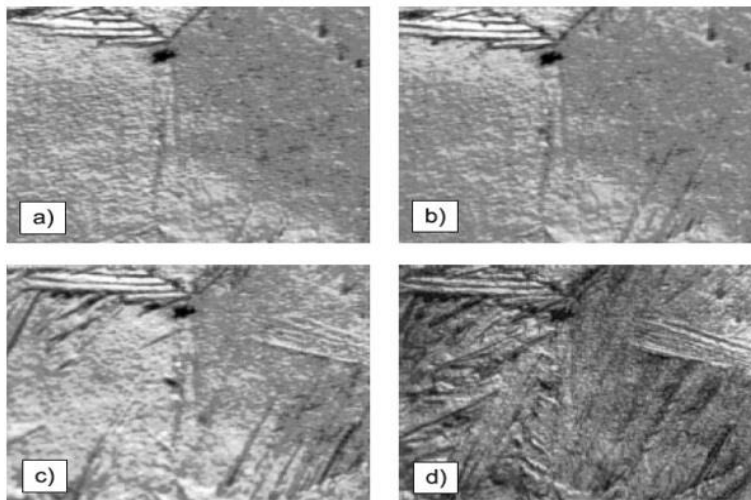


Figure 2.6 Example of nucleation and growth of the alpha phase into the (prior) β grains with cooling from the β -phase field (Peters, M., & Leyens, C 2003) [17].

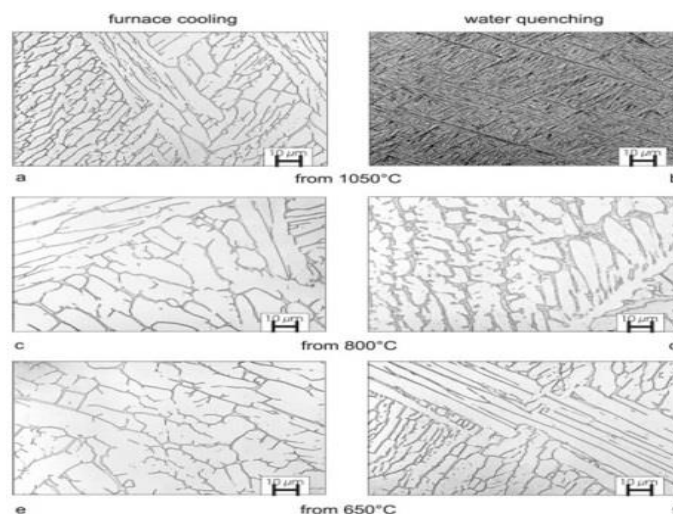


Figure 2.7 Microstructure of Ti-6Al-4V after slow cooling (50°C/h) and after quenching from 1050°C, 800°C, and 650°C. (Peters, M., & Leyens, C 2003) [17].

- Equiaxed microstructures: is due to recrystallization process, that provides for a first deformation, followed by a heat treatment (in an area below beta transus temperature) and an annealing, which is important to make equiaxed microstructure coarser (Peters & Leyens, 2003) [17].

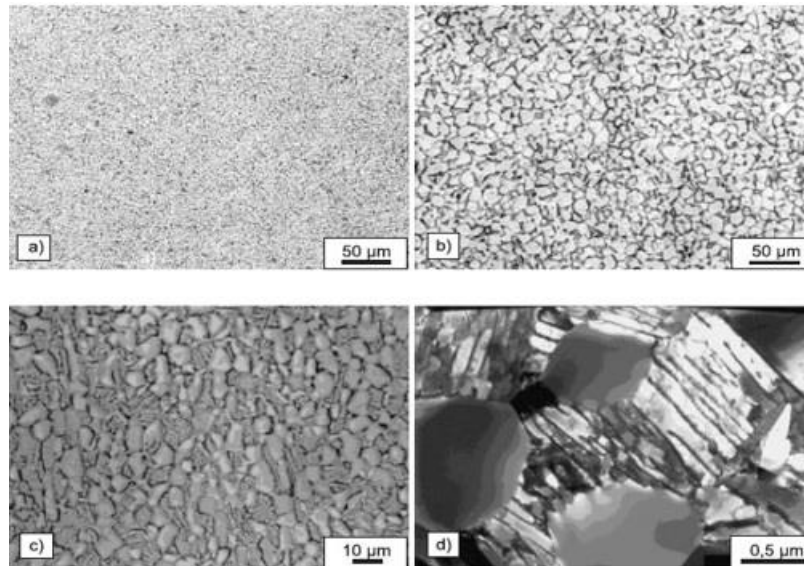


Figure 2.8 Equiaxed microstructures of Ti-6Al-4V via recrystallization: a) fine equiaxed; b) coarse equiaxed; c,d) bimodal (Peters, M., & Leyens, C 2003) [17].

Moreover, quenching above β transus temperature leads to a martensitic transformation of β , resulting in a very fine needle-like-microstructure (Peters & Leyens, 2003) [17]. Martensite can have two different shape: hexagonal α' martensite and orthorhombic α'' (ω) martensite (Fig. 2.9 and 2.10) (Peters & Leyens, 2003) [17].

The first type of martensite (hexagonal α' martensite) occurs when there is a low number of beta-stabilizers (as in the case of Ti-6Al-4V); the second one (orthorhombic α'' martensite) occurs when there is a high number of beta-stabilizers (Mo, V, Ta, Cr and so on, as in case of Ti15Mo).

In case of low number of alloying elements and high martensitic transformation temperature will be formed massive martensite; however, a high number of alloying elements and low martensitic transformation temperature will be formed acicular martensite (Ramskogler C. 2018) [8].

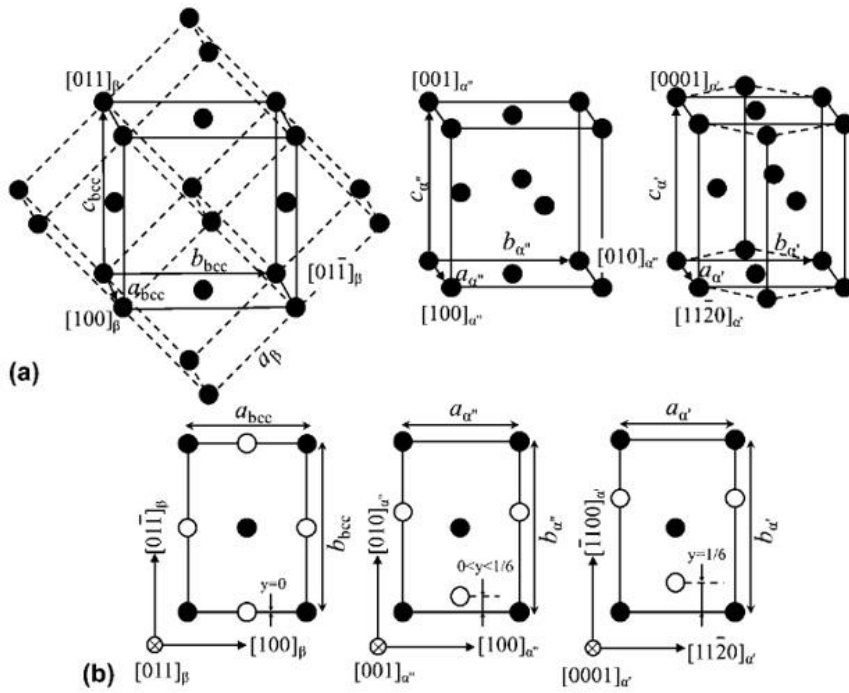


Figure 2.9 (a) Schematic representation of the crystal structures of β , α'' and α' phases (Conventional unit cells are indicated by dashed lines) and (b) their lattice correspondences (the solid and empty circles located respectively, at adjacent $(011)_{\beta}$ basal planes for the β phase, $(001)_{\alpha''}$ for the α'' phase and $(0001)_{\alpha'}$ for the α' phase) (Mei, Sun, & Wen, 2017) [21].

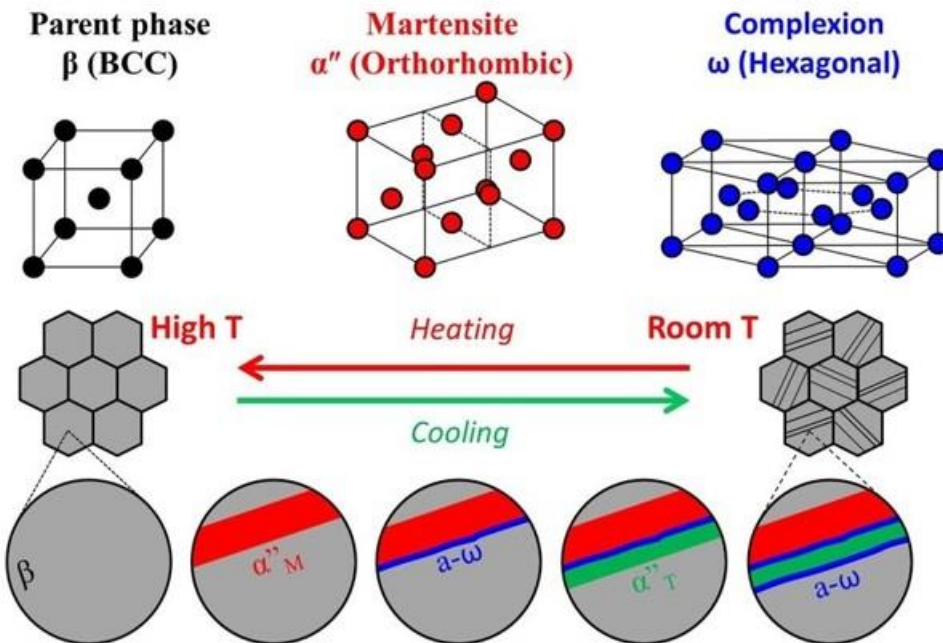


Figure 2.10 Crystal structure of the different phases of titanium alloy involved during heat treatment (Zhang, Tasan, Lai, Dippel, & Raabe, 2017) [22].

In addition to heat treatments, there are some other modifications that we can carry out in order to improve tribological (hardness) and biological (corrosion and wear resistance) properties of Titanium alloys, without changing bulk features(Liu, Chu, & Ding, 2004) [23]. These surface modifications can be divided in:

- Mechanical methods: grinding, polishing and blasting;
- Chemical methods: biochemical modifications, electrochemical treatments;
- Physical methods: in order to produce modified coatings on Ti-alloys using different kinds of energy (kinetic, electrical or thermal); one of the more important physical techniques is electron beam treatments in order to obtain different topographies on the Titanium surfaces.

By means of electron beam it's possible to realize different shapes on the surface to improve it or to improve mechanical properties of this. For instance in a study it was realized a hexagonal pattern on Ti-6Al-4V with concentric grooves (Figure 2.11) (Ramskogler, Warchomicka, Mostofi, Weinberg, & Sommitsch, 2017) [24].

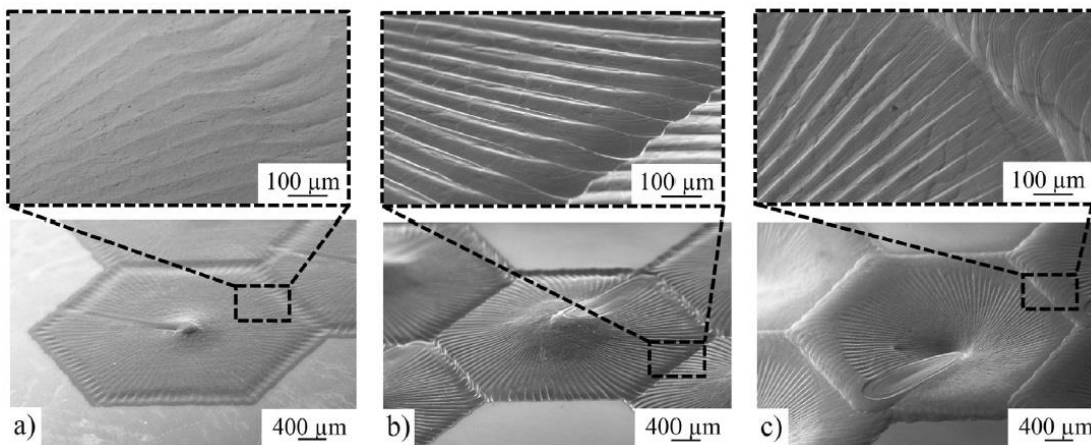


Figure 2.11 SE-SEM images a) hexagonal pin array $I = 0.8 \text{ mA}$ $v = 341 \text{ mm/s}$, b) hexagonal pin array $I = 2.5 \text{ mA}$ $v = 698 \text{ mm/s}$, c) hexagonal wall array $I = 2.5 \text{ mA}$ $v = 698 \text{ mm/s}$.

It's also important to remember how different topographies on the material could influence not only mechanical properties, but also cell and bacteria behavior, that sense micro structures on the surface. (Anselme, 2000) [25]. The presence of microstructures increases the air content of the surface and the hydrophobicity, as explained using Cassie-Baxter equation(Cheng & Rodak, 2005) [26] (Martines et al., 2005) [27].

INFLUENCE OF MICRO AND NANO TOPOGRAPHY ON THE BEHAVIOR OF CELLS AND BACTERIA

CELL RESPONSE

As is widely known, cells are able to sense the surrounding environmental and in particular, micro and nano structures and topographies. In fact, cells live in a physiological environment in which they are in contact with the extra cellular matrix (ECM) composed by a lot of micrometric structures and nanometer ones (Goodman, Sims, & Albrecht, 1996) [28] (Abrams, Goodman, Nealey, Franco, & Murphy, 2000) [29] (Pamula, De Cupere, Dufrene, & Rouxhet, 2004) [30]. These interactions between cells and other structures in the ECM are mediated by the contact guidance phenomenon (Ambrose, 1956) [31], according to which the orientation of cells is influenced by micro and nano topographies (such as micro and nano grooves) and different geometrical patterns (Wolf, Müller, Borgmann, Bröcker, & Friedl, 2003) [32] (Friedl, 2004) [33]. Thanks to this phenomenon is also possible to improve soft tissue, of which fibroblasts are the more representative cells, by means of topographical surface modification in order to guide fibroblasts and allow their preferential orientation by contact guidance (S. Ferraris et al., 2019) [34].

In order to understand better how this complex phenomenon works, first we need to explain how a cell can create interactions between itself and the ECM or another cell.

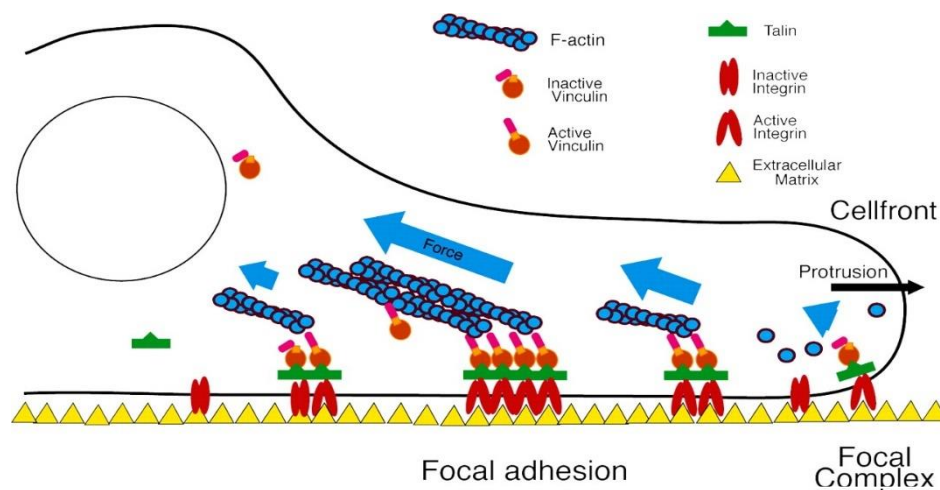


Figure 3.1 Model of cell movement (Humphries et al., 2007) [35].

In the link between the cell and matrix, adhesion proteins and integrins play the main importance role among the transmembrane proteins (Van der Flier & Sonnenberg, 2001) [36] (Giannone & Sheetz, 2006) [37]. Integrins allow cell-ECM contact by means of weak bonds but much higher dense, so in this way the cell is capable of moving easily attaching and detaching quickly its interactions. When a large amount of integrins are involved in adhesion it's possible to talk about focal adhesion or focal complex (Kanchanawong et al., 2010) [37] (Riveline et al., 2001) [38] (Ingber, 1997) [39].

However about cell-cell contact there are different proteins that play this important role, they are called cell adhesion molecule (CAMs) and they are cadherins, selectins and immunoglobulins (Rekka, Sathiyawathie, & Abilasha, 2019) [40].

All the cells are very sensitive to micrometer substrates, not only cells of hard tissues, but also the soft tissue cells, such as fibroblasts, and the most representative micrometer surface topography are micro grooves, widely investigated in literature (S. Ferraris et al., 2019) [34] (Sara Ferraris et al., 2018) [41]. Others studies have demonstrated how the majority of cells (fibroblasts, osteoblasts, neurites...) align themselves along the major axis of grooves and this alignment is enhanced by decreasing groove width and increasing groove depth (Rajnicek, Britland, & McCaig, 1997) [42].

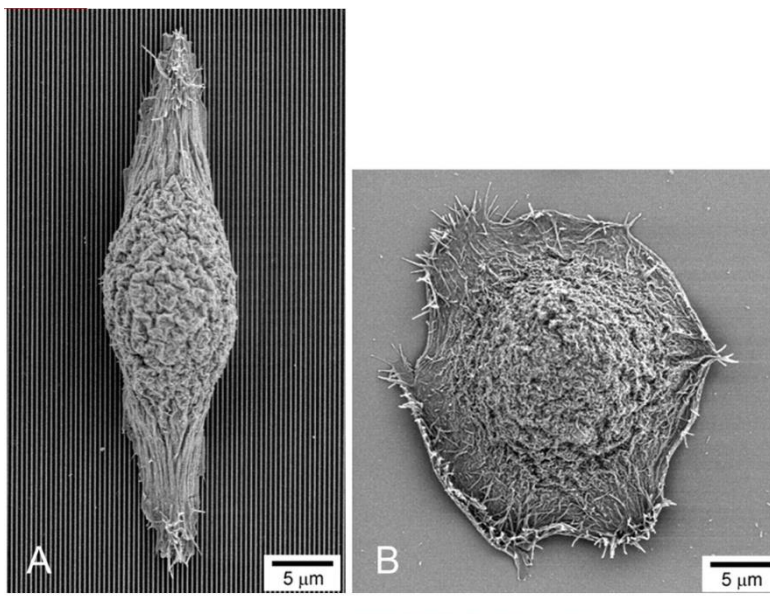


Figure 3.2 SEM images of human corneal epithelial cells. (A) Cell cultured on a silicon oxide substrate patterned with 70 nm wide ridges, on a 400 nm pitch. The groove depth was 600 nm. (B) Cell on a smooth silicon oxide substrate (Teixeira, Abrams, Bertics, Murphy, & Nealey, 2003) [43].

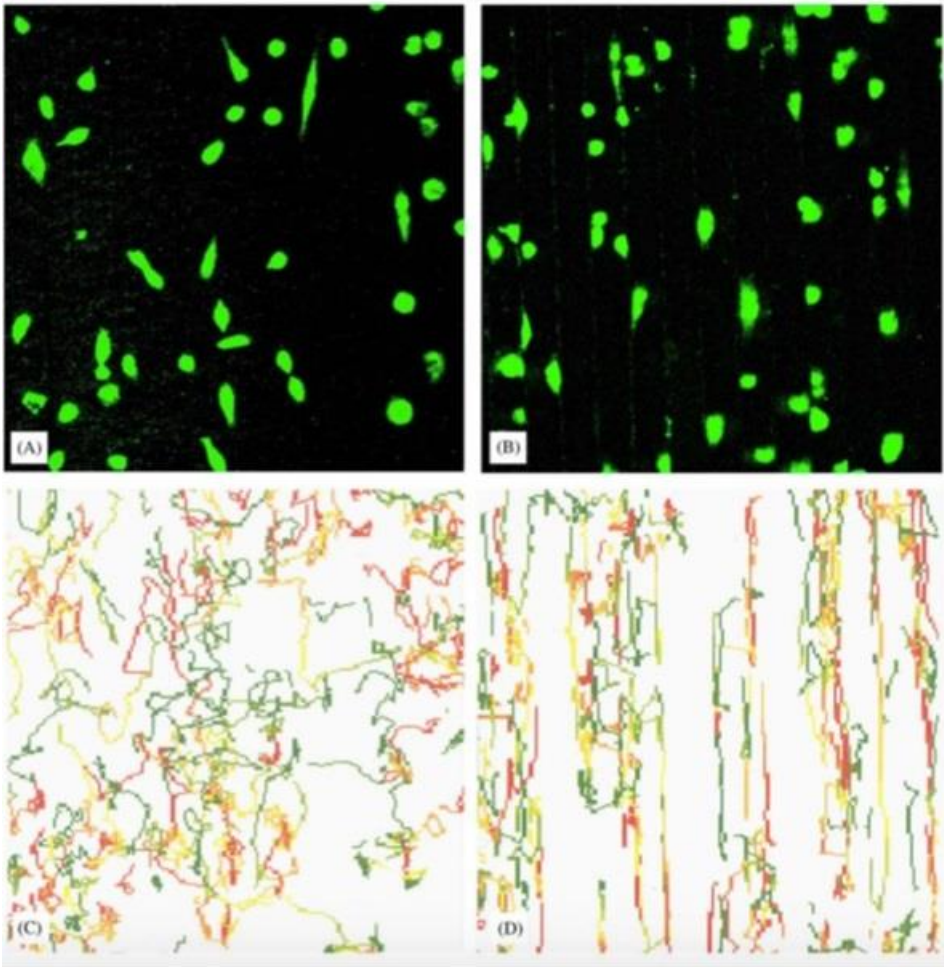


Figure 3.3 Analysis of cell behaviour. One representative picture of a series made of DiI labelled 3T3 fibroblast cells on the plane surface (A) and on the structured surface (B) (grooves depth: 22 μ m; ridges width: 22 μ m; spaced grooves: 18 μ m). The covered trails (trajectories) of the cells migrating on a plane surface (C) and structured surface (D) over an observation period of 24 h was drawn (Kaiser, Reinmann, & Bruinink, 2006) [44]

We talked before about integrins, focusing on their main role in focal adhesion and how cells are able to sense micrometer substrates; this is true, but it's also true that they can sense nanometer substrates (Cavalcanti-Adam et al., 2006) [45] because integrins are on nanometer scale (8-12nm). It was widely demonstrated that nanometer changes in topography could produce a cascade effect of biochemical stimuli on cell that lead a modification in gene expression and consequently a modification in the cellular behavior (Dalby, 2005) [46] (Dalby, Riehle, Sutherland, Agheli, & Curtis, 2004) [47].

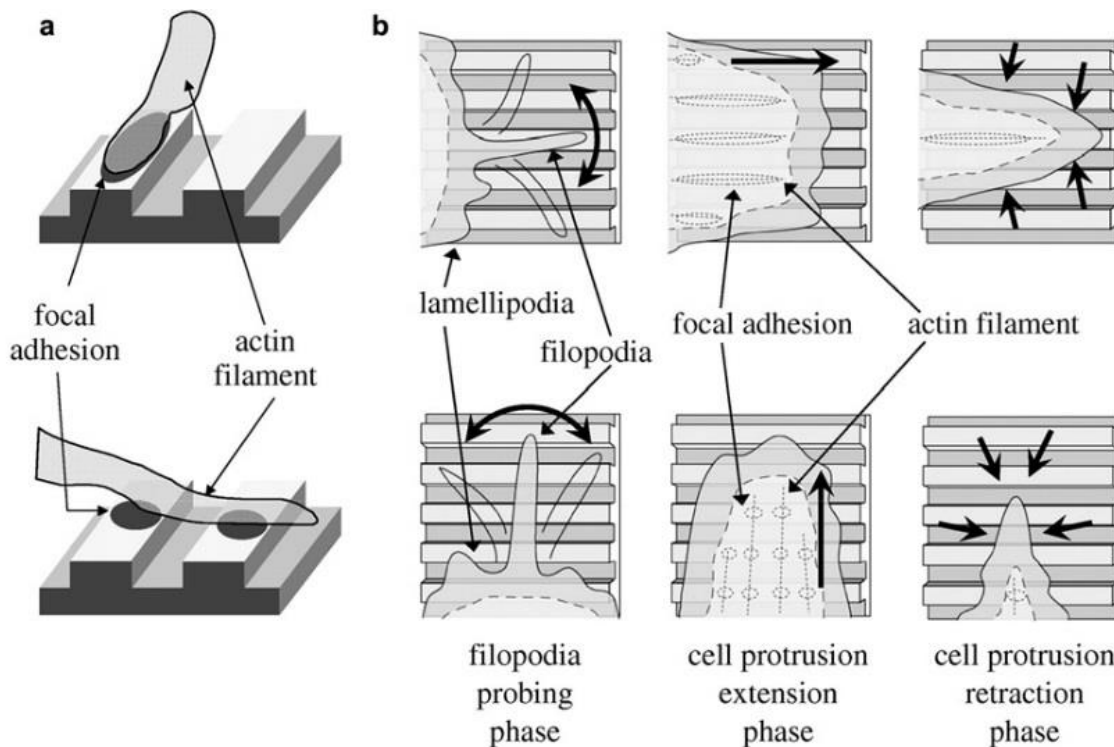


Figure 3.4 Model for cell alignment on the nanogrooved substrate. (a) Actin filaments parallel to the grooves form wide focal adhesions at filament terminations. On the other hand, termination of perpendicular filaments is fragmented because focal adhesions form only on the ridge. (b) Filopodia movements are isotropic, i.e. no specific direction was observed for their extension and retraction against the nanogrooved structure. This finding suggests that filopodia probing does not play a major role in cell alignment. Cell protrusions extended isotropically, but some that were perpendicular to the nanogrooved pattern retracted more rapidly than those parallel to the nanogrooved pattern. These cell protrusion dynamics force a cell to elongate and align along the nanogrooved pattern (Anselme et al., 2010) [48].

By the way, it's appropriate to explain well how nano topography could influence cell behavior because there a lot of features that play a significant role in this field:

1. Rugosity: this is one of the more important factors which can influence cell adhesion on a substrate. Cells are different from one another, in facts for instance fibroblasts are rugophobic (preferentially adhere on smooth surfaces) while osteoblasts are rugophilic (preferentially adhere on rough surfaces) (Sara Ferraris et al., 2018) [41].

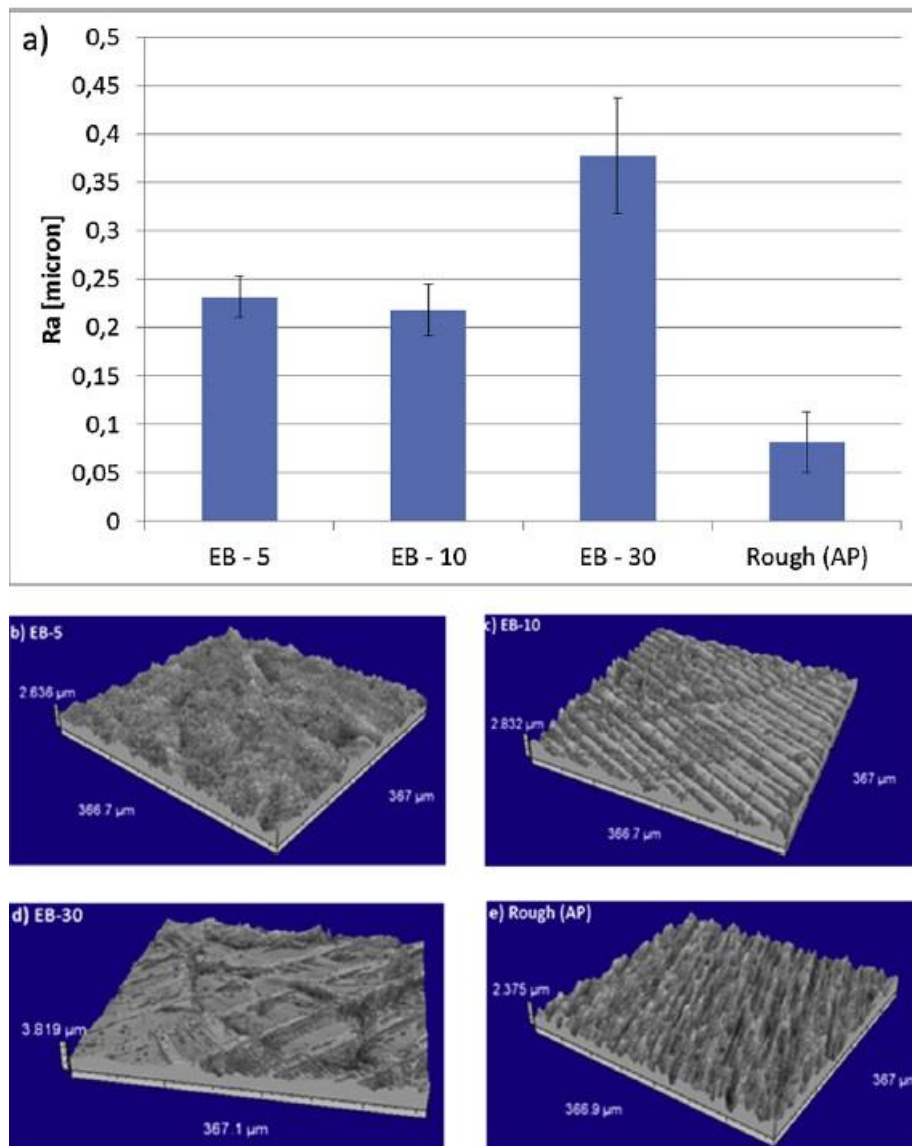


Figure 3.5 Roughness measurements and surface 3D reconstructions of the EB structured and mechanically roughened samples (AP) (S. Ferraris et al., 2019) [34].

In this study S.Ferraris et al. realized different samples with different nano topographies (EB5, EB10 and EB30) and measured the rugosity in order to allow fibroblasts adhesion and avoid bacterial adhesion;

2. Size: in the previous work they investigated also the influence of the size for cell adhesion. In facts they found that grooves with width higher than 100nm and lower than 70 μm, depth higher than 35 nm and with spacing between grooves lower than 2 μm allow contact guidance phenomenon on fibroblasts.

Also, Anselme et. Al investigated these features and they found that in case of islands on the surface, cells are able to respond to a value not lower than 13nm tall. In general islands <25nm tall increased cell adhesion and >40nm decreased cell adhesion. In case of nanopits, it was demonstrated that fibroblasts are able to sense topography down to 35nm using their filopodia. These results are due to the increased number of grain boundaries and consequently an increased surface energy, that influences protein absorption and cell adhesion. In conclusion, we can say that an increase in the size of features has a negative impact on cells (Anselme et al., 2010) [48]. Dalby et al. studied the influence of nanocolumns (160 nm high and 100 nm in diameter). They demonstrated decreased cell adhesion and spreading on the nanocolumns, characterized by smaller, fainter focal adhesions;

3. Surface energy: for small surface energies any increase in roughness is detrimental to cell adhesion; for intermediate surface energies the roughness has a minor effect on cell adhesion and for large surface energies there is an optimal roughness in order to promote and maximize cell adhesion (Anselme et al., 2010) [48];

Distance between nanofeatures: the minimum spacing required for the clustering of integrins and activation of focal complexes is in the range of 58-73nm. So, the distance between nanofeatures has to be considered a function of distance between focal adhesion. About organization, it was studied the adhesion and the differentiation of stem cells on different organized topography (square, hexagonal and random conformation of pits) and it was seen that the square topography (with average displacement of 20 and 50nm) were more positive for osteocalcin and osteopontin, two markers of osteoblast differentiation. This is a remarkable result because it was demonstrated that is possible to influence cell differentiation only with topographical stimuli, without chemical ones (Arnold et al., 2004) [49];

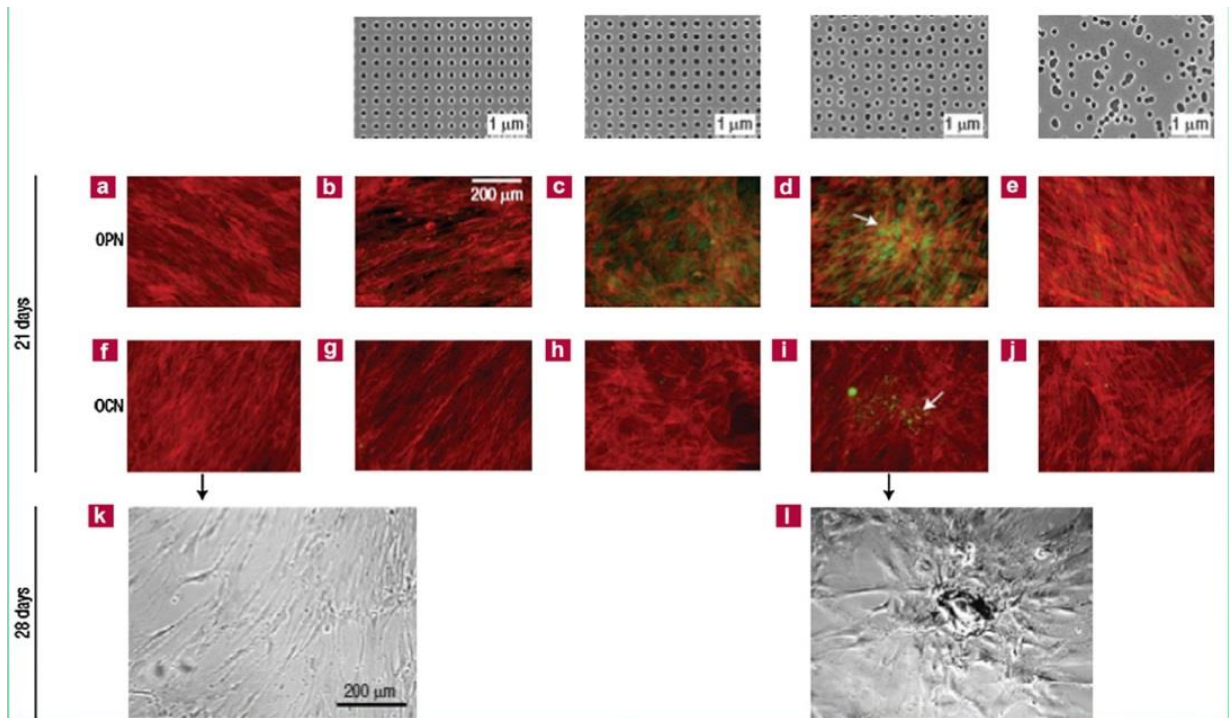


Figure 3.6 Directed differentiation of human mesenchymal stem cells (MSC) to the osteoblast lineage using nanopit substrates. The top row shows images of nanopit substrates fabricated by electron beam. All have 120 nm diameter pits with square (SQ), displaced square 20 (DSQ20), displaced square 50 (DSQ50) and random placements (RAND). (a and f) MSCs on the control. Note the fibroblastic appearance and no osteopontin (OPN) or osteocalcin (OCN) positive cells; (b and g) MSCs on SQ. Note the fibroblastic appearance and no OPN/OCN positive cells; (c, h) MSCs on DSQ20. Note OPN positive cells; (d and i) MSCs on DSQ50. Note OPN and OCN positive cells and nodule formation (arrows); (e and j) MSCs on RAND. Note the osteoblast morphology, but no OPN/OCN positive cells (Anselme et al., 2010) [48].

4. Cell type: different cells need different stimuli in order to carry out their physiological activities. For instance, smooth muscle cell proliferation is enhanced by nanostructure in comparison with endothelial cell proliferation that is decreased. Moreover, the nanotextured surfaces could be used to limit fibroblasts growth and slow down the formation of fibrous capsule around implants.

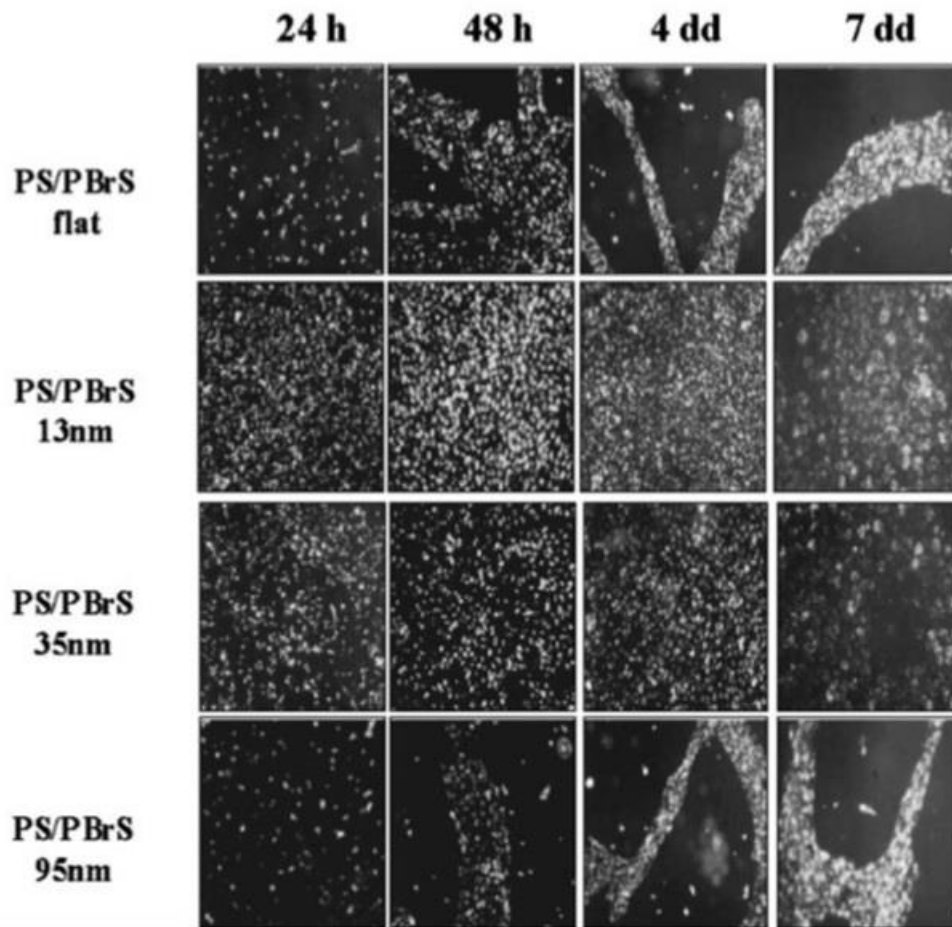


Figure 3.7 Responses of three different endothelial cell lines grown on polymeric nanostructured surfaces consisting of nanohills with increasing hill height (13, 35 and 95 nm (Buttiglieri et al., 2003) [50].

BACTERIA RESPONSE

Bacteria constitute a large domain of prokaryotic cells; they have a length of few microns and there are two types of them:

- Gram positive (*Bacillus Subtilis*, *Staphylococcus aureus*): they are characterized by one lipid membrane and one thick peptidoglycan layer (20-80nm);
- Gram negative (*Escherichia Coli*): they have two lipid membranes and a thin peptidoglycan layer (2-3nm) between them;

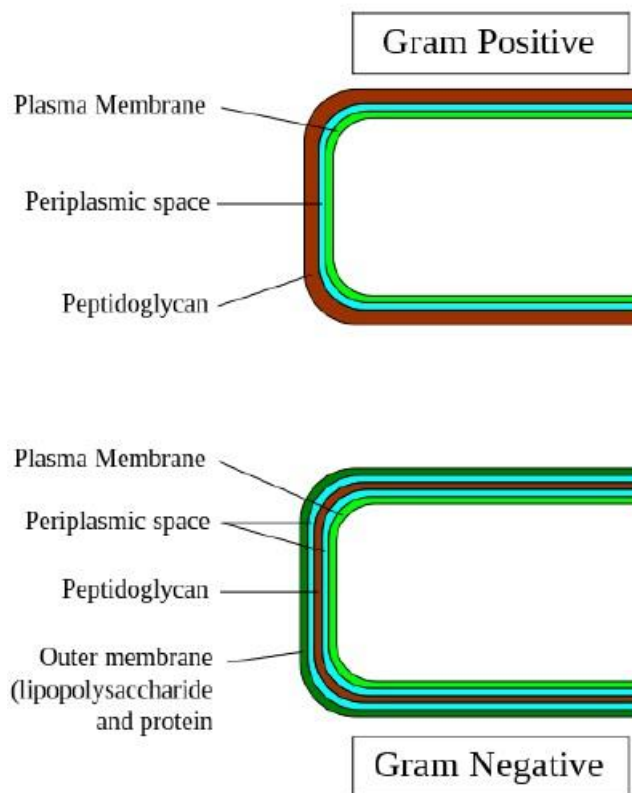


Figure 3.8 Gram Positive and Gram-Negative bacteria cell wall structure (Madigan, Martinko, Dunlap, & Clark, 2008) [51].

They can be very different each other in size and shape and some of them has the so called ‘fimbriae’ that aid them to adhere on a surface (Proft & Baker, 2009) [52] (Srivastava & Srivastava, 2003) [53].

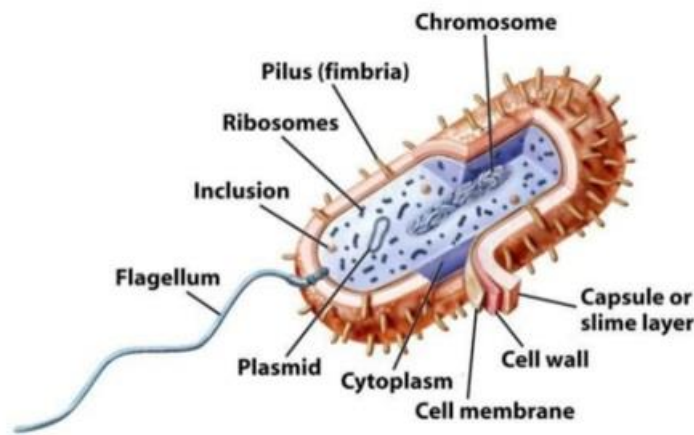


Figure 3.9 Prokaryotic cell (Proft & Baker, 2009) [52].

Nowadays it's not so clear how bacteria attach on a surface and which kind of mechanism allow the movement, nevertheless in some ways they can adhere on a surface or a medical device, infecting it and developing biofilm (Costerton 1999) [54]. Some proteinaceous features of the bacterial membrane (flagella, pili, and other fimbriae) have been shown to play a role in bacterial adhesion to surfaces and in the creation of biofilm (Van Houdt & Michiels, 2005) [55].

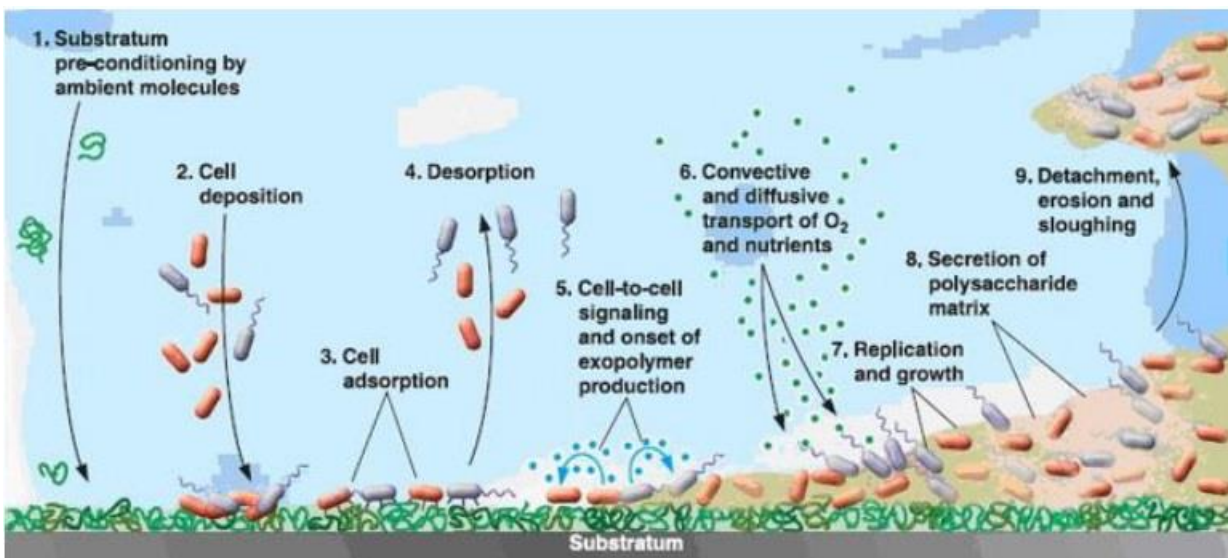


Figure 3.10 Different steps of the formation of biofilm on a generic substrate.

It's very important to study how biofilm works because bacterial infections and biofilm formation are the most common causes of medical implant failures or surgical removal, amputation and, in the most serious cases, death and this is widely known in literature. The main steps in biofilm formation are:

1. Adhesion of free-floating microorganisms on a surface;
2. Adhesion of bacteria on the surface; these interactions firstly are weak (mainly Van der Waals bonds and hydrophobic effects) and in a second moment become stronger, by means of pili. These interactions are called reversible and irreversible adhesions (Ploux, Ponche, & Anselme, 2011) [55].
3. Proliferation of the adherent bacteria and synthesis of biofilm matrix; in facts biofilm is just the assembly of bacteria and extracellular polymeric substance (EPS) (Branda, Vik, Friedman, & Kolter, 2005) [56];
4. The biofilm starts to increase and change its size and shape (Seyer et al., 2005) [57].

Bacteria, as cells, could be influenced by microtopography, but mostly by nanotopography being smaller than cells; but this is not true because they are smaller than cells but less deformable in shape, so bacteria are sensitive only for structures with the size of their same size, not lower, such as in the case of cells (Anselme, 2000) [48]. However, bacteria membrane fimbriae are very important in the role of bacterial adhesion because of their small size (diameters of 10nm or less; lengths from 100nm up to few microns); flagella are thicker (tens of nanometers in diameter), but all these bacteria features allow them to sense also nano topography structures (Srivastava & Srivastava, 2003) [53]. Several studies tried to find which kind of features really influence bacterial adhesion and most of them agree that roughness is one of the more important factors in this field; it is necessary to consider not to exceed the threshold value of 0.2 μ m of average surface roughness, widely explained in literature (Fröjd et al., 2011) [58] (S. Ferraris et al., 2019) [34] (Anselme, 2000) [48]. A specific study on transmucosal portion of dental implant revealed that an average surface roughness above 0.2 μ m increases biofilm formation and maturation and it's very important because dental field is the topic of this master thesis.(Teughels, Van Assche, Sliepen, & Quirynen, 2006) [59].

Jaione Valle et al. carried out some experiments of polystyrene surface modification microtopography by means of DLIP (direct laser interference patterning) in order to avoid bacterial adhesion; polystyrene polymer surfaces were patterned with periodical line (1D), pillar-like (2.5D) and a combination of lamella-like and line-like pattern (3D) by means of DLIP. These samples were tested in vivo and in vitro to evaluate the behavior of bacteria. The results revealed that line and pillar-like micro topographical patterns enhanced bacterial adhesion, a spatial period of $1\mu\text{m}$ induced higher bacterial attachment, than $5\mu\text{m}$. On the other hand, lamella-like topography caused a significant reduction of bacteria. They found in in-vivo tests the same results of in-vitro tests, where a significant lower colonization of bacteria was seen in mice with lamella-like structures. The reasons about why lamella-like structures reduce bacterial attachment could be find in the protruded features of the topographical surface, that provide a physical obstacle to prevent the expansion of the bacterial clusters. This is true in steady and in fluid flow conditions; in facts in the latter case the effect of lamella-like structures is amplified (Valle et al., 2015) [60].

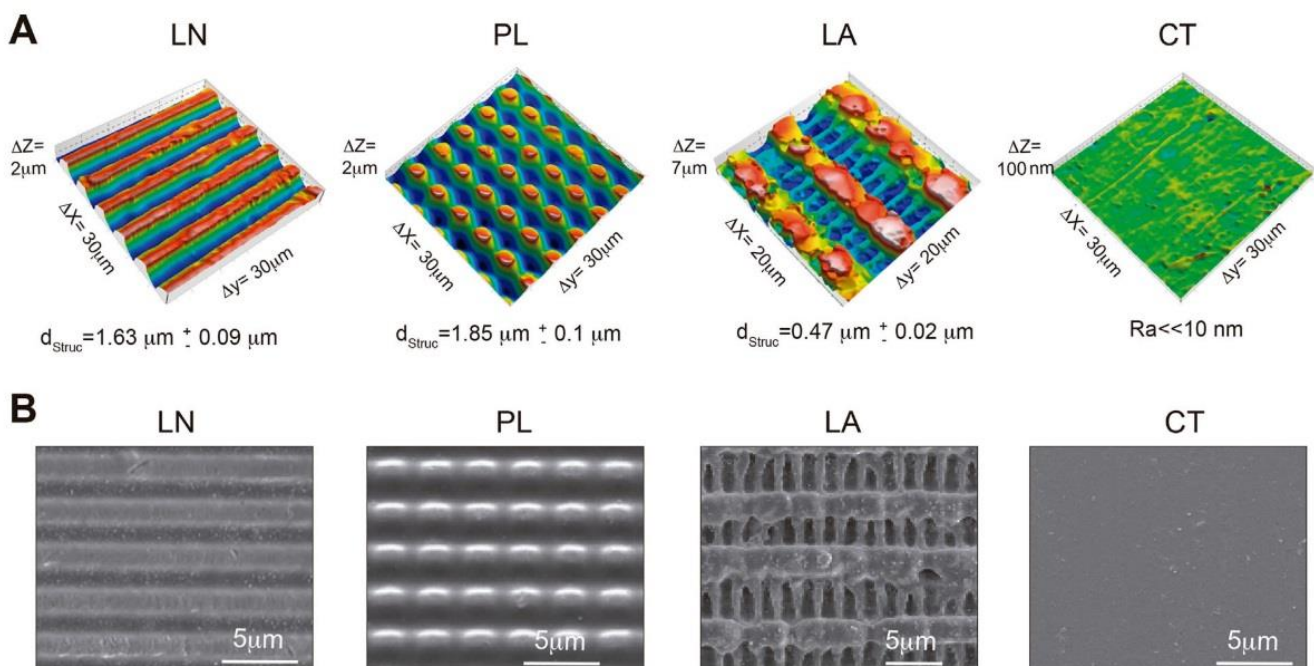


Figure 3.11 Images from confocal (A) and scanning electron microscopy (B) of PS polymeric surfaces structured by Direct Laser Interference modified surfaces (CT). The laser fluence was kept constant at 0.5 J cm^{-2} . Patterning technique. Periodic arrays of line-like (LN, $L \approx 5\text{mm}$), pillar-like (PL, $L \approx 5\text{mm}$), lamella-like (LA, $L \approx 2\text{mm}$) structures and non-modified surfaces (CT) (Valle et al., 2015) [60].

Puckett et al. studied the adhesion of *Staphylococcus aureus*, *Staphylococcus epidermidis*, and *Pseudomonas aeruginosa* on conventional Ti, nanorough Ti produced by electron beam evaporation, and nanotubular and nanotextured Ti produced by two different anodization processes. The nanotextured and nanotubular Titanium were found to be amorphous, while nanorough and conventional Titanium presented a crystalline structure, in fact, the conventional Ti contained rutile TiO_2 , while the nanorough Ti contained anatase TiO_2

The nanorough Ti substrates resulted the best for minimize bacterial adhesion, compared to the other ones, and this is due to the large amount of absorption of proteins (fibronectin in particular), that inhibits bacterial adhesion and promotes osteoblasts proliferation.

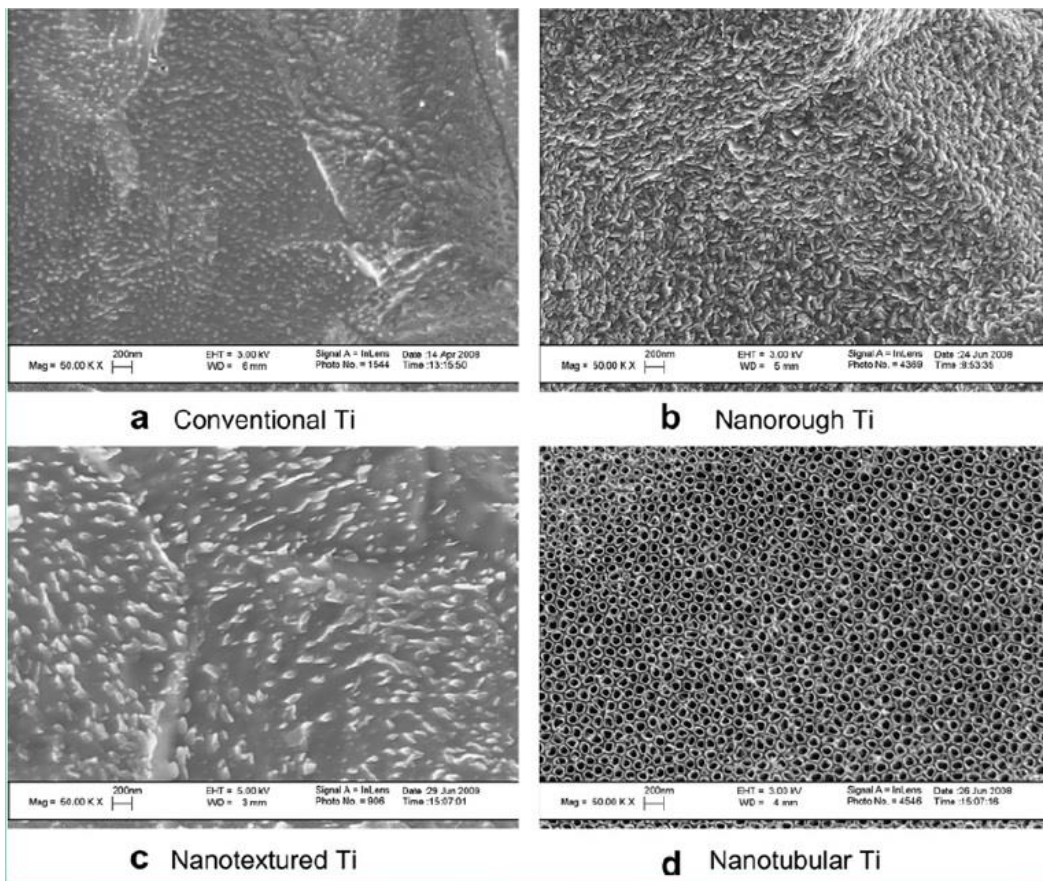


Figure 3.12 SEM micrographs of Ti before and after electron beam evaporation and anodization: (a) conventional Ti as purchased from the vendor; (b) nanorough Ti after electron beam evaporation; (c) nanotextured Ti after anodization for 1 min in 0.5% HF at 20 V; (d) nanotubular Ti after anodization for 10 min in 1.5% HF at 20 V (Puckett, Taylor, Raimondo, & Webster, 2010) [61].

Moreover, it's interesting to notice that another study was focused on nanotubular and nanotextured substrates discovering that the higher number of bacterial colonies were formed on these surfaces, compared with conventional Ti. Probably this is due to fluorine present on nanotubular and nanotextured Ti, that promotes bacterial adhesion (Puckett, Taylor, Raimondo, & Webster, 2010) [61] or more probably this is due to the antibacterial properties of the anatase TiO₂, as shown by some researches (Del Curto et al., 2005) [62] (Yang, Uchida, Kim, Zhang, & Kokubo, 2004) [63].

Ferraris et al. in a study of 2018 realized 3 different grooved patterns (5, 10 and 30 μm) with EB, maintaining average roughness below 0.2 μm, in Titanium surfaces in order to support soft tissues and avoid bacterial adhesion and proliferation as requested in the collar region of transmucosal dental implants and in percutaneous devices. They used gingival human primary fibroblasts (HGFs) to evaluate in vitro cytocompatibility; while cells viability was determined by the metabolic colorimetric alamar blue assay; to evaluate bacterial adhesion it was used Staphylococcus aureus in culture for 2 hours and the viable bacteria number was evaluated by CFU count (colonies forming units) (S. Ferraris et al., 2019) [34].

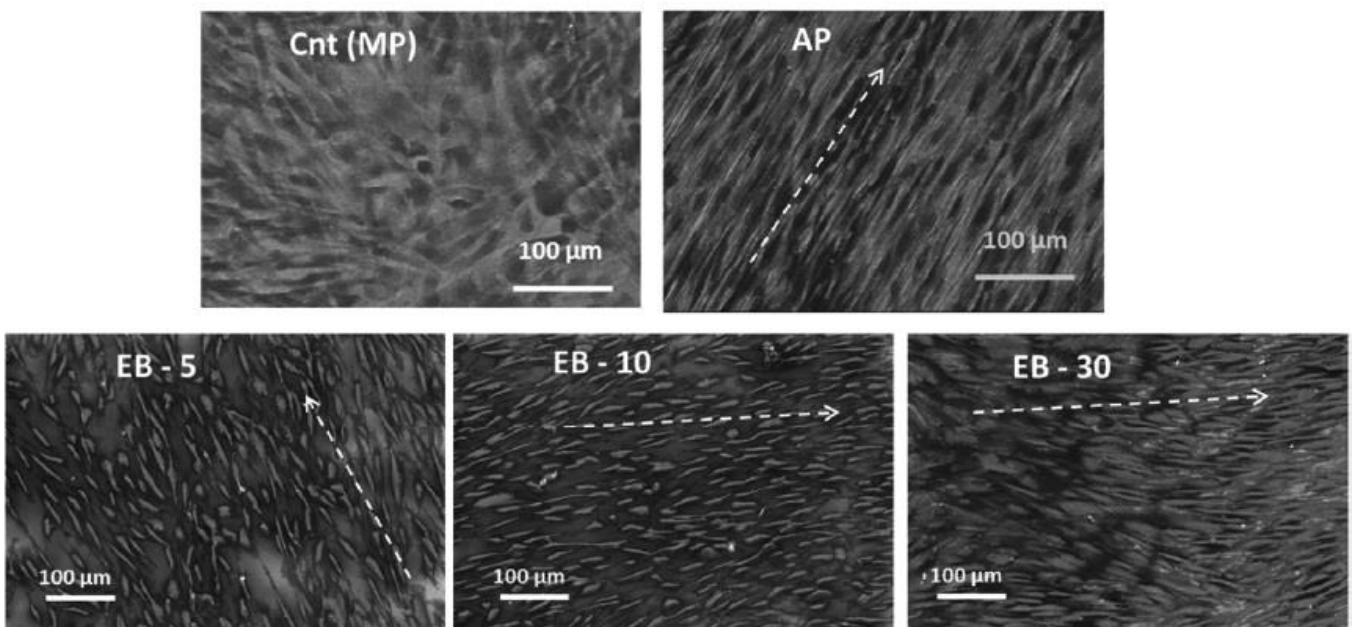


Figure 3.13 Representative FESEM images of reference mirror polished (MP) and mechanically roughened (AP) samples and EB surface structured ones after 48 cell culture. Arrows indicate grooves direction (S. Ferraris et al., 2019) [34]

EB-5 is not completely effective to stimulate fibroblasts alignment, EB-30 is effective in cells orientation, but not so effective for cells alignment (because grooves spacing result larger than what required); EB-10 grooves show a good level of cells alignment and orientation;

Bacterial adhesion is not encouraged by any analyzed surfaces (because of the roughness) and EB surface structuring introduced anti-adhesive properties after 2h culture; EB structuring was not effective in bacteria death, but in decreasing the number of adherent bacteria in the first stage of culture.

In conclusion it's possible to say that a lot of studies did experiments about bacterial adhesion and it's not so easy to define a unique method to apply in order to avoid infections by bacteria. It's possible to summarize all these methods and draw conclusions:

- Puckett et al.: they used conventional and nanorough Titanium surfaces and nanotubular and nanotextured Titanium surfaces. They used electron beam to structure the surfaces and after that they observed a lot of nanometer features on the substrates. Staphylococcus aureus and Staphylococcus epidermidis were observed on these surfaces and they saw a reduction in bacterial adhesion, due to nanometer topographies;
- X. Wang et al: they created nanopores with 150-200nm in diameter on carbon fiber reinforced polyetheretherketone and used HGFs and Streptococcus mutans to evaluate biological behavior. They find that nanoscale surface inhibited bacterial reproduction (Wang et al., 2016) [64];
- Ferraris et al.: in a study of 2017 realized keratin electrospun nanofibers on Ti Grade 2; the nanogrooves (0.1-0.2 μm) were realized by means of keratin nanofibers and were seeded HGFs and Staphylococcus aureus. They noticed an increase in fibroblast adhesion, proliferation and alignment and in the same time of bacterial biofilm adhesion (S. Ferraris et al., 2017) [65];
- Mitik-Dineva et al.: they etched (by hydrofluoric acid) glass surfaces in order to improve roughness in glasses and avoid bacterial adhesion. For this purpose they used different marine bacteria, but they discovered that on etched surfaces the amount of bacteria was increased (Mitik-Dineva et al., 2009) [66];

- Truong et al.: they used commercially pure Titanium (Grade 2) and realized nanometer grain structure (grain size was about 170-200nm). Staphylococcus aureus and Pseudomonas aeruginosa were used to test bacterial adhesion, but they saw at the end of the experiments that Staphylococcus aureus increased his propension to attach on the surface, while for the second bacterium was less high this propension (Truong et al., 2010) [67].

MATERIALS AND METHODS

In this thesis were used three different materials with different features:

- Titanium Grade 2: commercially pure Titanium (α alloy) with density (at 20°C) = 4.51g/cm³, β -transus temperature=913±15°C, Young's modulus=105-110GPa, specific heat=523J/(KgK), ultimate tensile strength=345MPa, Yield strength=250MPa (Ramskogler et al., 2017) [8];
- Ti-6Al-4V: α + β alloy with density (at 20°C) = 4.53g/cm³, β -transus temperature=1020±5°C, Young's modulus=105-116GPa, specific heat=526J/(KgK), ultimate tensile strength=1009-1054MPa, Yield strength=924MPa (Ramskogler et al., 2017) [8];
- Ti-15Mo: β metastable alloy with density (at 20°C) = 5.4g/cm³, β -transus temperature=774±14°C, Young's modulus=78GPa (in β annealed condition) 106 (in α + β annealed condition), specific heat=500J/(KgK), ultimate tensile strength=775-785MPa, Yield strength=715-730MPa (Ramskogler et al., 2017) [8];

SAMPLES POLISHING

There were used Ti-6Al-4V samples and Ti Grade2 samples with dimensions of 15mmx15mm, while Ti-15Mo had different dimensions (10mmx15mm) and all of them had a thickness of 2mm. To polish the samples was used a "Struers Tegramin-30 machine" (Fig. 4.1) with a metallic disk where were pasted about 6-8 samples per time, by means of adhesive tape and glue, close to the edge of the disk and equidistant as much as possible in order to give the same strength per sample.



Figure 4.1 Struers Tegramin-30 polishing machine.



Figure 4.2 Metallic disk with 8 Ti-6Al-4V base material samples.

After positioning the disk in the machine were set the parameters of the machine in order to obtain a mirror polishing on the surface, but before were opened the air and water valves:

- Specimen holder method was selected;
- Force: 15N per 8 sample= 120N;
- Time: 3 minutes for the first 2 steps with 320 and 500 grit size of Silicon Carbide abrasive papers (SiC papers); 5 minutes for P800, P1200, P2400, P4000 SiC abrasive papers;
- Round per minute: 100rpm in co-rotation mode and all the process was performed under water lubrication;



Figure 4.3 Setting parameters of polishing machine.

After every step the abrasive paper was changed, the disk removed, and the samples were washed with water and ethanol and well dried. After these steps were used different chemical solution in order to polish very well every sample and reach a mirror shape; a 1 μ m carbon solution was used for 5 minutes with 120N of force and 100rpm; a MD-chem cloth with OPS Nondry (nondrying colloidal silica suspension for final polishing) and distilled water with the same parameters of the other steps. To remove OPS the samples were polished for other 5 minutes without OPS and only with water.

The same process was performed for TiGrade2 and Ti-15Mo, with the only difference that in this last case (Ti-15Mo) the base material was already quite smooth, and the first paper used was P800.

After polishing the specimens resulted very smooth and the surface was like a mirror (Fig. 4.4).

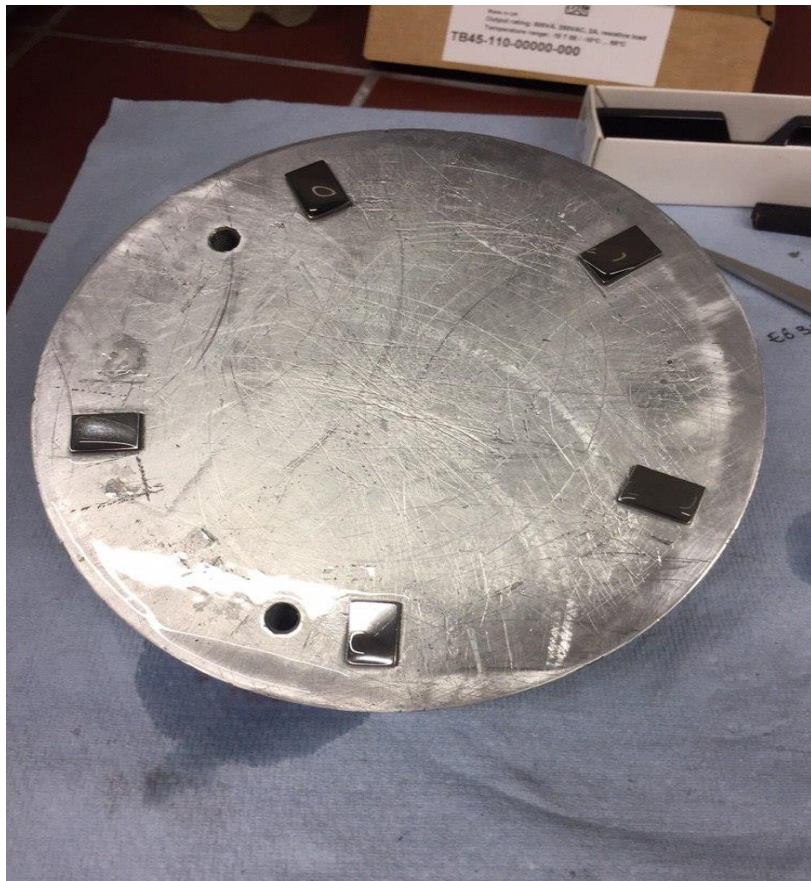


Figure 4.4 Specimens after the last polishing step.

ELECTRON BEAM STRUCTURING

Electron Beam Welding machine was used to realize grooves on the surface of the samples and produce surface microstructures; the machine used was the “Pro-beam Kammeranlage K14” (Fig. 4.5).



Figure 4.5 Pro-beam Kammeranlage K14.



Figure 4.6 Sample holder with Ti-6Al-4V samples.

It was used a sample holder for the specimens (Fig. 4.6), and it was placed in the vacuum chamber (Fig. 4.7).

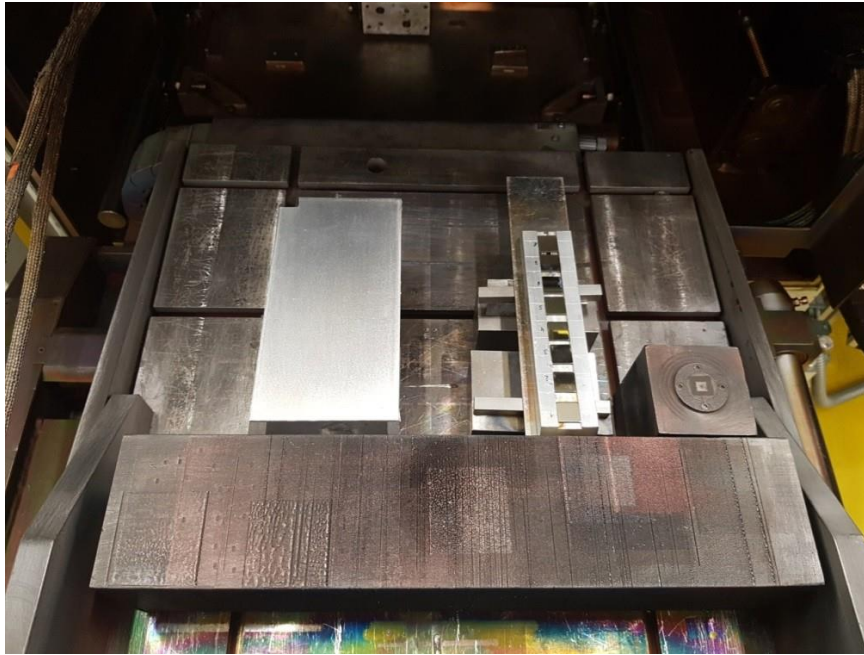


Figure 4.7 Vacuum chamber of the electron beam welding machine.

There were used different parameters on different Titanium alloys, they are showed in Tab. 4.1.

Type of alloy	Distance between lines [μm]	HV (Voltage) [kV]	I (Current) [mA]	Velocity [mm/s]	PVZL	Total time [s]	Vacuum Value [mbar]
Ti-6Al-4V	30	150	1,3	853	4687	3,871	2,0 E-4
	10	150	1,3	3333	1200	4,4325	2,0 E-4
Ti-15Mo	30	150	0,8	853	4687	3,871	2,0 E-4
	10	150	0,8	3333	1200	4,4325	2,0 E-4
TiGrade2	30	150	0,8	853	4687	3,871	2,0 E-4
	10	150	0,8	3333	1200	4,4325	2,0 E-4

Tab. 4.1 Electron beam parameters.

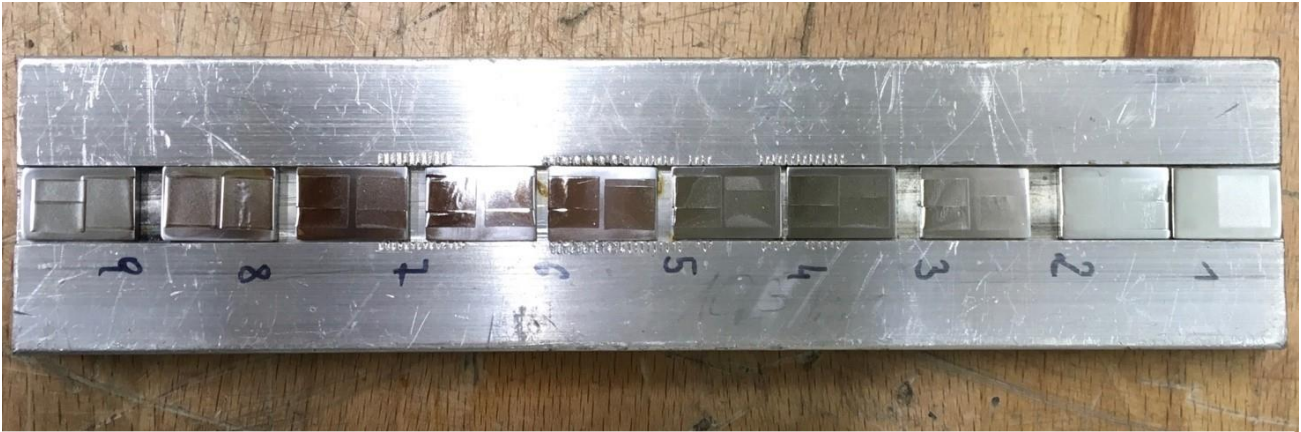


Figure 4.8 Sample holder with structured specimens, after electron beam process.

The machine is able to focus an electron beam with the desired parameters, so we can choose the speed and the power, by the current. The chamber is in vacuum in order to improve the process and accelerate electrons by an electric field, while the orbit is controlled by a magnetic field. The heat required to melt the material and create the microstructure on it is obtained by the kinetic energy of shooting of electrons to the material.

The machine is composed by a tungsten cathode and an anode; the free electrons are produced when the cathode is heated up to a certain temperature, while is generated a high voltage between anode and cathode that forces the free electrons emission towards the anode (Ramskogler et al., 2017) [8].

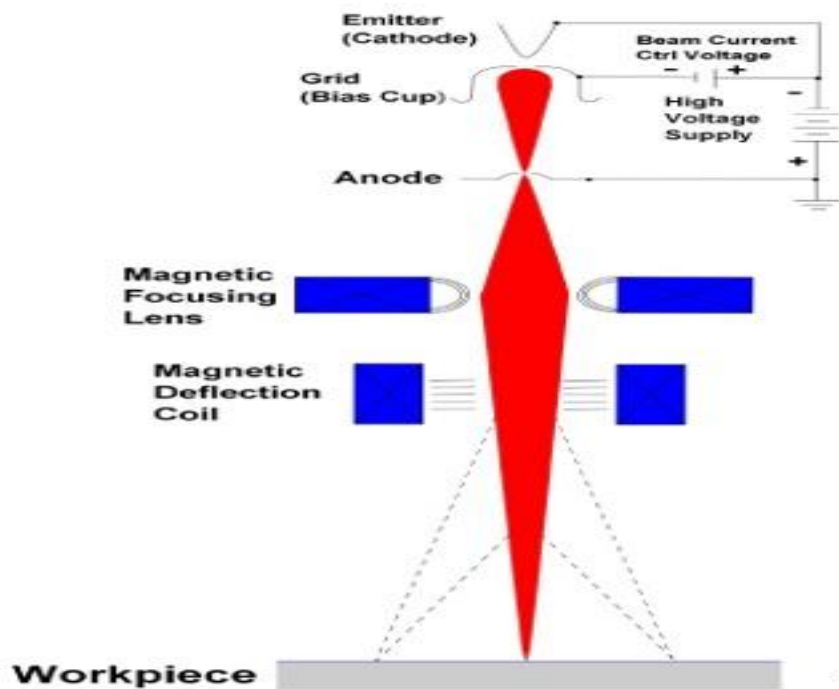


Figure 4.9 Electron beam welding technique.

The high voltage value (HV) is proportional to the electron's speed, while the magnetic field influences the electrons by means of Lorentz force:

$$\vec{F}_L = q \cdot (\vec{E} + \vec{v} \times \vec{B})$$

Where q is the electric charge; E is the external electric field, B is the magnetic field and v is the instantaneous velocity.

The electrons in the high-speed focused beam affect the materials causing heating, melting and local evaporation, that become the so called “keyhole”, that is generating by moving electron beam and by the deposit of material in the opposite direction of welding one; this material solidifies at the backside of the beam resulting in a protrusion at the beginning and an intrusion at the end of the weldment (Nightingale, 1989) [68].

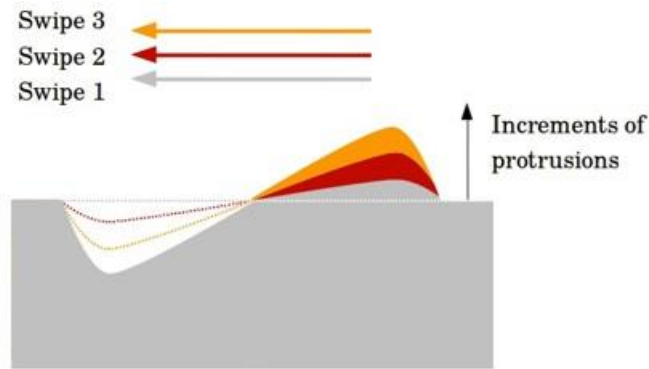


Figure 4.10 Effect of the repeated beam swipes.

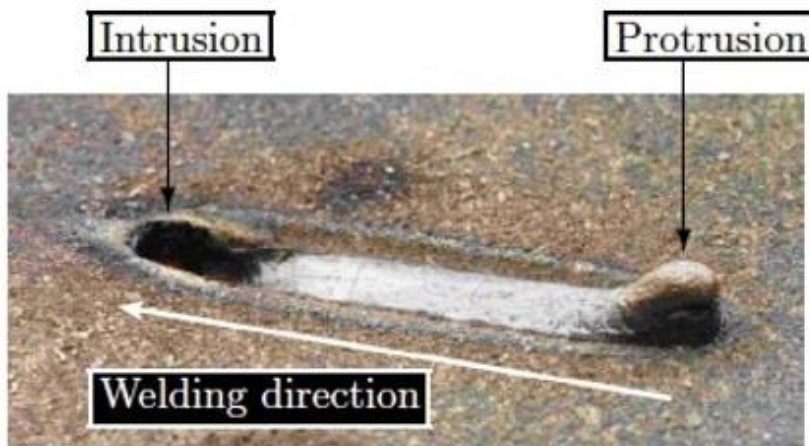


Figure 4.11 Effect of the protrusion and intrusion by a single swipe (B. Dance and A. Buxton, 2007) [69].

To create the microstructure on the surface by means of electron beam we have to move the beam in the same path repeatedly, creating in this way an increment of protrusion height and an increment in intrusion depth (Fig. 4.10).

It's also possible to create different figures and geometries on the material surface, modifying Matlab parameters and the electron beam path. In this thesis were realized grooves spaced each other of 10 and 30 μ m for a total structured area of 7x7mm in order to obtain two structured areas for each sample and evaluate the effect of the grooves on bacterial adhesion and if the different spacing between them could influence the effect on bacteria.

CUTTING SAMPLES

As told before it's possible to obtain two different structured areas for each sample, so, for this reason we need to cut the samples in the middle in order to obtain two structured surfaces after the cutting. To cut the samples was used "Struers Accutom-10" machine and the cut samples had dimensions of about 7x15mm (for Ti-6Al-4V and TiGrade2) and 7x10mm (for Ti-15Mo). Was used also a cutting plate (carbide cut-off wheel 10S15 with HV=70-400) for soft non-ferrous metals.



Figure 4.12 Struers Accutom-10 machine in work phase with the glass closed.

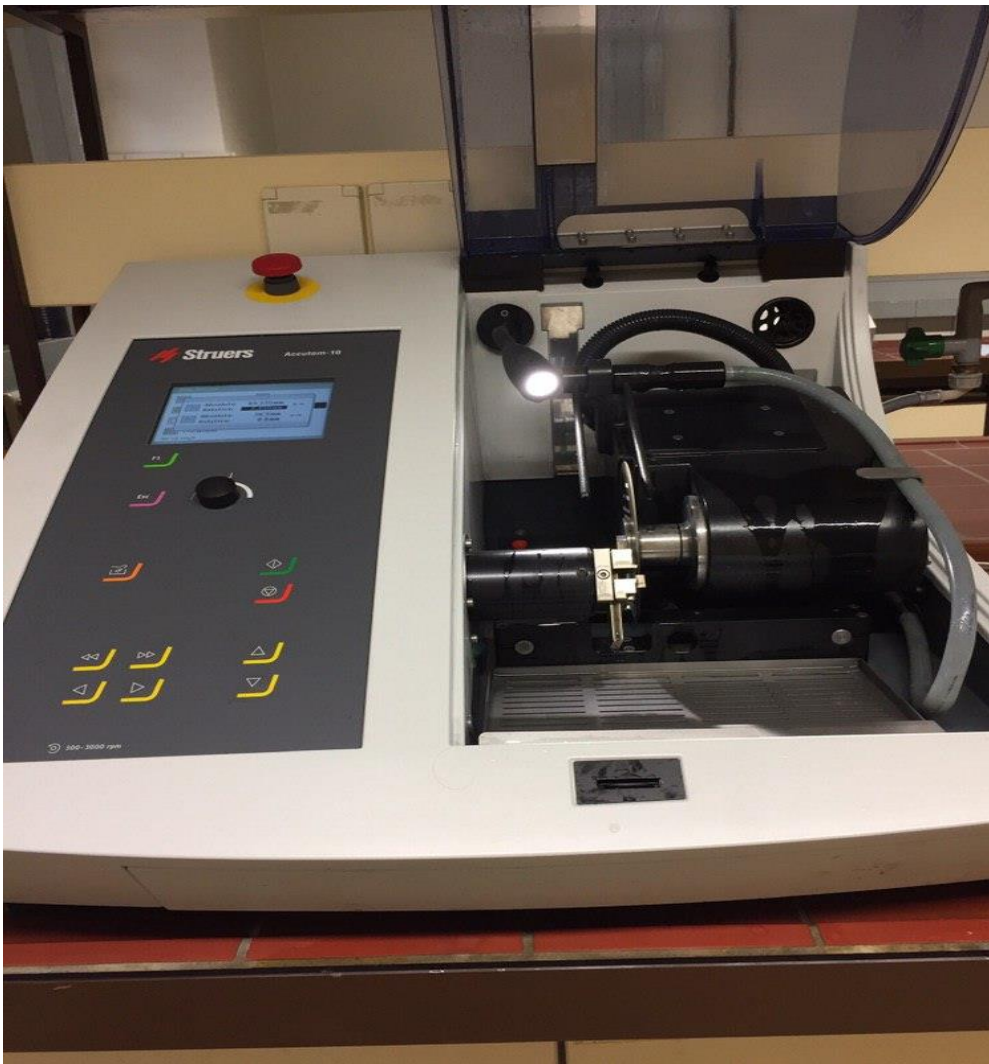


Figure 4.12 Struers Accutom-10 machine in detail.



Figure 4.13 Ti-15Mo cut samples.

After the cutting, the samples were washed very well with water and ethanol in order to clean them and remove any kind of carbide residual from the cutting plate.

HEAT TREATMENTS

After cutting the samples, it was used the Dilatometer, an instrument that measures volume changes caused by heat treatment. The dilatometer presents a vacuum chamber under pressure ($5 \cdot 10^{-4}$ mbar) in an inert atmosphere after cleaning of chamber by Argon flooding to avoid samples oxidation, where were inserted the samples. First a thermocouple was welded in the middle of the sample, very close to the edge in order to don't influence the rest of the surface; after welding the thermocouple was assembled in the chamber and the sample was fixed in the middle of the coil generating heat. The chamber was closed and the gas (Argon) starts to flow until was reached the right pressure, then the experiment was carried out. Several experiments were carried out on Ti-6Al-4V and Ti-15Mo.

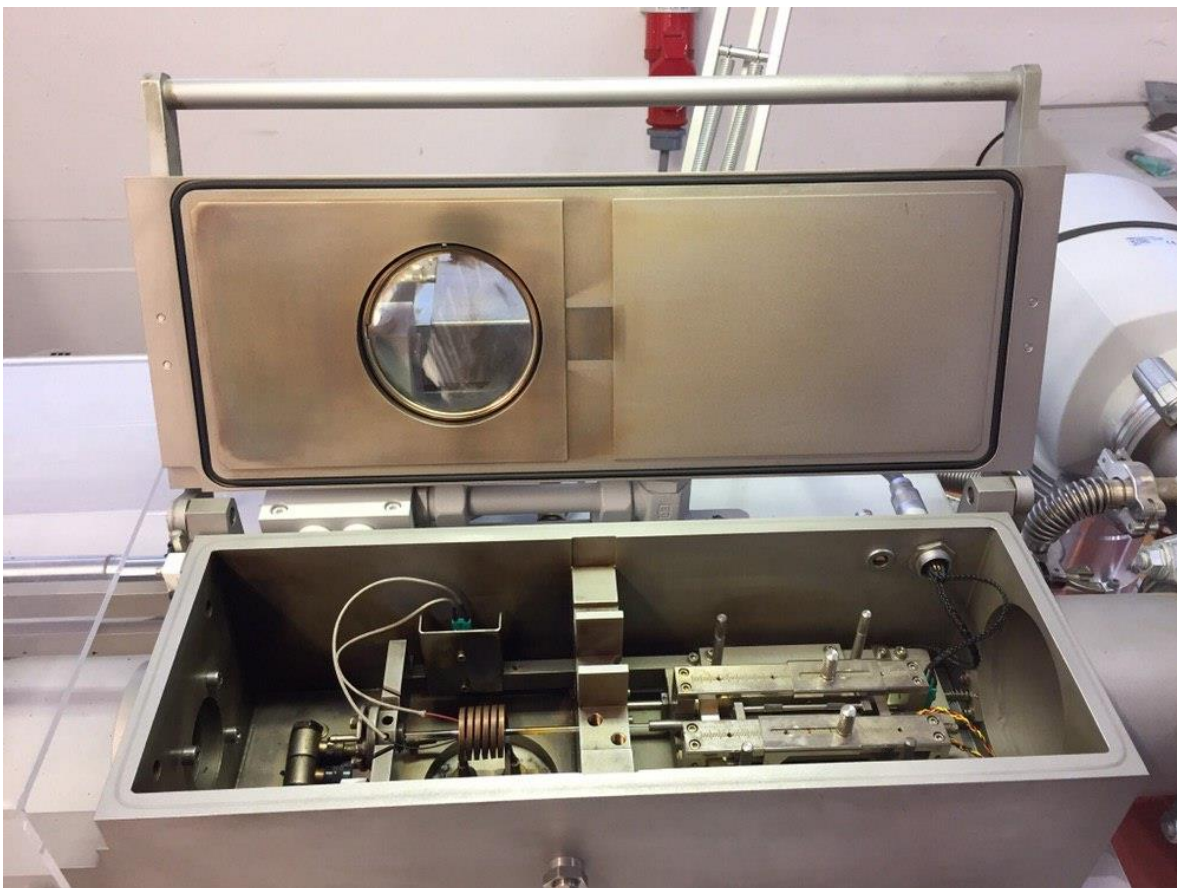


Figure 4.14 Dilatometer.

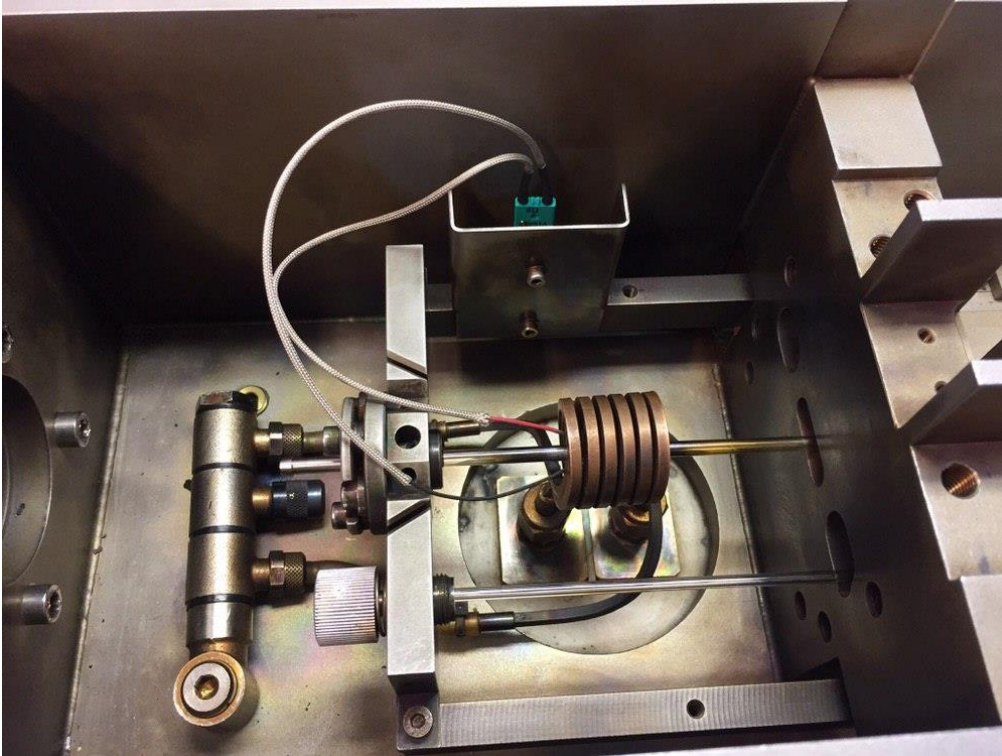


Figure 4.14 Thermocouple welded on the sample in the coil.

1. Ti-6Al-4V:

- Argon Quenching in beta phase (1050°C);
- Heating rate: 300K/min;
- Temperature: 950°C with holding time: 4 hours;
- Cooling rate: 1K/min up to 850°C; 200K/min up to room temperature;

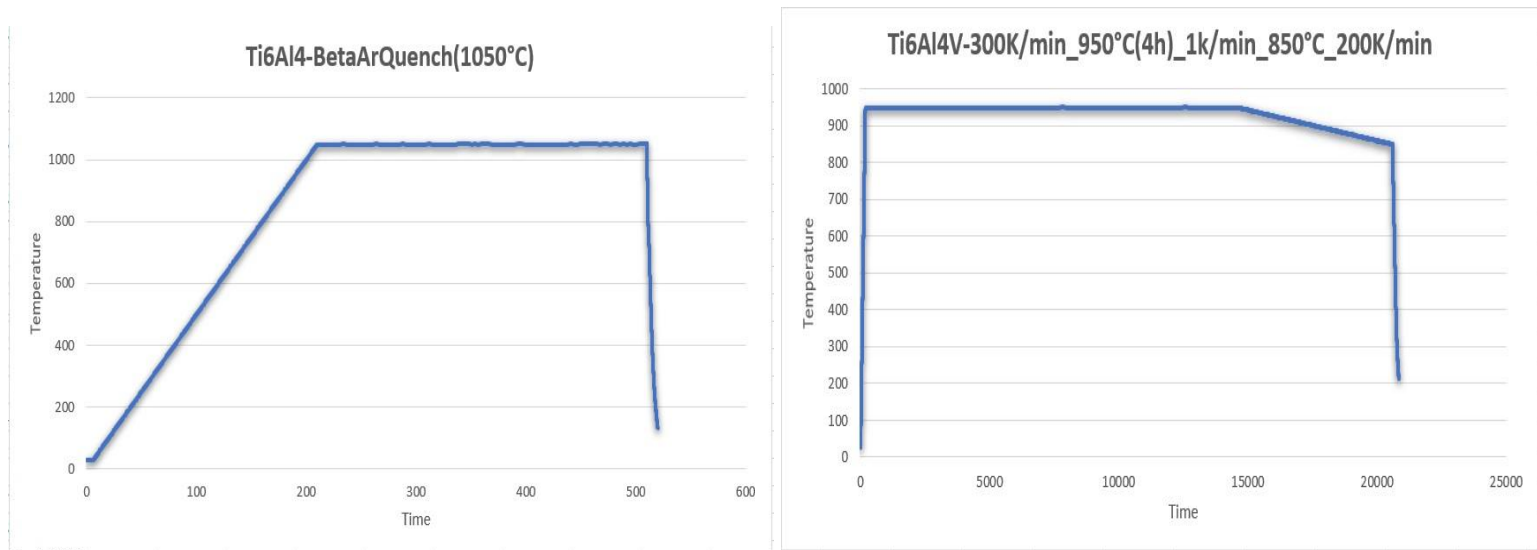


Figure 4.15 Ti-6Al-4V first heat treatment.

This HT was performed in order to convert martensite in lamellar shaping in the base material and rapid quenching leads to a very fine needle-like martensitic microstructure.

- Argon Quenching in beta phase (1050°C);
- Heating rate: 300K/min;
- Temperature: 800°C with holding time: 2 hours;
- Cooling rate: 200K/min;

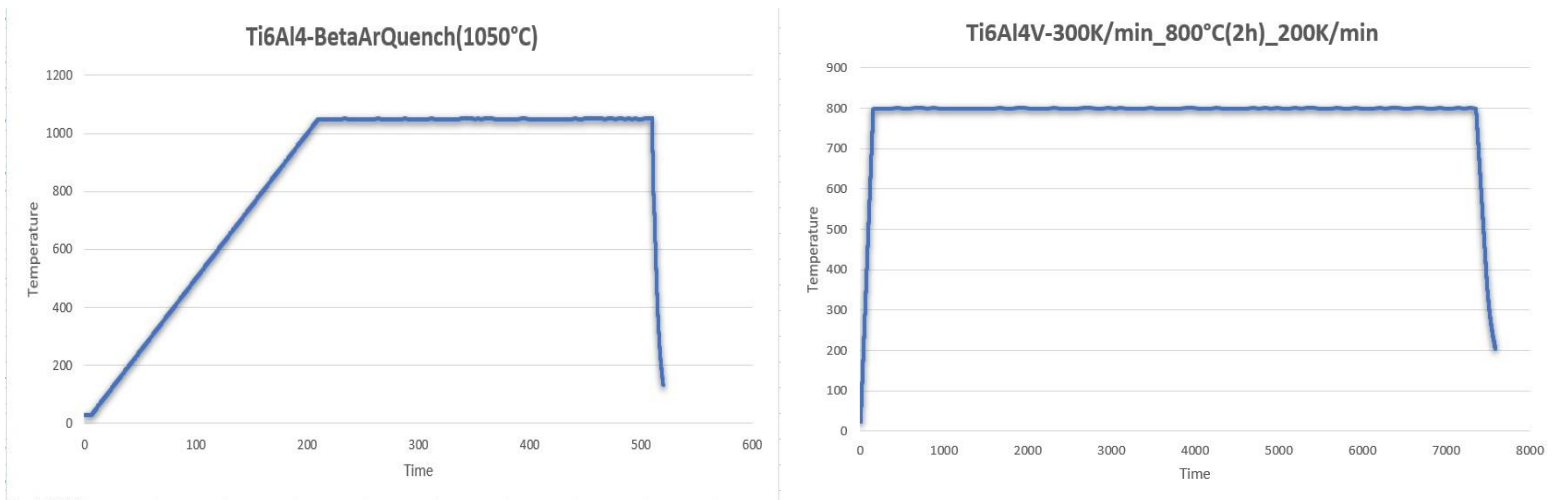


Figure 4.15 Ti-6Al-4V second heat treatment.

- Heating rate: 300K/min;
- Temperature: 1030°C with holding time: 5 minutes;
- Cooling rate: 20K/min (slow cooling rate);

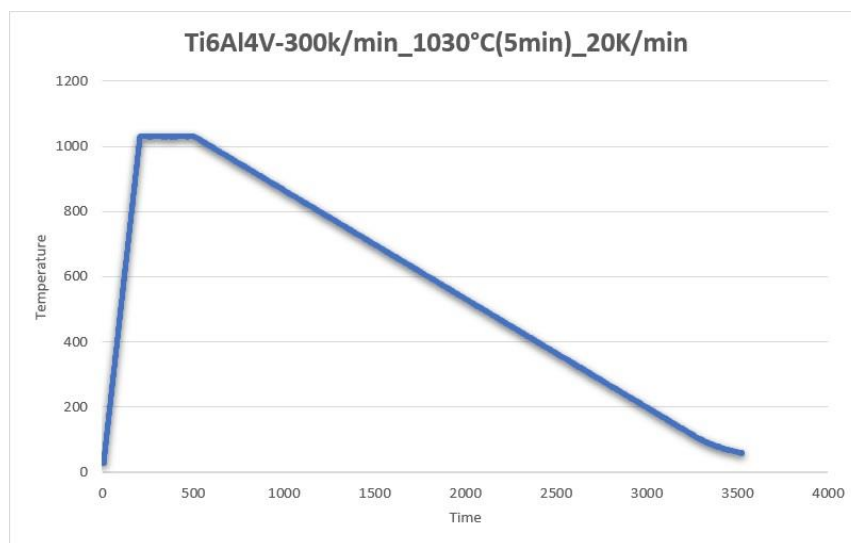


Figure 4.15 Ti-6Al-4V third heat treatment.

The HT was performed above beta transus temperature in order to see beta phase on the surface after the heating. The slow cooling rate allows the formation of packaging of lamellae in different directions, evident in the cross section of the material.

- Heating rate: 300K/min;
- Temperature: 1030°C with holding time: 5 minutes;
- Cooling rate: 300K/min (fast cooling rate);

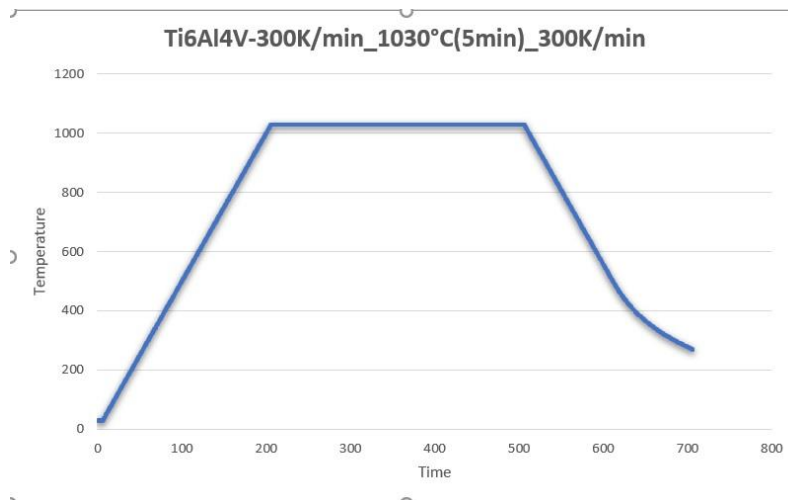


Figure 4.16 Ti-6Al-4V fourth heat treatment.

The HT was performed above beta transus temperature in order to see beta phase on the surface after the heating. The aim of this treatment is to form alpha lamellae on the sample surface by fast cooling, because a faster cooling rate could generate finer lamellae.

- Heating rate: 300K/min;
- Temperature: 800°C with holding time: 2 hours;
- Cooling rate: 200K/min (fast cooling rate);

The HT was performed below beta transus temperature in order to stabilize the martensite microstructure. The aim of this treatment is to form alpha lamellae on the sample surface by fast cooling, because a faster cooling rate could generate finer lamellar shaping

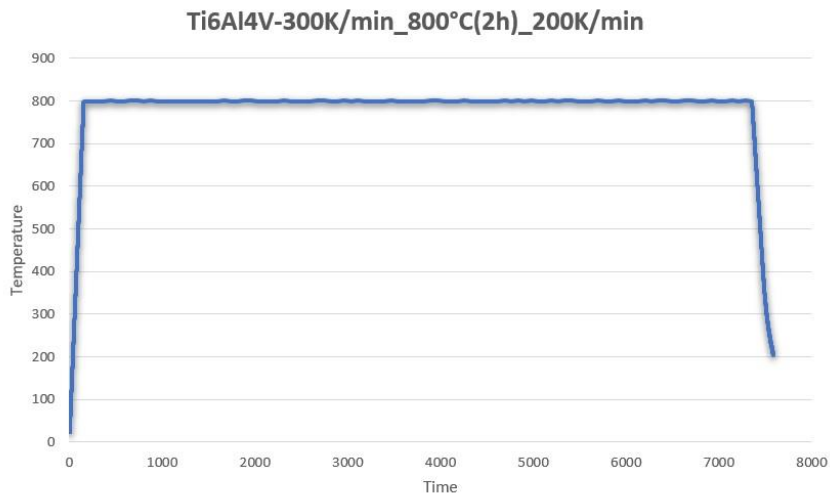


Figure 4.17 Ti-6Al-4V fifth heat treatment.

- Heating rate: 300K/min;
- Temperature: 950°C with holding time: 4 hours;
- Cooling rate: 1K/min up to 850°C; 200K/min up to room temperature

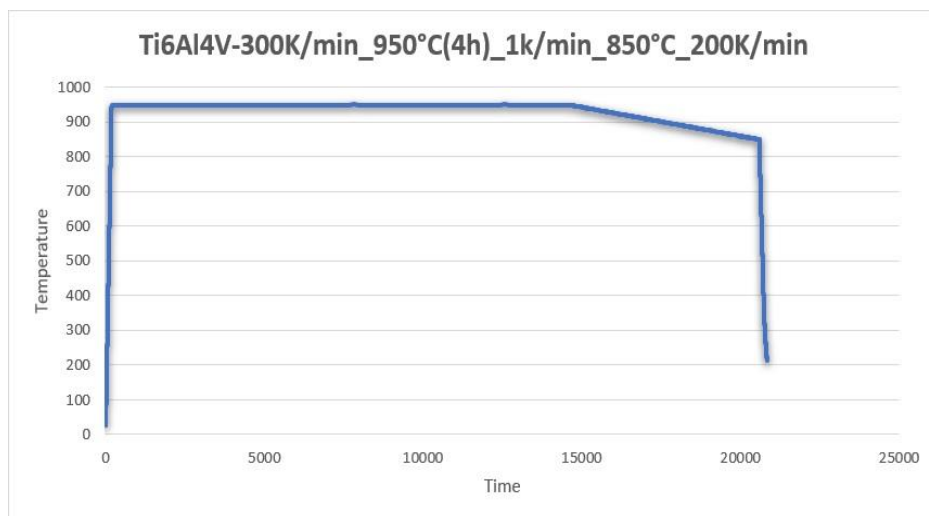


Figure 4.18 Ti-6Al-4V sixth heat treatment.

The HT was performed below beta transus temperature but for an higher holding time in order to evaluate the effect of the recrystallization on the martensite.

2. Ti-15Mo:

- Argon Quenching in beta phase (850°C);
- Heating rate: 300K/min;
- Temperature: 550°C with holding time: 1 hours;
- Cooling rate: 200K/min;

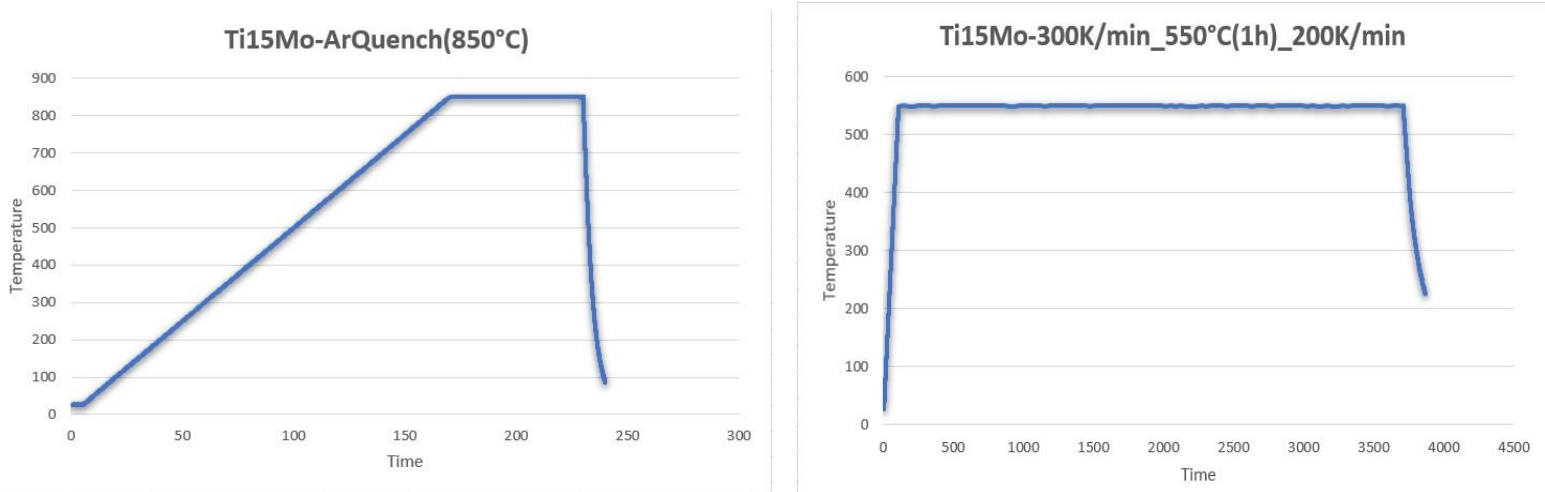


Figure 4.19 Ti-15Mo first heat treatment.

- Heating rate: 300K/min;
- Temperature: 850°C with holding time: 5 min;
- Cooling rate: 20K/min (slow cooling rate);

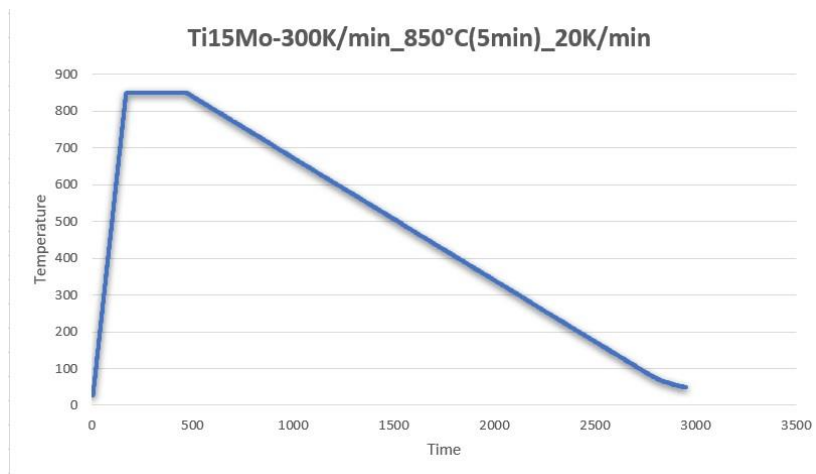


Figure 4.20 Ti-15Mo second heat treatment.

- Heating rate: 300K/min;
- Temperature: 650°C with holding time: 4 hours;
- Cooling rate: 200K/min;

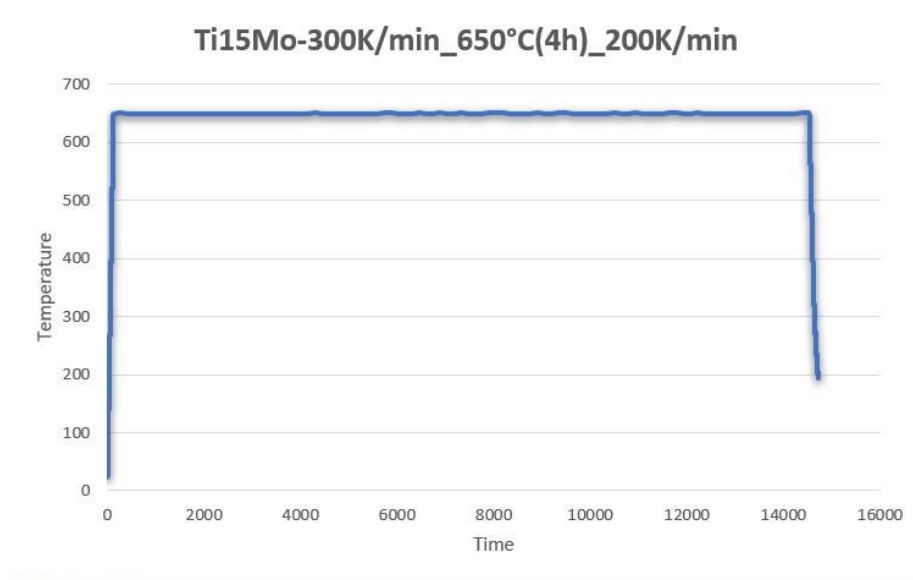


Figure 4.21 Ti-15Mo third heat treatment.

The HT was performed to evaluate the influence of the heating rate and temperature on the precipitation of α in the β matrix.

- Heating rate: 300K/min;
- Temperature: 650°C with holding time: 1 hours;
- Cooling rate: 200K/min;

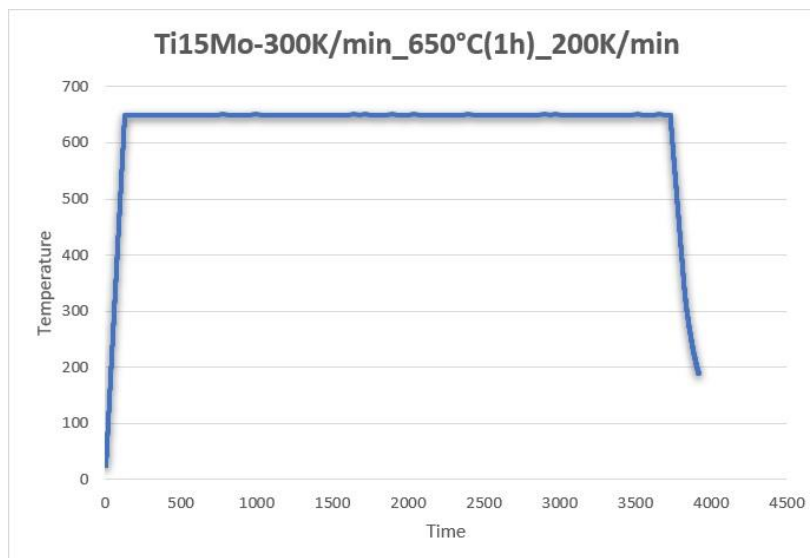


Figure 4.21 Ti-15Mo fourth heat treatment.

- Heating rate: 300K/min;
- Temperature: 550°C with holding time: 1 hours;
- Cooling rate: 200K/min;

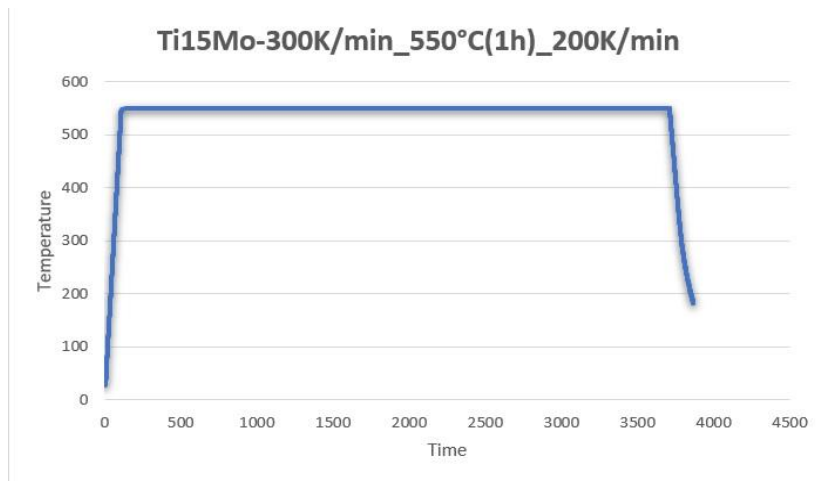


Figure 4.22 Ti-15Mo fifth heat treatment.

METALLOGRAPHY

Some of the total samples were used to analyze the cross section and see the differences between structured and base material in order to study the transition area between them. To do this was used “Struers citopress-30” mounting press with a thermosetting resin (PolyFast powder) hot mounted with the specimens. The parameters used were:

- Amount of PolyFast: 20ml;
- Temperature: 180°C;
- Time: 3 minutes for heating and 1.5 minutes for cooling;
- Pressure: 250bar;



Figure 4.23 Samples mounted with PolyFast powder.



Figure 4.24 Struers CitoPress-30.

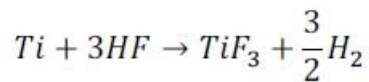
After mounting, the samples were fixed in a sample holder (another kind of metallic disk) for grinding and polishing in order to recognize clearly the surface.

The polishing protocol was almost the same, but this time we started from P520 for 5 minutes in single specimen mode with 15 N per sample and 150rpm in co-rotation. The same was done for P800, P1200, P4000. Then it was used Diamond 9 μ m and Diamond 1 μ m cloth with the appropriate solution and finally OPS Nondry solution for a variable time, depending on the observation, in fact if we wanted to observe the cross section by light optical microscope (LOM) it was polished for 5 minutes, else if we wanted to observe the surface by scanning electron microscope (SEM) it was polished for 10 minutes.

ETCHING

After metallography process and polishing it was used a chemical composition based on Hydrofluoric acid (HF) in order to make more visible at microscope the nanostructure of the Ti-6Al-4V and Ti-15Mo samples. The samples were etched selectively in order to modify microstructural features, such as crystal structure, composition and stress.

The etching reaction is:



Were tested different concentration of chemical solution until optimal surface treatment was achieved. The first try was less aggressive and was composed by:

- HF: 2ml;
- Nitric acid: 4ml;
- Distilled water: 94ml;

The second one was more aggressive and composed by:

- HF: 3ml;
- Nitric acid: 6ml;
- Distilled water: 91ml;

Ti-6Al-4V EB structured was immersed in the more aggressive solution for 90s while Ti-15Mo was immersed in the solution just for 50s.

FINAL POLISHING

A final polishing was carried out on EB30 Ti-6Al-4V and EB30 Ti-15Mo in order to remove the grooves on the surface, but maintaining the microstructure, due to electron beam process. This process was done in order to see how the microstructure can influence bacterial behavior in comparison with the grooves. The final polishing protocol provided:

- Force: 10N per sample in single specimen mode;
- Round per minute: 100rpm in co-rotation mode;
- Time: 2 minutes for P2000 SiC abrasive paper, 1 minute for P4000, 10 minutes for Diamond 1 μ m cloth with Nap DiaDuo-2 solution and 10 minutes for 0.25 μ m carbon paste;

The OPS Nondry with MD-Chem cloth has not been used in order to avoid solution residual on the surface of the material and compromise in this way bacterial behavior. Finally the samples were washed in water and ethanol and well dried.

SAMPLE PREPARATION FOR BIOLOGICAL TESTS

Some Ti-6Al-4V and Ti-15Mo samples were prepared and brought to Politecnico di Torino in order to do biological tests with bacteria.

1. Ti-6Al-4V (35 samples in total):

- 5 BM: base material polished up to 0.25 μm paste with the same protocol shown before;
- 5 EB10: electron beam structuring with 10 μm spacing between the lines, without any polishing;
- 5 EB30 + POL: electron beam structuring with 30 μm spacing between the lines, with final polishing in order to make the grooves disappear;
- 5 EB10 + HT1: electron beam structuring with 10 μm spacing between the lines, with heat treatment 1 (950°C_4h_1K/min_850°C);
- 5 EB30 + HT1 + POL: electron beam structuring with 30 μm spacing between the lines, with heat treatment 1 (950°C_4h_1K/min_850°C), with final polishing in order to make the grooves disappear;
- 5 EB10 + HT2: electron beam structuring with 10 μm spacing between the lines, with heat treatment 2 (1030°C_5min_300K/min);
- 5 EB30 + HT2 + POL: electron beam structuring with 30 μm spacing between the lines, with heat treatment 2 (1030°C_5min_300K/min), with final polishing in order to make the grooves disappear;

2. Ti-15Mo (25 samples in total):

- 5 BM: base material polished up to 0.25 μm paste with the same protocol shown before;
- 5 EB10: electron beam structuring with 10 μm spacing between the lines, without any polishing;
- 5 EB30 + POL: electron beam structuring with 30 μm spacing between the lines, with final polishing in order to make the grooves disappear;
- 5 EB10 + HT: electron beam structuring with 10 μm spacing between the lines, with heat treatment (850°C_5min_20K/min);
- 5 EB30 + HT + POL: electron beam structuring with 30 μm spacing between the lines, with heat treatment (850°C_5min_20K/min), with final polishing in order to make the grooves disappear;

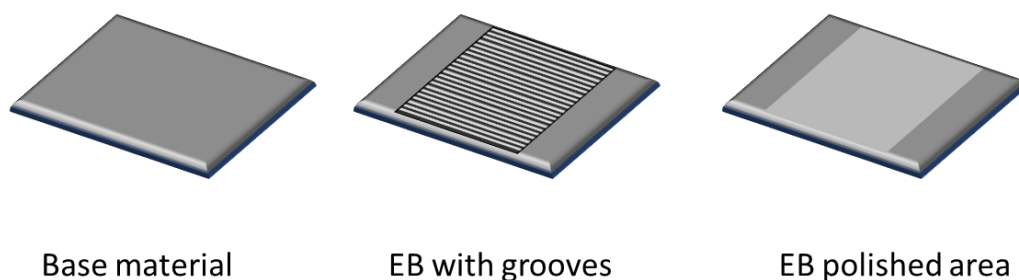


Figure 4.25 Different conditions of the samples. 1-Base material; 2-Electron Beam structured; 3-Electron Beam structured and final polishing in order to make the grooves disappear.

The samples were brought to Turin and to eliminate any contamination during the travel another cleaning process was achieved in Turin.

First, all the process was performed under fume hood and there, the samples were immersed in acetone with the structured part upwards and the base material in contact with the beaker bottom. After this the beakers with the samples and acetone were covered with aluminum foils and inserted in the ultrasonic bath for 5 minutes. After this period the samples were immersed in other beakers with ultrapure water under the fume hood and then reinserted in the ultrasonic bath for other 10 minutes. This last step was repeated with clean ultrapure water. After drying the samples were inserted in Petri dishes.

MATERIAL'S CHARACTERIZATION METHODS

Scanning Electron Microscope (SEM)

A scanning electron microscope is a type of microscope that scans a focused electron beam over a surface in order to produce an image and this one is the result of the interaction between the primary electrons in the beam and the sample; it was developed to improve the resolution of the others microscopes, in facts it can reach a resolution better than 1nm, and to overcome the issue of wavelength in light optical microscopes. It's composed by an electronic source, that generates the beam, an anode, that accelerates that beam and a series of electromagnetic lenses and finally an objective lens, which can deflect the beam (Stokes, 2008) [70]. It could be composed also by an Energy Dispersive Spectroscopy (EDS) to detect the chemical composition of the materials.

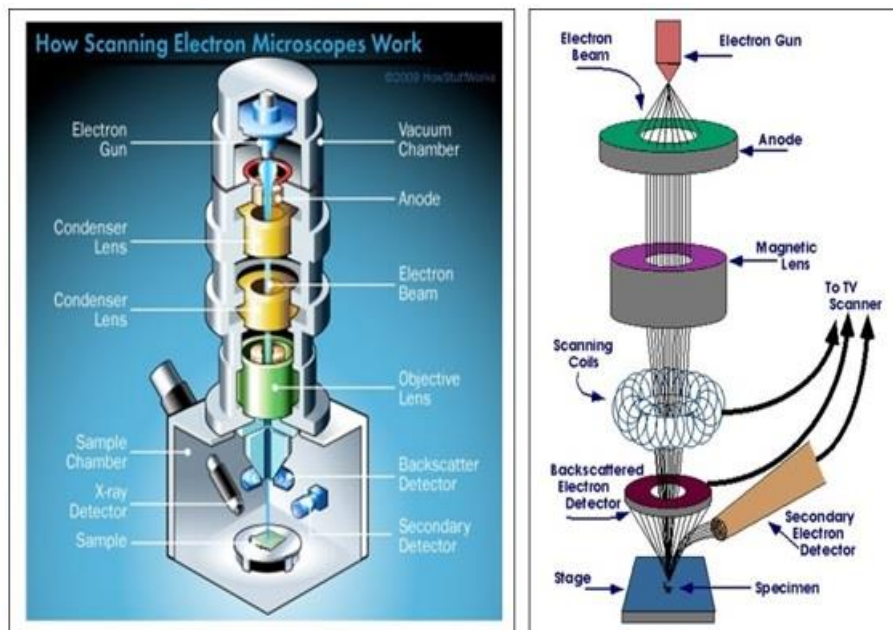


Figure 5.1 Scanning electron microscope [71].

The sample is mounted on a stage in a high vacuum chamber, while the electron beam penetrates the sample for few microns to create the image and allow that this one is displayed on the screen of a computer.

SEM can be used in two different mode:

- SE (secondary electrons): uses secondary electrons that can be detected;
- BSE (backscattered electrons): the backscattered electrons occur from elastic collisions between electrons and atoms, collisions that induce electron trajectory changes;

Field Emission Scanning Electron Microscope (FESEM)

The Field Emission Scanning Electron Microscope works like the scanning electron microscope, but it can reach higher resolution and energy range. To produce the electron beam that hit the sample in this case are emitted primary electrons by the source and then accelerated by an electrical field gradient; this beam is focused and deflected by some lenses. From this process are emitted secondary electrons with an angle and a velocity related to the surface structure of the sample and they are caught by a detector, which produces an electronic signal, amplified and transformed in a picture in the computer screen. In biological field FESEM is used to see small biological particles and organelles, such as DNA or cell components [72].

Light Optical Microscope (LOM)

The light optical microscope uses the visible light and a system of lenses to magnify the images. It is composed by an ocular lens, that is a cylinder with two lenses, where it's possible to see, by eyes, the images. It's also possible to change the objective lenses in order to change the magnification from 10 to 100 times. The sample, even in this case, is positioned on a stage and is illuminated by a light in a hole at the center of the stage [73].

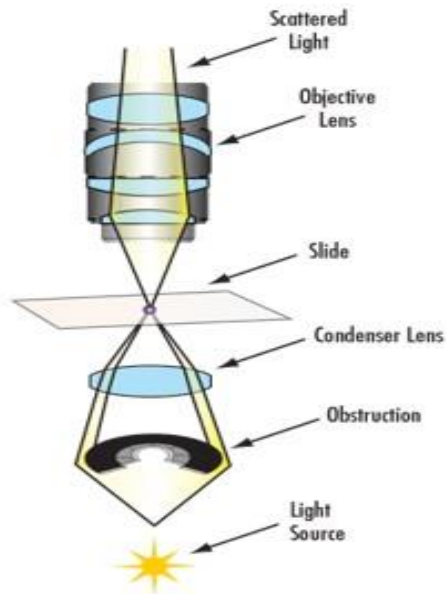


Figure 5.2 Light optical microscope [72].

WETTABILITY TEST

The wettability test was performed at Politecnico di Torino by means of optical microscope Kruss DSA 100 in order to calculate the contact angle between the liquid (pure water) and the material. The equipment consists of a support plate for the sample, on which a liquid drop is placed through a micrometric pipette, a light source and a telescope connected to the software.



Figure 5.3 Optical microscope Kruss DSA 100.

The contact angle is the angle formed by a liquid where the liquid, the gas and the solid intersect each other. The balance of these three phases is described by Young equation:

$$\gamma_{SV} = \gamma_{SL} + \gamma_{LV} \cos \theta_Y$$

Where θ is the contact angle, while γ_{sv} , γ_{sl} and γ_{lv} are the interfacial tensions between solid and gas, solid and liquid, liquid and gas respectively.

There are different possibilities:

- Contact angle $< 90^\circ$: the drop spreads on the surface and this one is hydrophilic;
- Contact angle $> 90^\circ$: the drop has a round shape and doesn't spread around; the surface is hydrophobic [74].

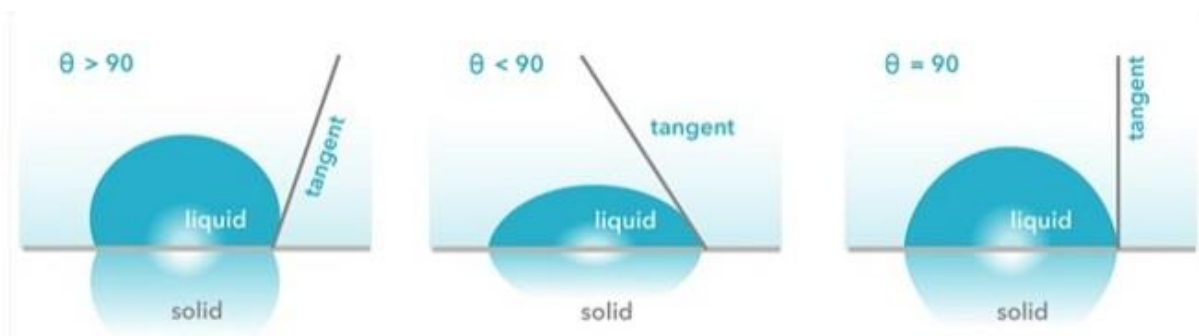


Figure 5.4 Different contact angles [75].

It was used pure water, placed on the surface of the material by a micrometric pipette, in a drop of $5\mu\text{l}$. Two drops were placed for each sample and were tested three samples for each type of specimen:

- Ti-6Al-4V BM;
- Ti-6Al-4V EB 10 and Ti-6Al-4V EB 30 + POL;
- Ti-6Al-4V EB 10 + HT (950°C-4h-850°C) and Ti-6Al-4V EB 30 + HT + POL;
- Ti-6Al-4V EB 10 + HT (1030°C) and Ti-6Al-4V EB 30 + HT + POL;
- Ti-15Mo BM;
- Ti-15Mo EB 10 and Ti-15Mo EB 30 + POL;
- Ti-15Mo EB 10 + HT (850°C) and Ti-15Mo EB 30 + HT + POL;

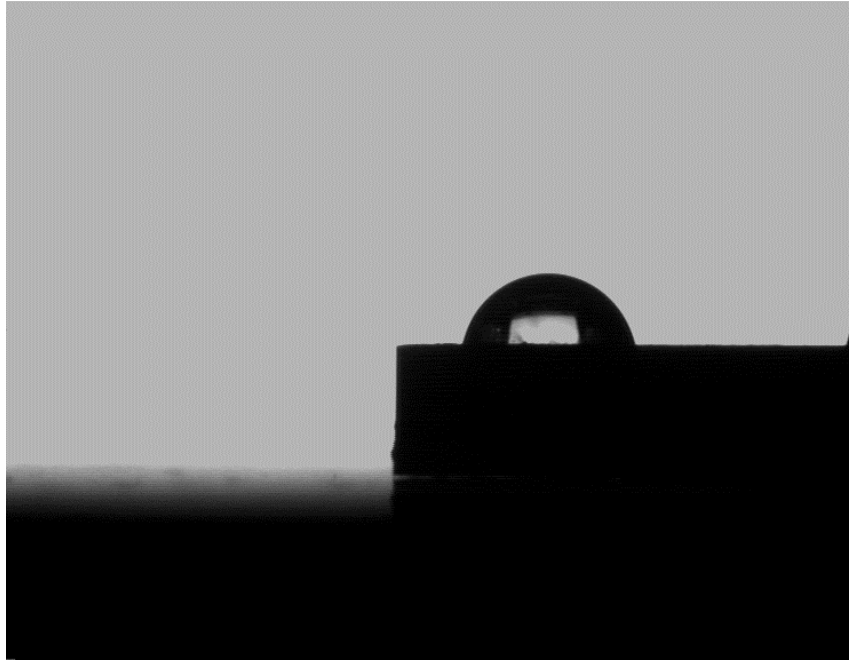


Figure 5.5 Example of a drop on Ti-15Mo surface.

SURFACE ROUGHNESS

Surface roughness it's a very important feature to study bacteria behavior, in facts in literature it possible to find, as told before, the threshold value of $0.2\mu\text{m}$, below which bacterial adhesion decreases. We can have different roughness parameters, but the most used is the average roughness Ra , defined as the arithmetic average of the absolute distances of the roughness profile to the mean line.

$$Ra = \frac{1}{L} \int_0^L |y(x)| dx$$

This roughness value is necessary, but not sufficient to completely define the morphological features of the surface, so we have to define Rt (maximum height of the profile), Rz (average distance between 5 highest peaks 5 lowest valleys) and Rq (the square mean of the deviation of the profile points from the midline), too. Rq is defined as:

$$Rq = \frac{1}{L} \int_0^L |y^2(x)| dx$$

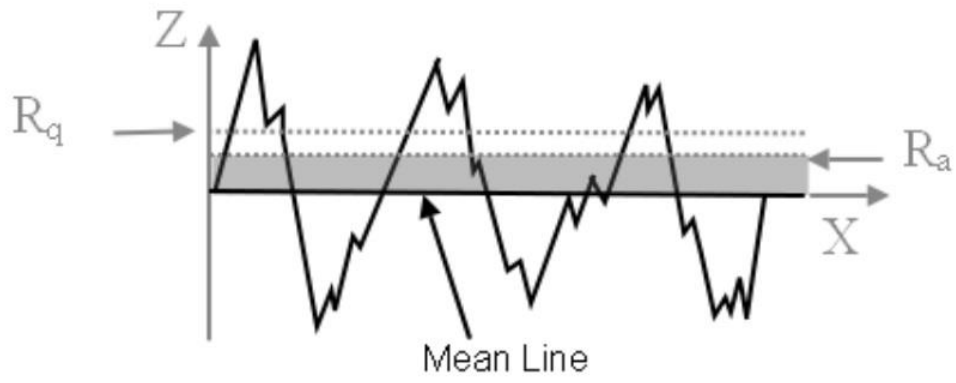


Figure 5.6 Roughness parameters [76].

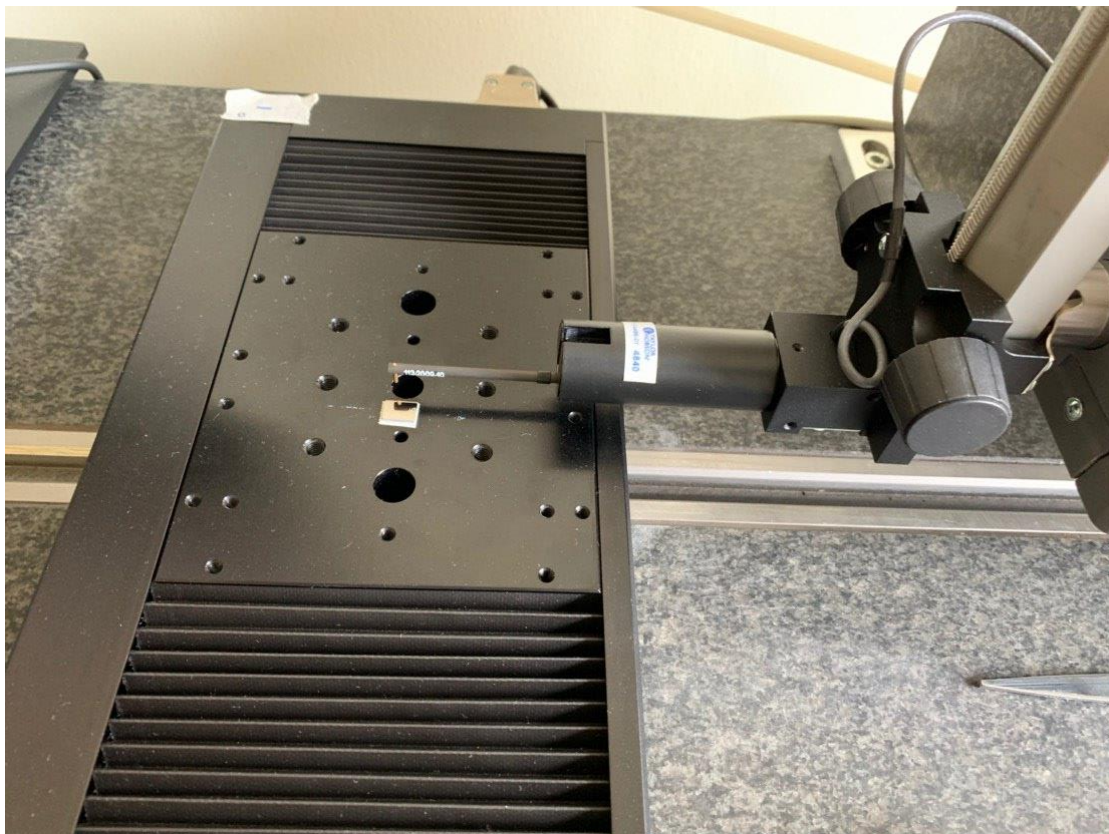


Figure 5.7

For this purpose, it was used the profilometer Intra Touch-Taylor Hobson (Fig. 5.7) and the measurements were performed one time per each sample, and were used 3 samples for every kind of material:

- Ti-6Al-4V BM;
- Ti-6Al-4V EB 10 and Ti-6Al-4V EB 30 + POL;
- Ti-6Al-4V EB 10 + HT (950°C-4h-850°C) and Ti-6Al-4V EB 30 + HT + POL;
- Ti-6Al-4V EB 10 + HT (1030°C) and Ti-6Al-4V EB 30 + HT + POL;
- Ti-15Mo BM;
- Ti-15Mo EB 10 and Ti-15Mo EB 30 + POL;
- Ti-15Mo EB 10 + HT (850°C) and Ti-15Mo EB 30 + HT + POL;

X-RAY DIFFRACTION (XRD)

X-ray diffraction is used to obtain information about the crystallographic structure of the materials, chemical composition and physical properties. This is a non-destructive method, based on constructive interference of monochromatic X-rays. It's composed by a cathode ray tube that generates X-ray, which in turn are filtered to produce monochromatic radiation and collimated to hit the sample. The constructive interference is produced when Bragg's Law is satisfied:

$$n\lambda = 2d \sin\theta$$

Where θ is the angle formed between beam and crystalline plane; λ is the wavelength of the radiation; d is the distance between two adjacent planes and n is the diffraction order.

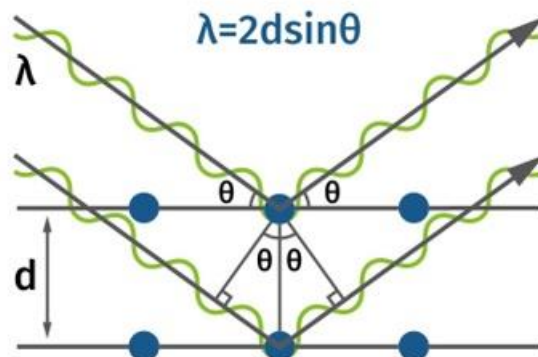


Figure 5.8 X-ray diffraction (Bragg's Law) [77].

BIOLOGICAL CHARACTERIZATION

BACTERIAL CHARACTERIZATION

The samples were brought to Novara for the bacterial characterization into a 12 multiwell plate in order to avoid any contamination and damage. There, all the samples were sterilized at 180°C for 1 hour in a stove. It was used a commercial (LB) bacterial soil with vegetable proteins at 37°C for 24-48-72 hours to allow the bacterial growth and was used *Staphylococcus aureus* (SA, commercial, multi-drug resistant, ATCC 43300) to test bacterial behavior on the samples.

After 72h of direct contact, colony forming unit (CFU) were counted. Bacteria were detached from the surface of the material by vortex and sonicator (3 times, 30 seconds each) and then 100 µl of supernatant were collected from each well and used to perform six-serial ten-fold dilutions, mixing 20 µl of bacterial suspension with 180 µl of sterile saline (0.9% NaCl). Twenty µl were then collected from each dilution, spotted onto plates containing LB agar medium, and incubated for 24h at 37°C.

$$CFU = [N \cdot Df \cdot \text{Serial Dilution}]$$

N=number of colonies;

Df=dilution factor (10, because we have 20µl in 200µl);

Finally, was carried out a statistic analysis in order to know how relevant the results were.

RESULTS AND DISCUSSION

Ti-6Al-4V

Ti-6Al-4V was structured by means of electron beam and then observed by SEM, in order to see the surface.

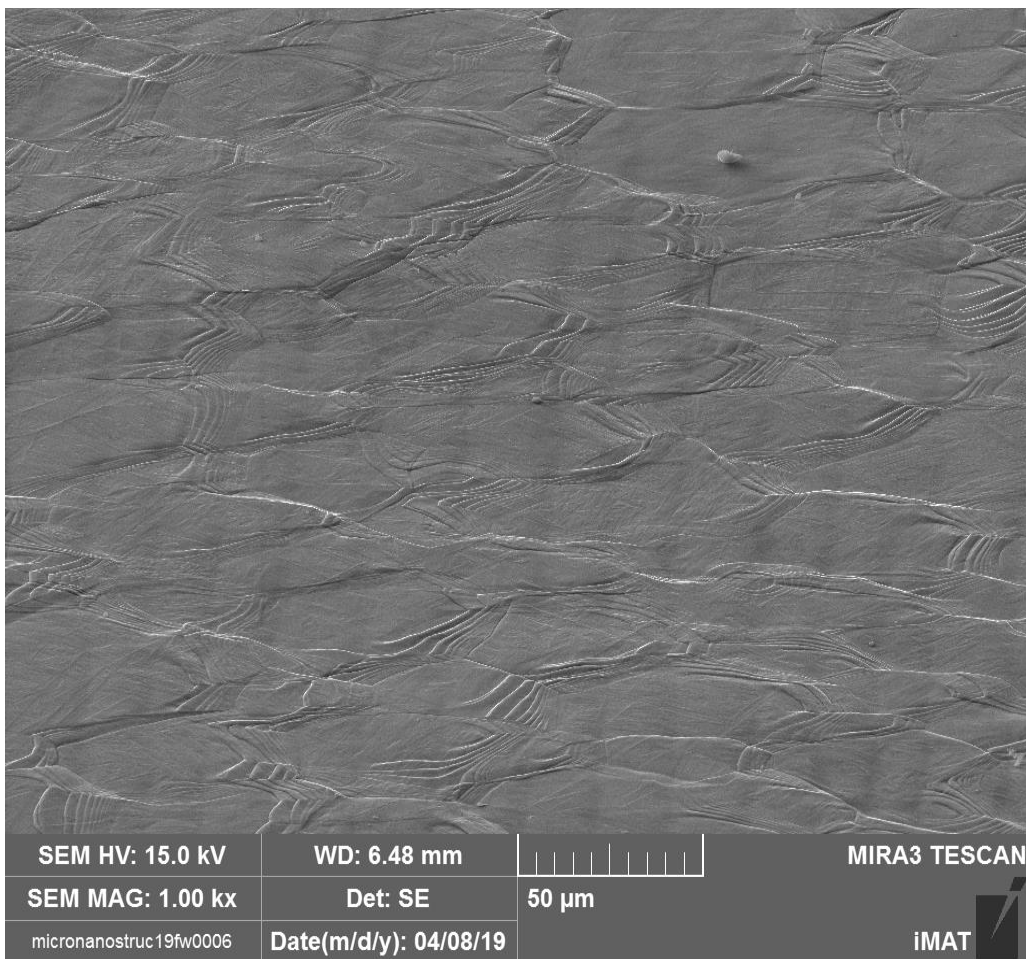


Figure 6.1 Ti6Al4V EB10 seen by SEM at 1000x magnification and 60° tilt angle. We can see clearly grain boundaries and the micro structuring of the surface with an average distance between the lines of about 20 μm . We can also observe martensite shaping

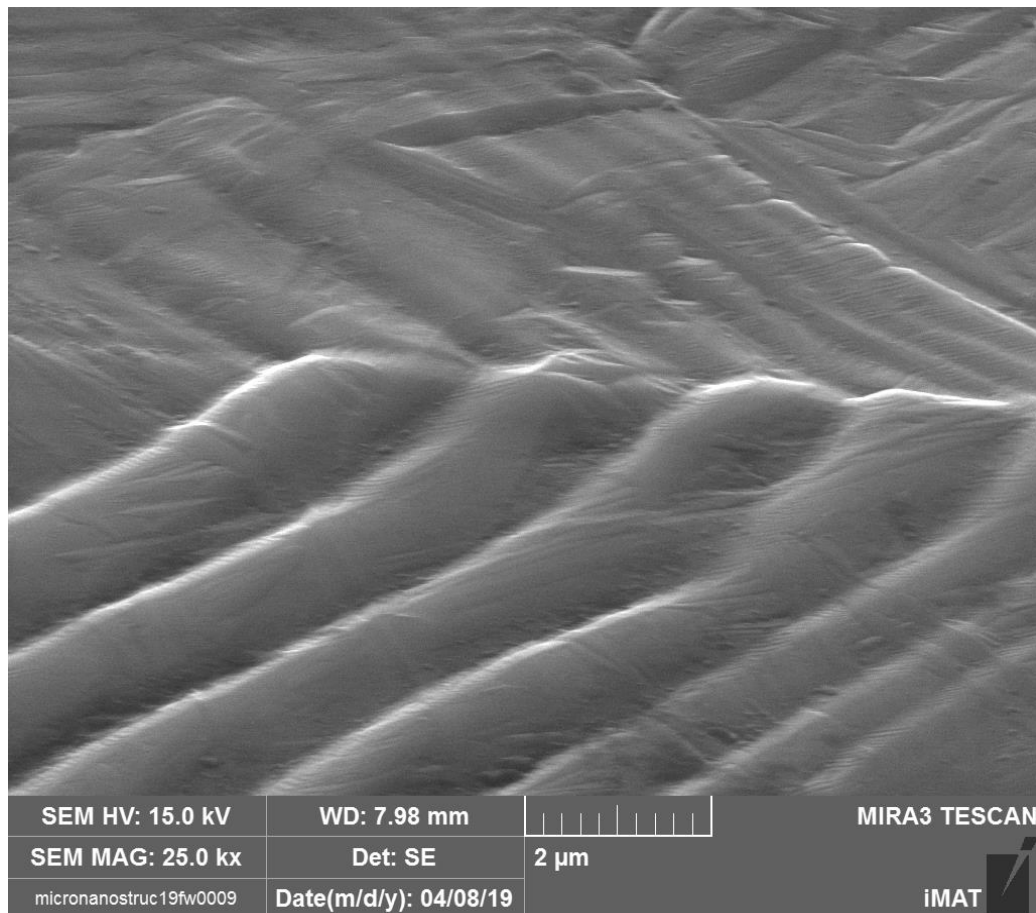


Figure 6.2 Ti6Al4V EB10 seen by SEM at 25000x magnification and 60° tilt angle. Grain boundary detail.

From the previous images it is possible to see clearly the martensite on the surface and the grooves, 10μm spacing each other. To see better the grooves, it's necessary to tilt the sample by at least 60°.

The effect of the heat treatments on the Ti-6Al-4V was widely observed even by means of LOM, in order to see the transition area between the structured area and the base material.

The first heat treatments were carried out without any electron beam structuring to evaluate the martensite conversion in lamellar shaping in the base material; for this purpose was performed a heat treatment in beta phase, Argon quenched, and then was reached a temperature of 950°C for a holding time of 4 hours, followed by a very slow cooling rate (1K/min) up to 850°C.

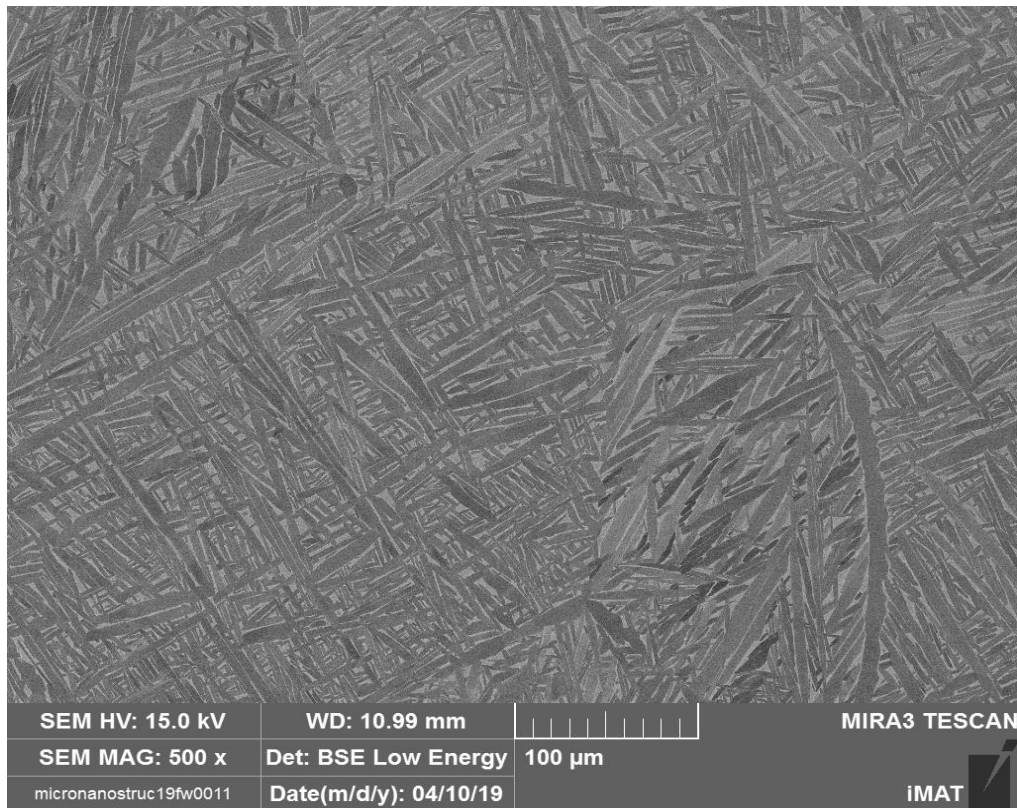
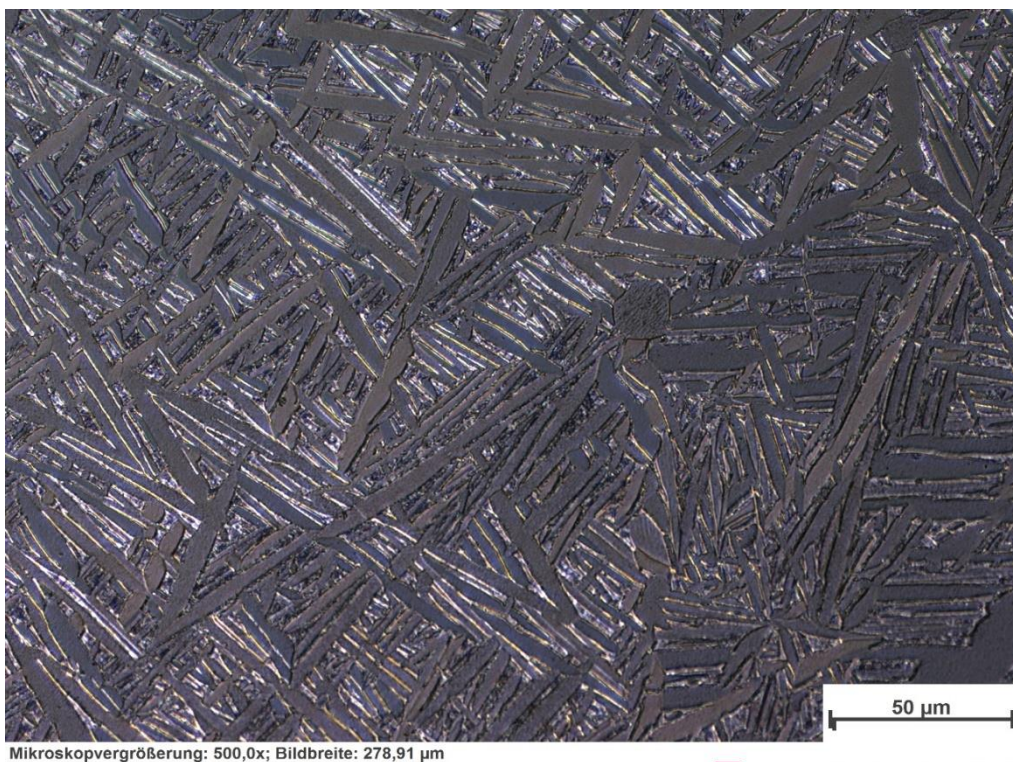


Figure 6.3 Ti6Al4V HT (β Argon quench + 950°C (4h) 1K/min up to 850°C 200K/min up to room temperature) seen by SEM at 500x magnification. The HT temperature is lower than β -transus temperature, so we can see easily the characteristic coarse α lamellar shape in β matrix, because of the slow cooling rate.



Bildname: micronanostruc19_e0074.jpg



Figure 6.4 Ti6Al4V HT (β Argon quench + 950°C (4h) 1K/min up to 850°C 200K/min up to room temperature) and etched material seen by LOM at 500x magnification with polarized light in the cross section. We can recognize the different contrast and light between lamellae with different orientations.

Another heat treatment is without Argon quenching and with a heating rate of 300K/min up to 1030°C, holding time of 5 minutes and then a cooling rate of 20K/min up to room temperature. The HT was performed above beta transus temperature in order to see beta phase on the surface after the heating. The slow cooling rate allows the formation of packaging of lamellae in different directions, evident in the cross section. The material was structured by electron beam, in this case before the heat treatment and it was used the EB10 to see the surface and EB30 to see the cross section.

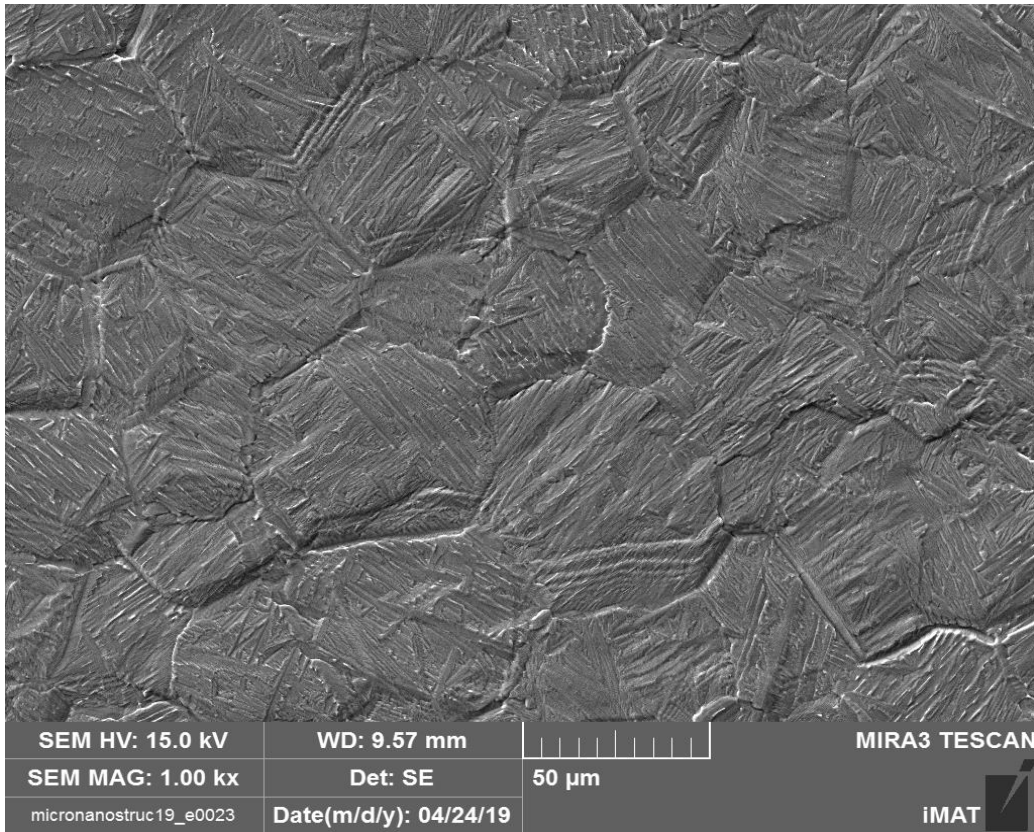


Figure 6.5 Ti6Al4V EB10 HT (Heating rate: 300K/min; Temperature: 1030°C with holding time: 5 minutes; Cooling rate: 20K/min) Tilt 20° seen by SEM at 1000x magnification.

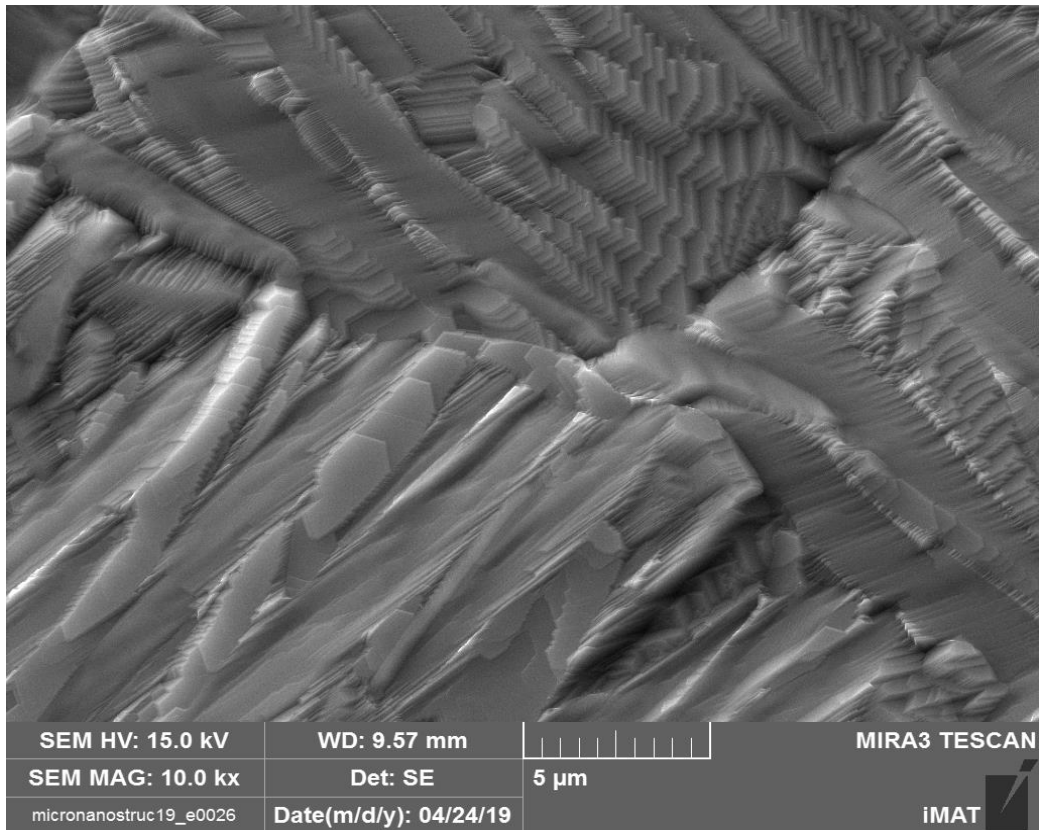


Figure 6.6 Ti6Al4V EB10 HT (Heating rate: 300K/min; Temperature: 1030°C with holding time: 5 minutes; Cooling rate: 20K/min) Tilt 20° seen by SEM at 10000x magnification. Grain boundary detail.

The previous picture is very important because it shows the nano structure of the material, in fact it's possible to see this characteristic nano stairs-like structure of Ti-6Al-4V treated at 1030°C. This structure it's even clearer tilting the sample by 40° (Fig6.7).

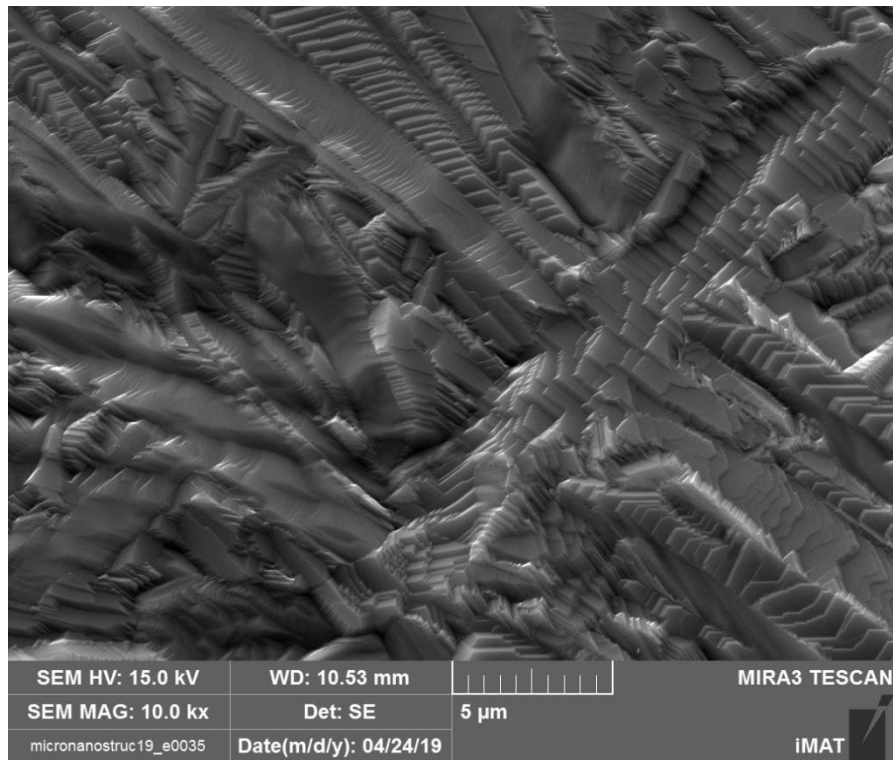


Figure 6.7 Ti6Al4V EB10 HT (Heating rate: 300K/min; Temperature: 1030°C with holding time: 5 minutes; Cooling rate: 20K/min) Tilt 40° seen by SEM at 10000x magnification.

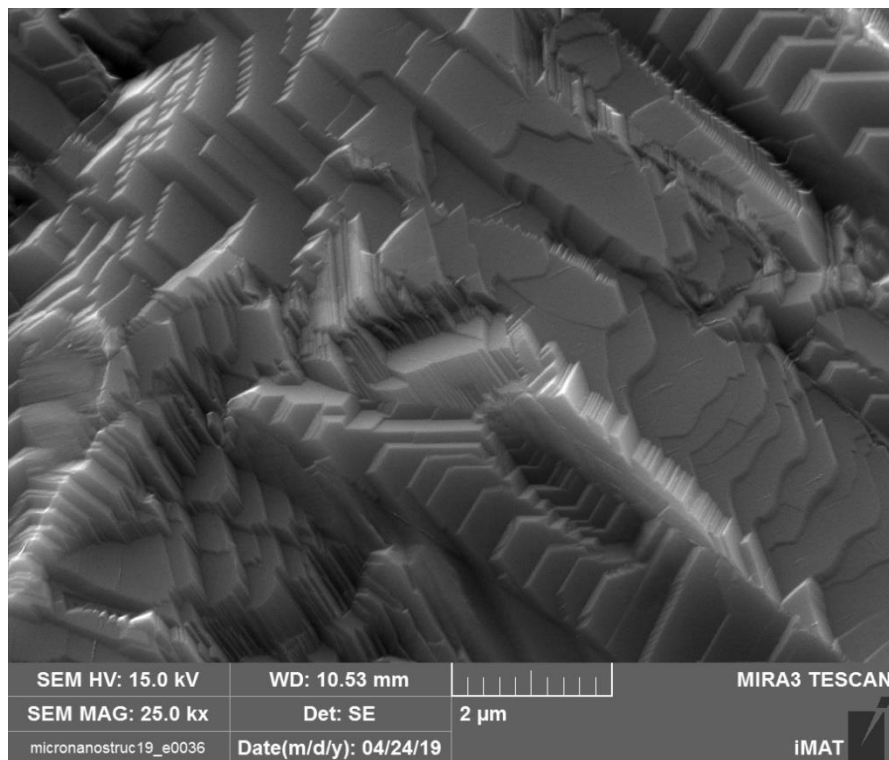


Figure 6.8 Ti6Al4V EB10 HT (Heating rate: 300K/min; Temperature: 1030°C with holding time: 5 minutes; Cooling rate: 20K/min) Tilt 40° seen by SEM at 25000x magnification.

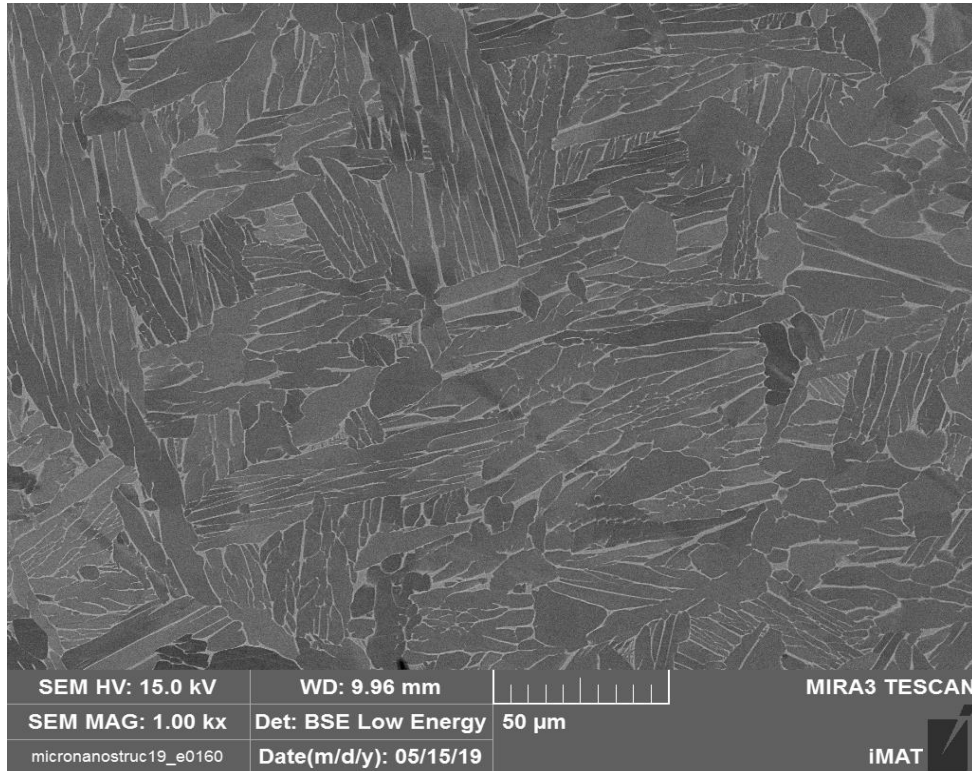


Figure 6.9 EB30 Ti-6Al-4V HT (Heating rate: 300K/min; Temperature: 1030°C with holding time: 5 minutes; Cooling rate: 20K/min) seen by SEM at 1000x magnification in the cross section. Detail of base material. The slow cooling rate allows the creation of thicker laths and coarser ones.

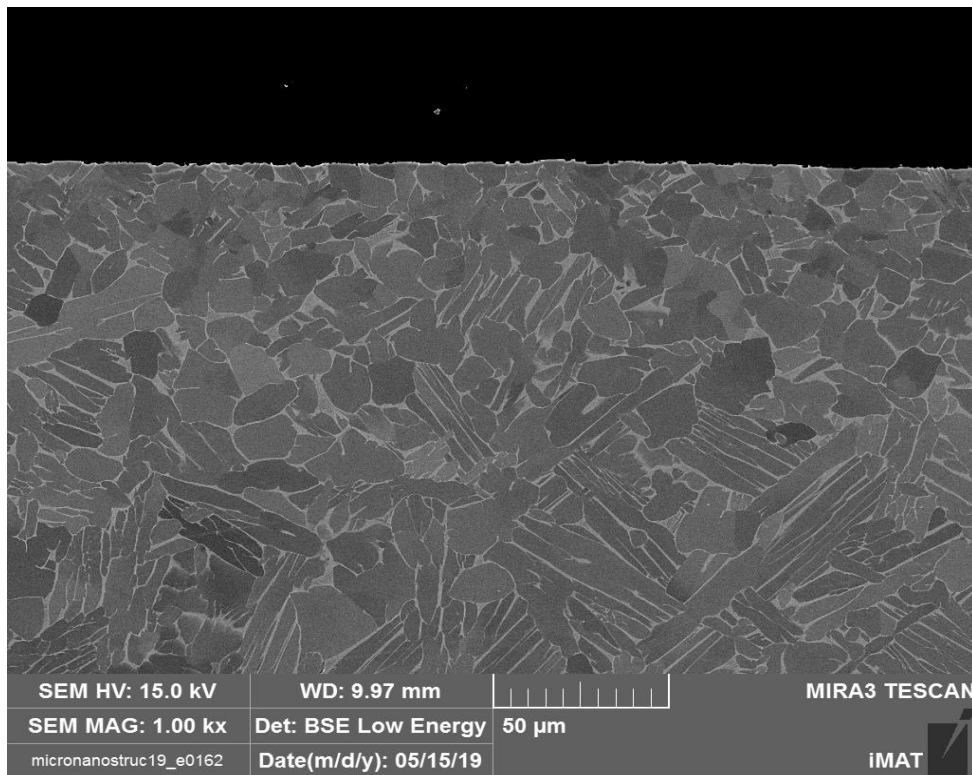


Figure 6.10 EB30 Ti-6Al-4V HT (Heating rate: 300K/min; Temperature: 1030°C with holding time: 5 minutes; Cooling rate: 20K/min) seen by SEM at 1000x magnification in the cross section.

In the previous pictures it's possible to see the cross section of EB30 Ti-6Al-4V (Fig. 6.9 and Fig.6.10) and, the coarse laths in the microstructure, due to the slow cooling rate of this heat treatment. In Fig.6.10 it is shown the transition area between the base material (in the low part of the picture) and the structured area (in the upper part of the picture); in facts in the base material there are coarse lamellae, while in the structured area we have different geometries, maybe packaging of lamellae, growing in the screen direction.

In order to see finer α laths we need to carry out a heat treatment with a faster cooling rate, so it was performed a heat treatment with a heating rate of 300K/min up to 1030°C (holding time 5 minutes) and a cooling rate faster (300K/min) up to room temperature.

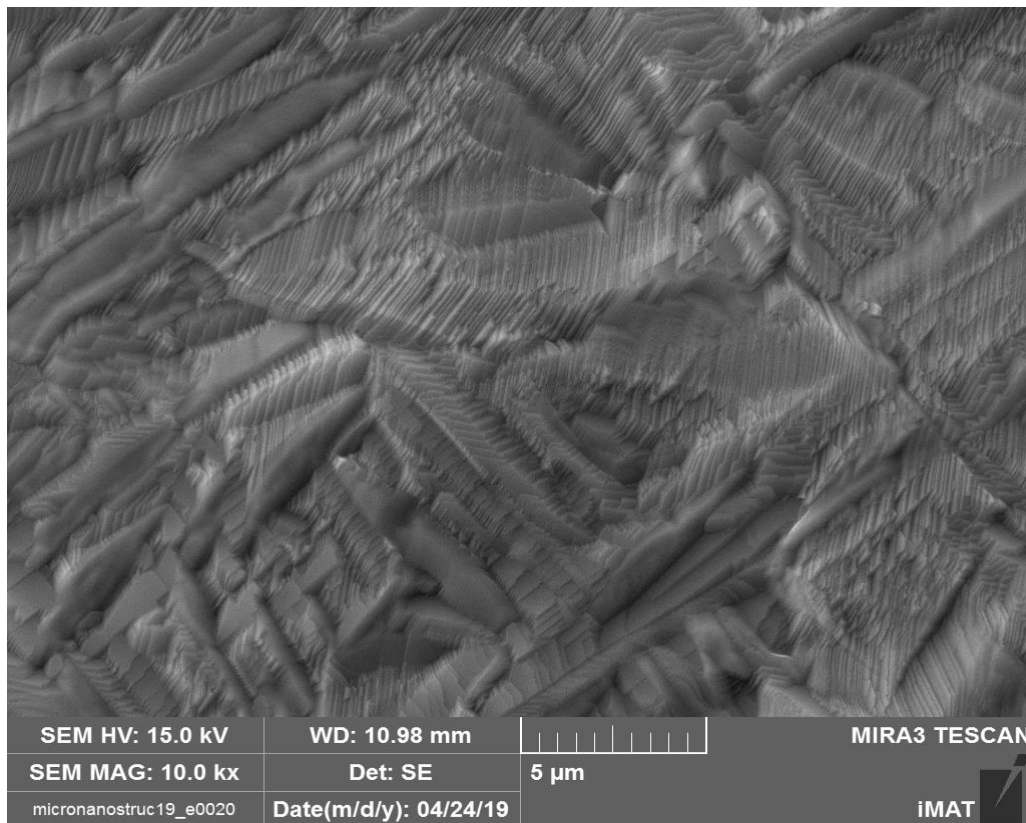


Figure 6.11 Ti-6Al-4V HT (Heating rate of 300K/min up to 1030°C with a holding time 5 minutes and a cooling rate faster 300K/min up to room temperature) EB10 - Tilt 20° seen by SEM at 10000x magnification. Detil of characteristic stairs-like shaping of the material.

In this picture the nano stairs-like structure is clearly finer than the other one; this is due to the faster cooling rate (300K/min) that produce finer laths on the microscale level and finer stairs-like shape on the nanoscale level.

There were realized some pictures of the cross section of the material, by means of SEM, too.

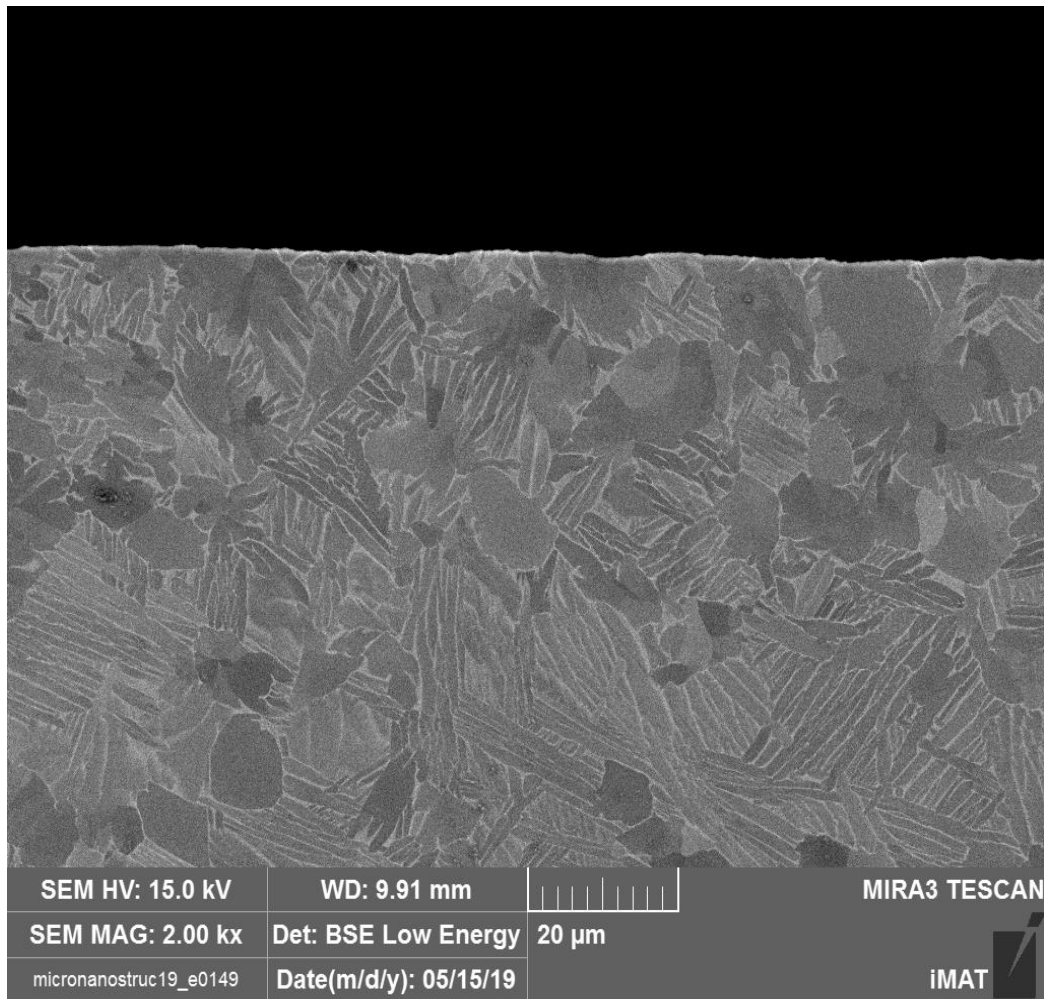


Figure 6.12 Ti-6Al-4V HT (Heating rate of 300K/min up to 1030°C with a holding time 5 minutes and a cooling rate faster 300K/min up to room temperature) EB30 seen by SEM at 2000x magnification. Detil of transition area and finer alpha laths.

A different heat treatment was tested on Ti-6Al-4V in order to stabilize the martensite microstructure and it was performed below beta transus temperature. The final aim is to form alpha lamellae on the sample surface by fast cooling, because a faster cooling rate could generate finer lamellar shaping (Fig. 6.14).

It was used a heating rate of 300K/min up to 800°C (holding time two hours) and a cooling rate of 200K/min.

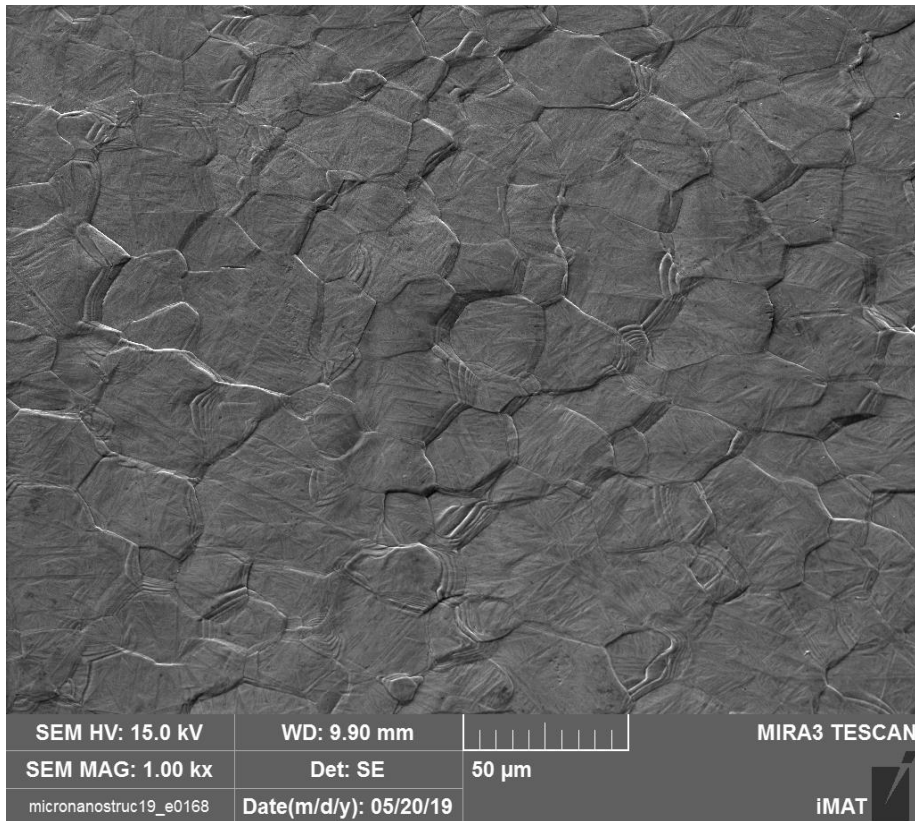


Figure 6.13 Ti-6Al-4V HT (Heating rate of 300K/min up to 800°C with holding time two hours and a cooling rate of 200K/min) EB10 seen by SEM at 1000x magnification ant tilt angle of 40°. It's possible to see clearly the grain boundaries on the surface.

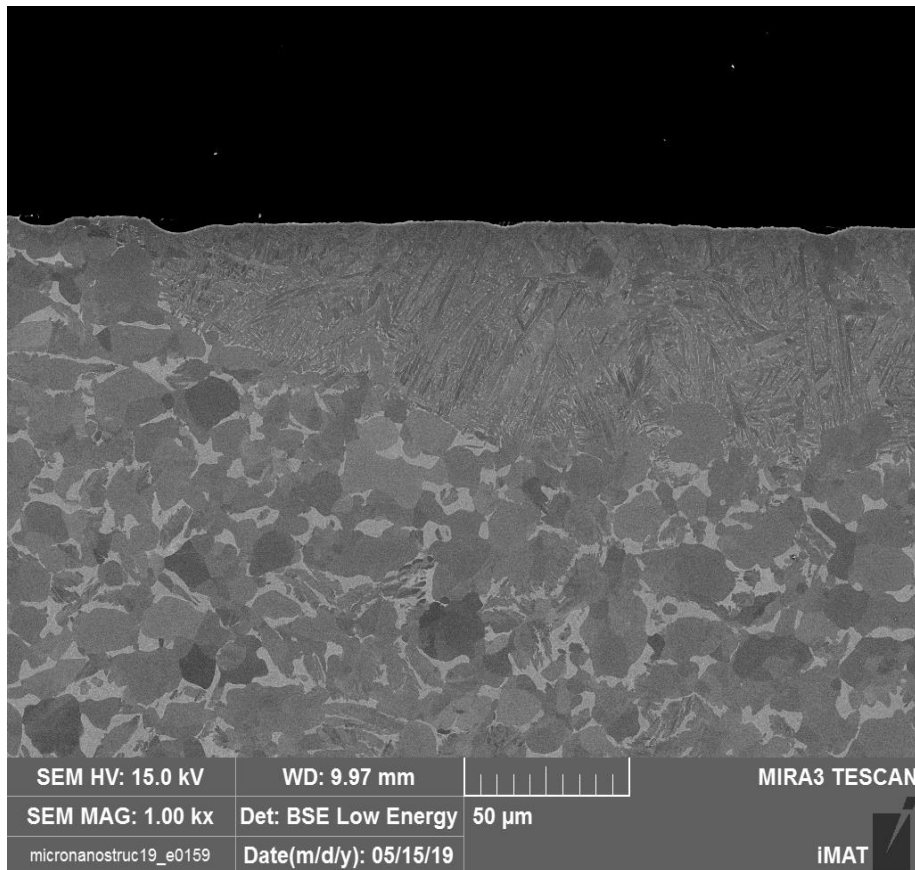


Figure 6.14 Ti-6Al-4V HT (Heating rate of 300K/min up to 800°C with holding time two hours and a cooling rate of 200K/min) EB30 seen by SEM at 1000x magnification

In the last picture (Fig. 6.14) it's shown the transition phase between the base material and the structured area. It's possible to see very clearly the differences between the two areas, the upper part characterized by lamellae and the lower part, characterized by alpha phase.

The last heat treatment tested was the one with a heating rate of 300K/min up to 950°C for a holding time of 4 hours, then 1K/min up to 850°C and finally a cooling rate of 200K/min up to room temperature. It was performed below beta transus temperature but for a higher holding time in order to evaluate the effect of the recrystallization on the martensite.

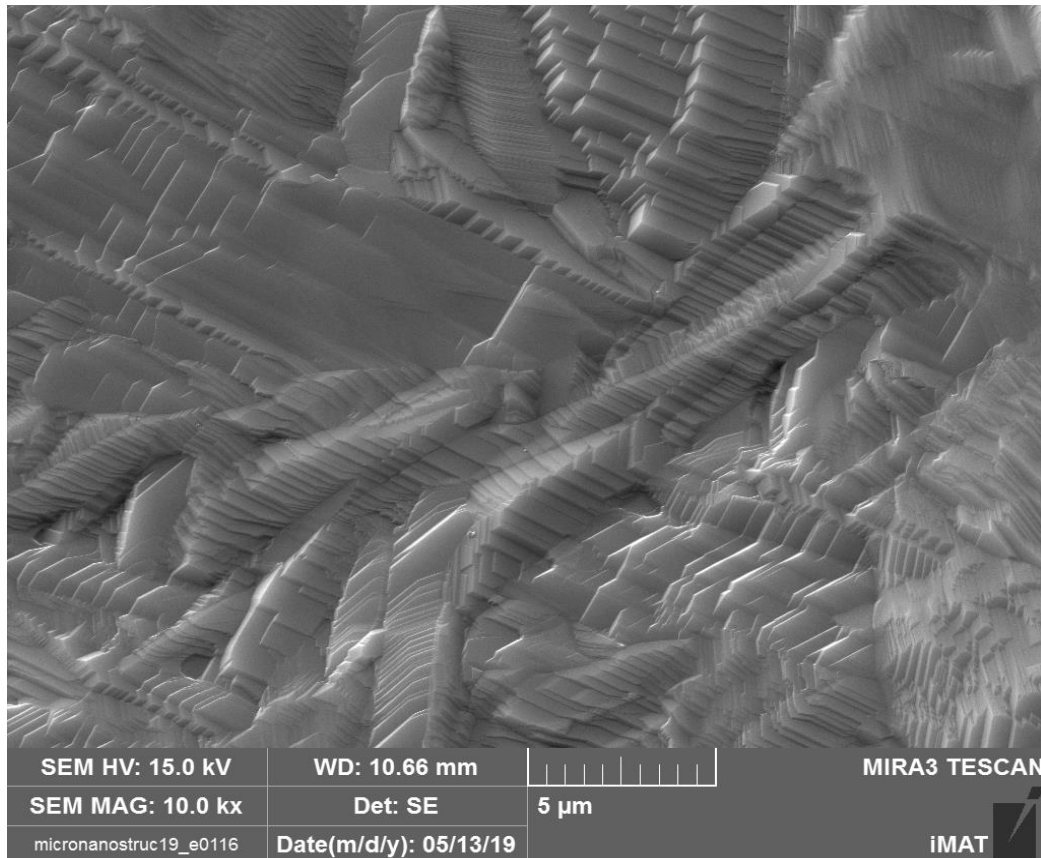


Figure 6.15 EB10 Ti-6Al-4V HT (300K/min up to 950°C for a holding time of 4 hours, then 1K/min up to 850°C and cooling rate of 200K/min up to room temperature) seen by SEM at 10000x magnification and tilt angle 40°. Surface detail.

After all the heat treatments the EB10 Ti-6Al-4V were brought to Politecnico di Torino for the biological tests, while EB30 Ti-6Al-4V were polished another time by means of the protocol of final polishing described above in order to make the grooves disappear, maintaining the microstructure. We observed EB30 Ti-6Al-4V after final polishing protocol in order to see if the grooves were disappeared, but the microstructure was still visible.

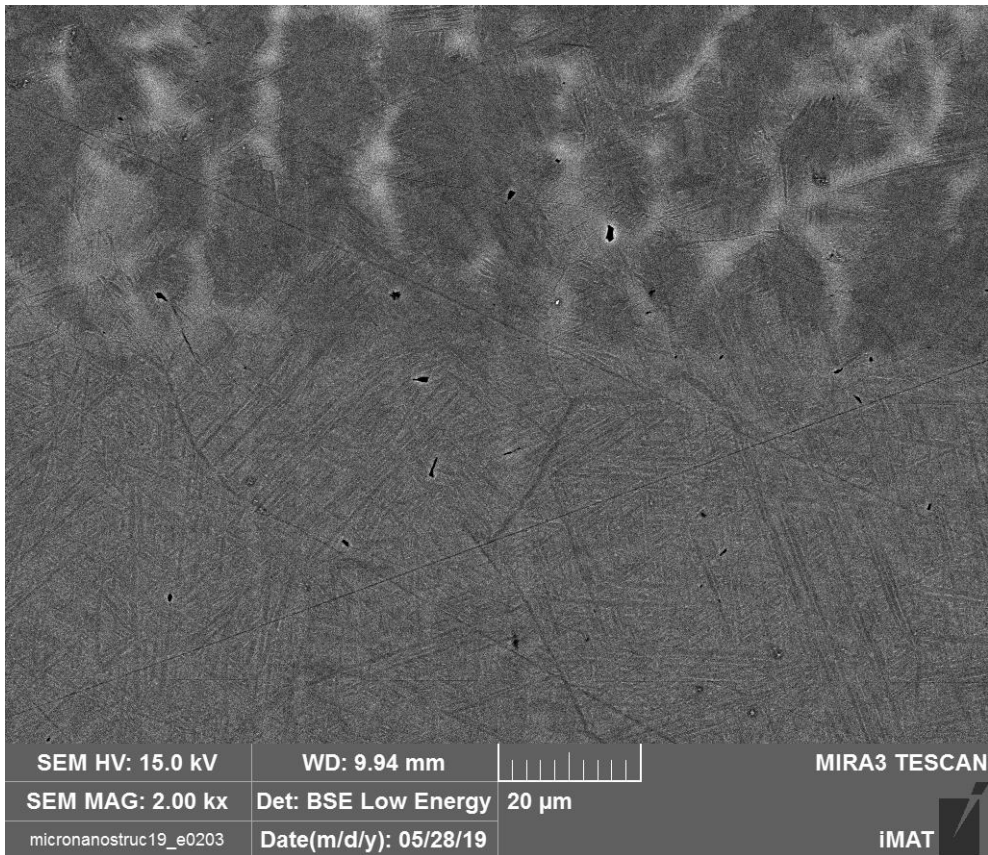


Figure 6.16 EB30 Ti-6Al-4V seen by SEM at 2000x magnification. Transition area between the structured area (lower part) and the base material (upper part).

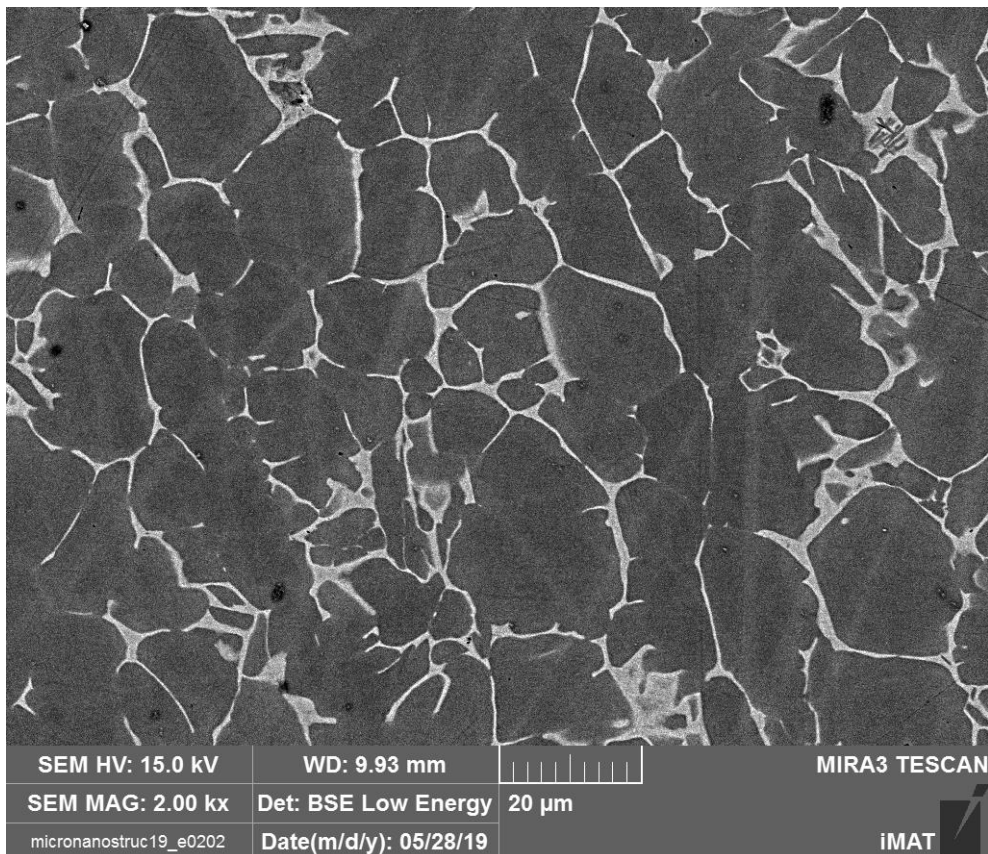


Figure 6.17 EB30 Ti-6Al-4V seen by SEM at 2000x magnification. Detail of base material.

In the previous pictures there is Ti-6Al-4V EB30 without any heat treatment polished in order to see the differences between the base material and the structured area, characterized by finer α laths.

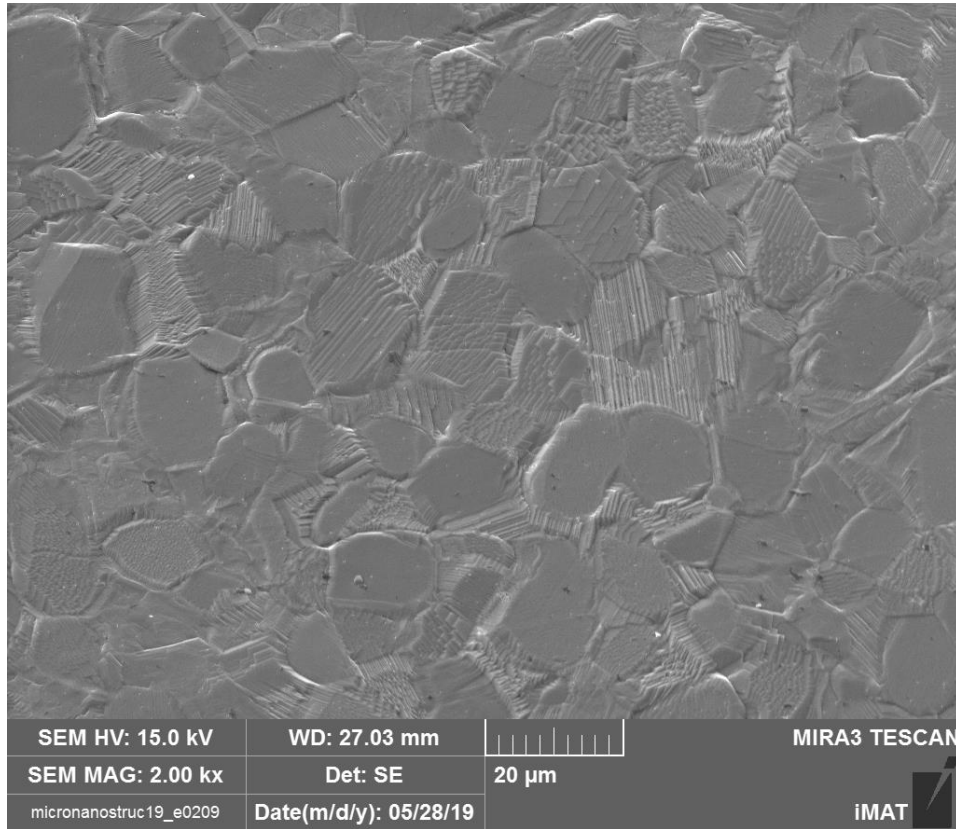


Figure 6.18 EB10 Ti-6Al-4V HT (950°C-4h-850°C) seen by SEM at 2000x magnification – Tilt 40°. Detail of base material.

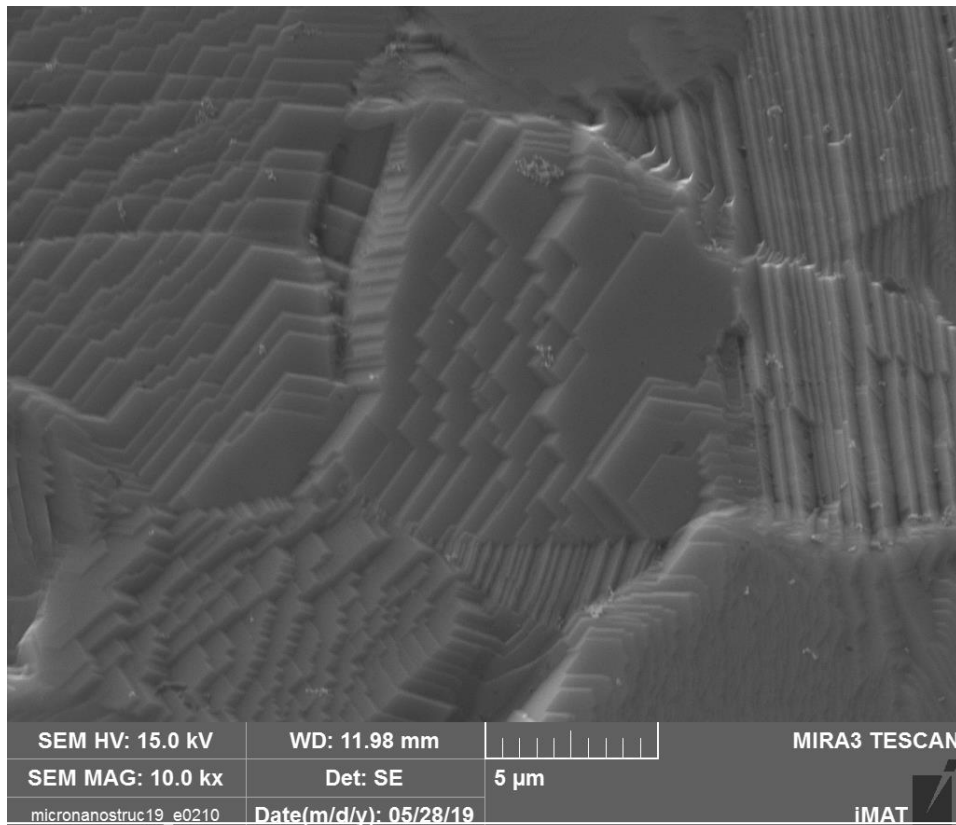


Figure 6.19 EB10 Ti-6Al-4V HT (950°C-4h-850°C) seen by SEM at 10000x magnification – Tilt 40°. Thicker nano-stairs like topography.

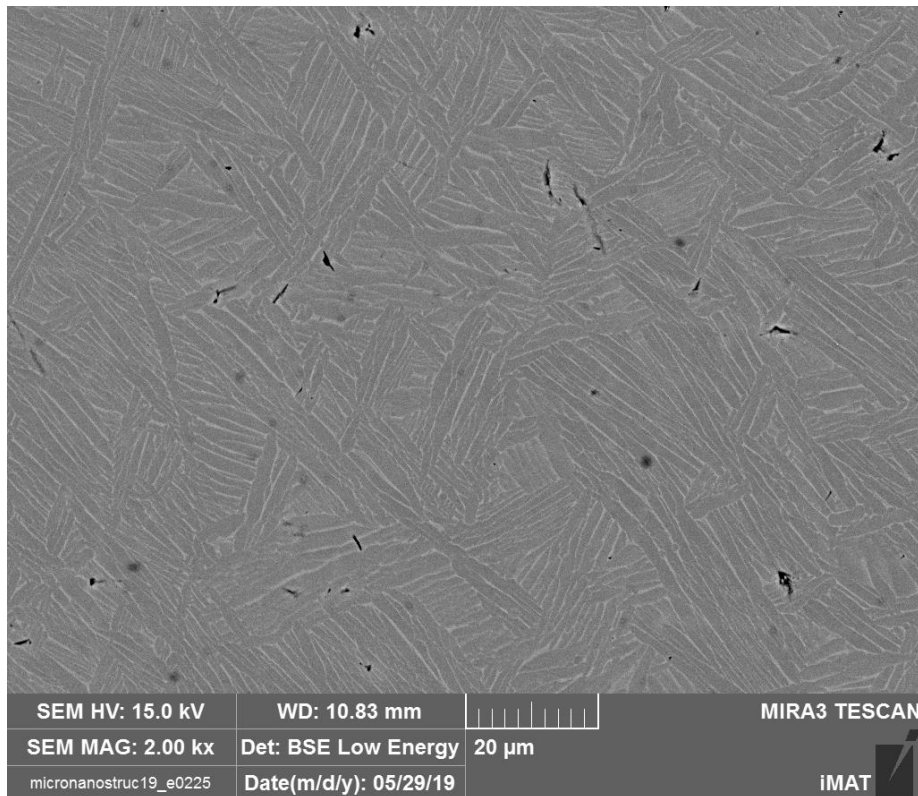


Figure 6.20 EB30 Ti-6Al-4V HT (1030°C-20K/min) after polishing seen by SEM at 2000x magnification. Structured area detail.

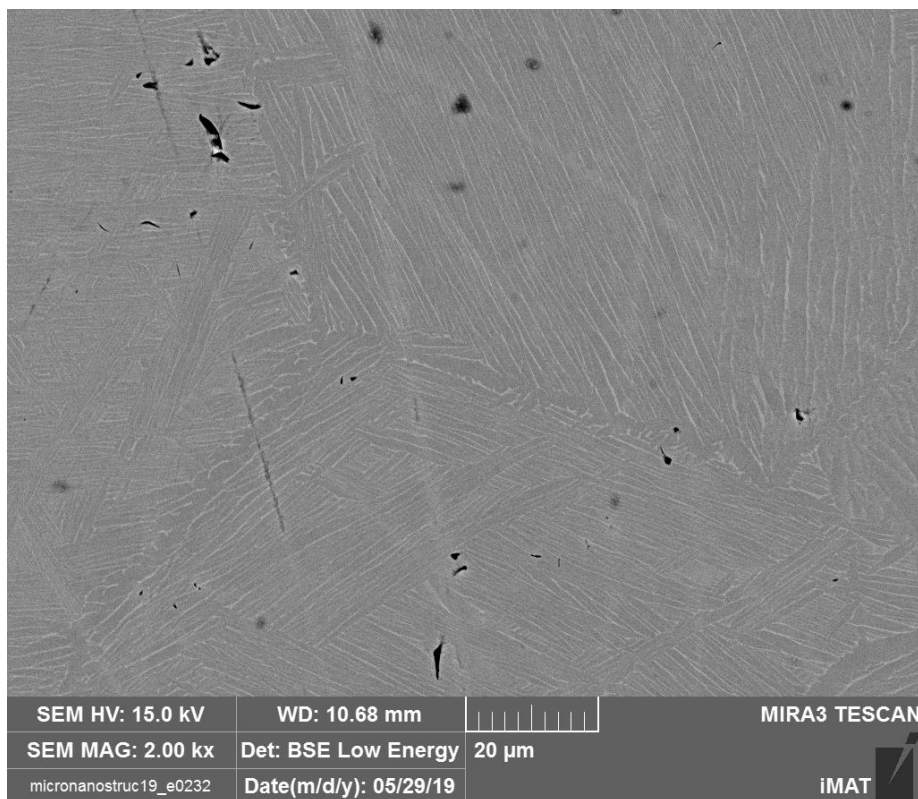


Figure 6.21 EB30 Ti-6Al-4V HT (1030°C-20K/min) after polishing seen by SEM at 2000x magnification. Structured area detail.

After final polishing is impossible to see anymore the grooves, but it's still possible to see the microstructure and the difference between base material and structured area.

Ti-15Mo

Different heat treatments were tested on Ti-15Mo in order to evaluate the changing of microstructure; the first heat treatment was carried out with Argon quenching in β phase and then a heating rate of 300K/min; temperature of 550°C for a holding time of 1 hour and then a cooling rate of 200K/min up to room temperature.

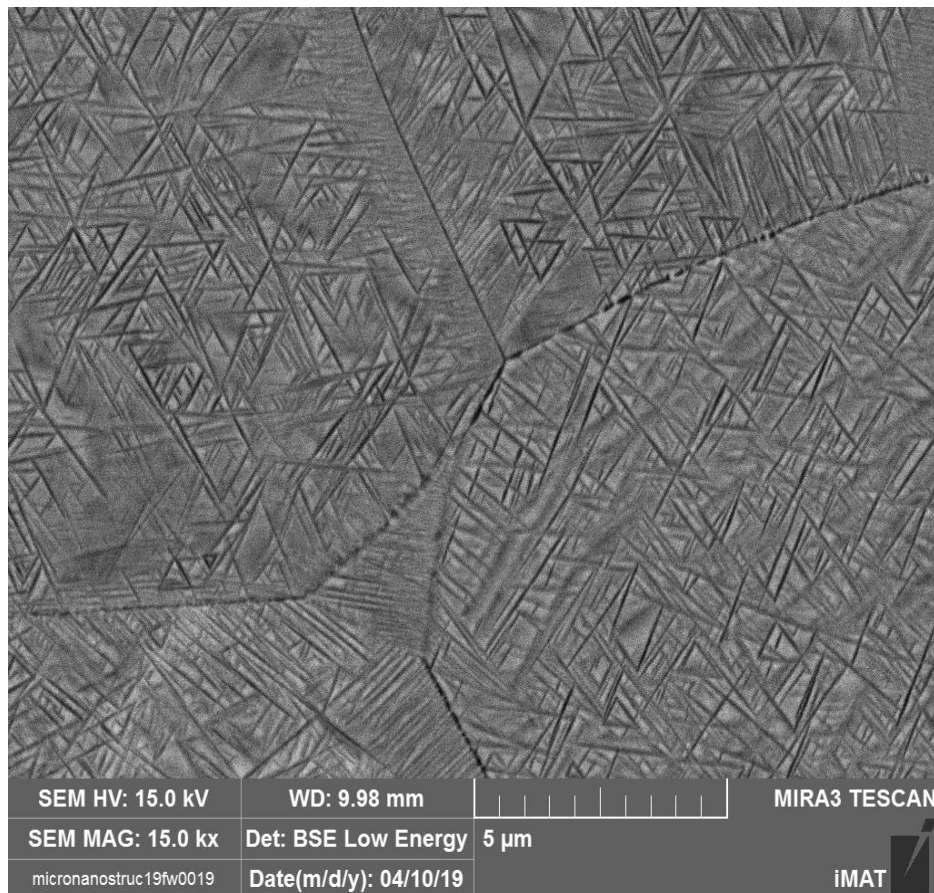


Figure 6.22 Ti15Mo HT (Argon quenching in β phase, heating rate of 300K/min; temperature of 550°C for a holding time of 1 hour and cooling rate of 200K/min up to room temperature) cross section seen by SEM at 15000x magnification. The quenching was performed in beta field and we can observe some triangle shape figures in the grains.

Another heat treatment was performed in β transus temperature with a slow cooling rate. Heating rate: 300K/min; temperature: 850°C with holding time: 5 min and cooling rate: 20K/min (slow cooling rate);

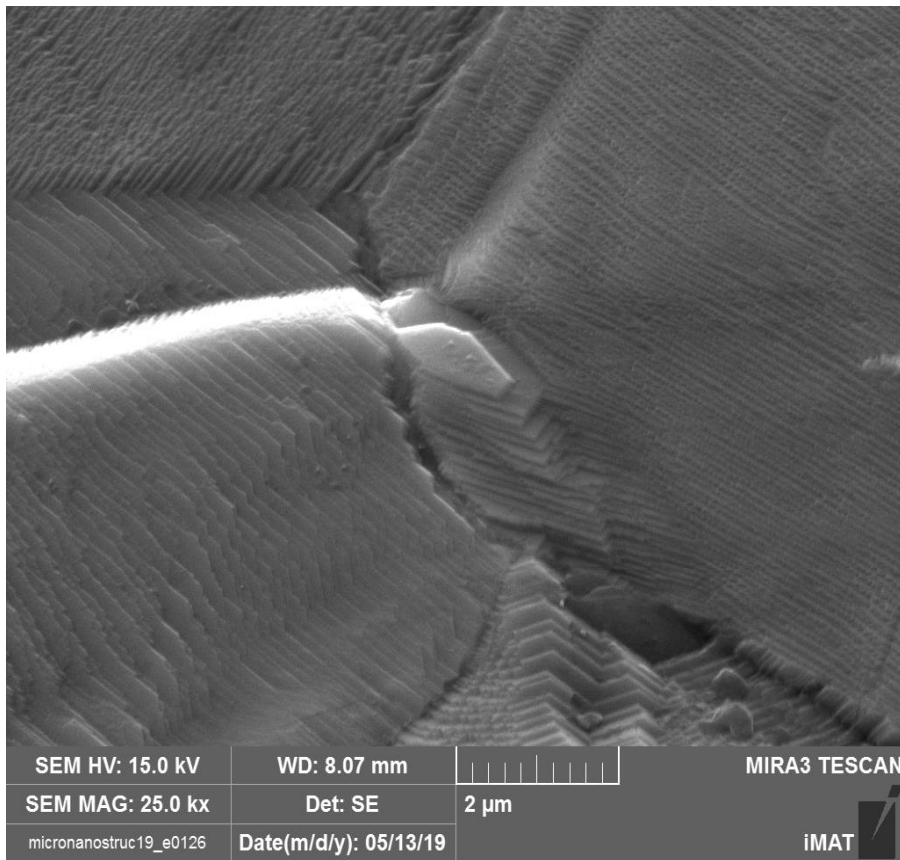


Figure 6.23 EB30 Ti15Mo HT (Heating rate: 300K/min; temperature: 850°C with holding time: 5 min and cooling rate: 20K/min); seen by SEM at 25000x magnification and tilt angle 40°. Grain boundary detail.

The following heat treatment was performed to evaluate the influence of the heating rate and temperature on the precipitation of α in the β matrix. Heating rate: 300K/min; temperature: 650°C with holding time: 4 hours and cooling rate: 200K/min;

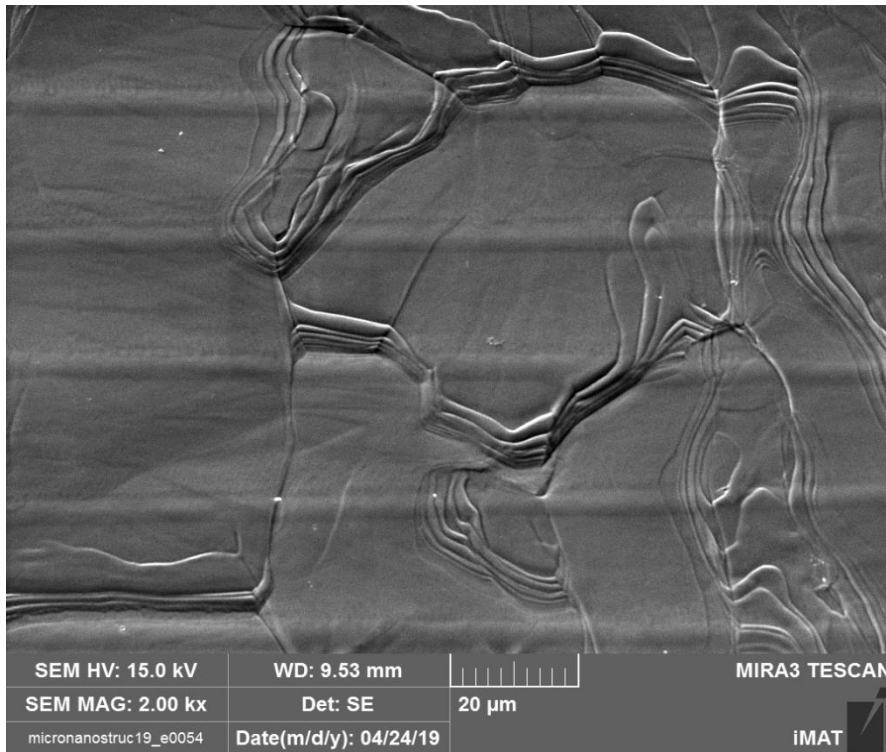


Figure 6.24 Ti15Mo EB30 HT (Heating rate: 300K/min; temperature: 650°C with holding time: 4 hours and cooling rate: 200K/min) - Tilt 40° seen by SEM at 2000x magnification. The EB structuring is very clear.

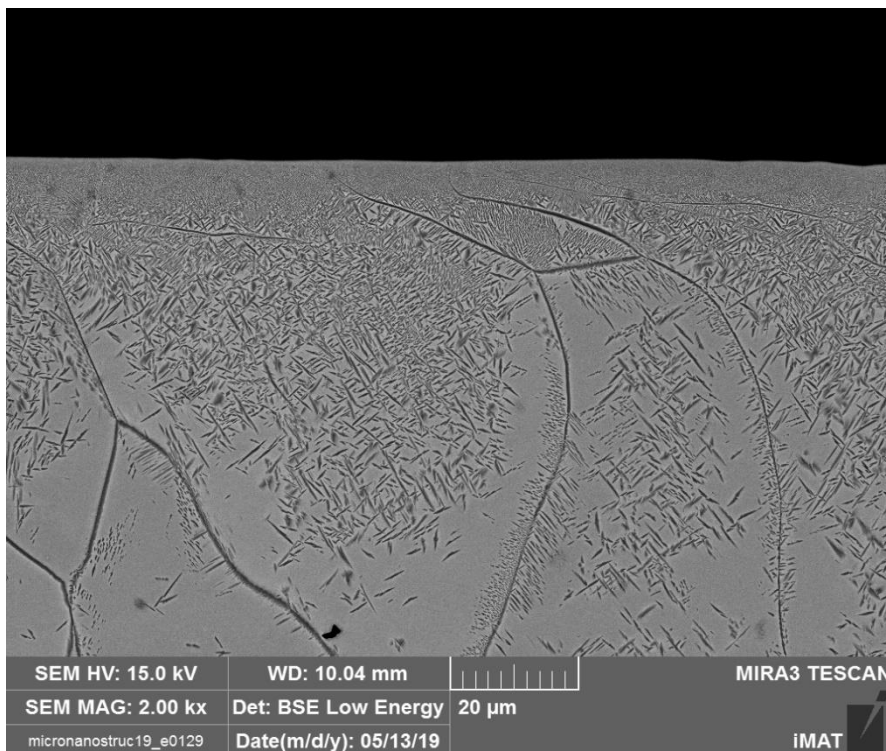


Figure 6.25 EB30 Ti15Mo HT (Heating rate: 300K/min; temperature: 650°C with holding time: 4 hours and cooling rate: 200K/min) cross section seen by SEM at 2000x magnification and tilt angle 40°. There are differences in topography in the upper and in the lower part.

In conclusion the last heat treatment carried out was the one with a heating rate: 300K/min; temperature: 650°C with holding time: 1 hours and a cooling rate: 200K/min;

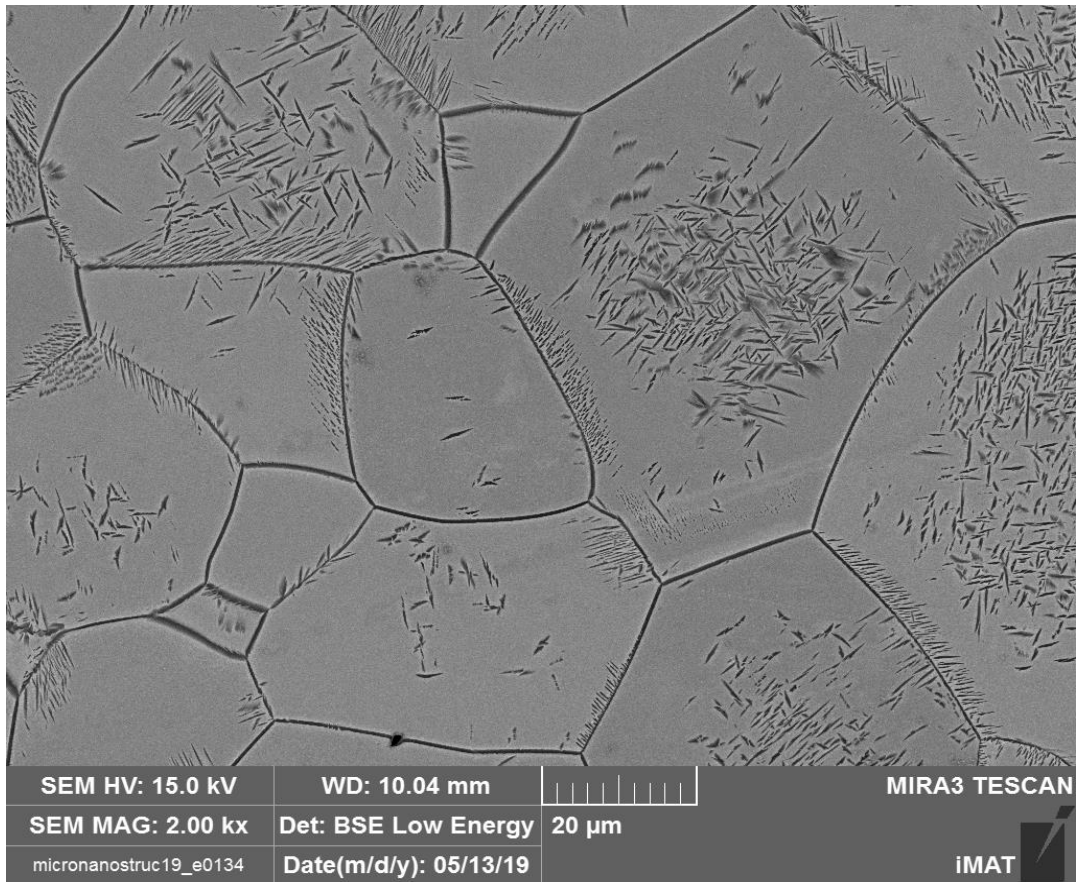


Figure 6.26 EB30 Ti15Mo HT (Heating rate: 300K/min; temperature: 650°C with holding time: 1 hours and a cooling rate: 200K/min) seen by SEM at 2000x magnification and tilt angle 40°. Detail of base material area: in the grains we can find some very fine laths.

SURFACE ROUGHNESS

Surface roughness was evaluated in the direction perpendicular to the grooves (in case of structured samples) and were carried out three measurements for each sample. In the table are shown the three values of surface roughness, the average and the standard deviation. All the values are in microns.

Sample Type	First value of Ra	Second value of Ra	Third value of Ra	Mean	Standard deviation
Ti64BM	0,024	0,025	0,021	0,023	0,002
Ti64EB10+HT1	0,203	0,255	0,24	0,233	0,027
Ti64EB10+HT2	0,265	0,314	0,285	0,288	0,025
Ti64EB30+HT1+POL	0,012	0,014	0,017	0,014	0,003
Ti64EB30+HT2+POL	0,03	0,028	0,025	0,028	0,003
Ti64EB10	0,242	0,28	0,241	0,254	0,022
Ti64EB30+POL	0,035	0,023	0,031	0,03	0,006
Ti15BM	0,029	0,024	0,028	0,027	0,003
Ti15EB10	0,141	0,194	0,201	0,179	0,033
Ti15EB30	0,031	0,028	0,033	0,031	0,003
Ti15EB10+HT	0,388	0,393	0,27	0,35	0,07
Ti15EB30+HT+POL	0,035	0,031	0,031	0,032	0,002

Tab 6.1 Surface roughness. HT1: 950°C(4h)_1K/min_850°C_200K/min;
HT2: 1030°C(5min)_300K/min; HT: 850°C (5min)_20K/min;

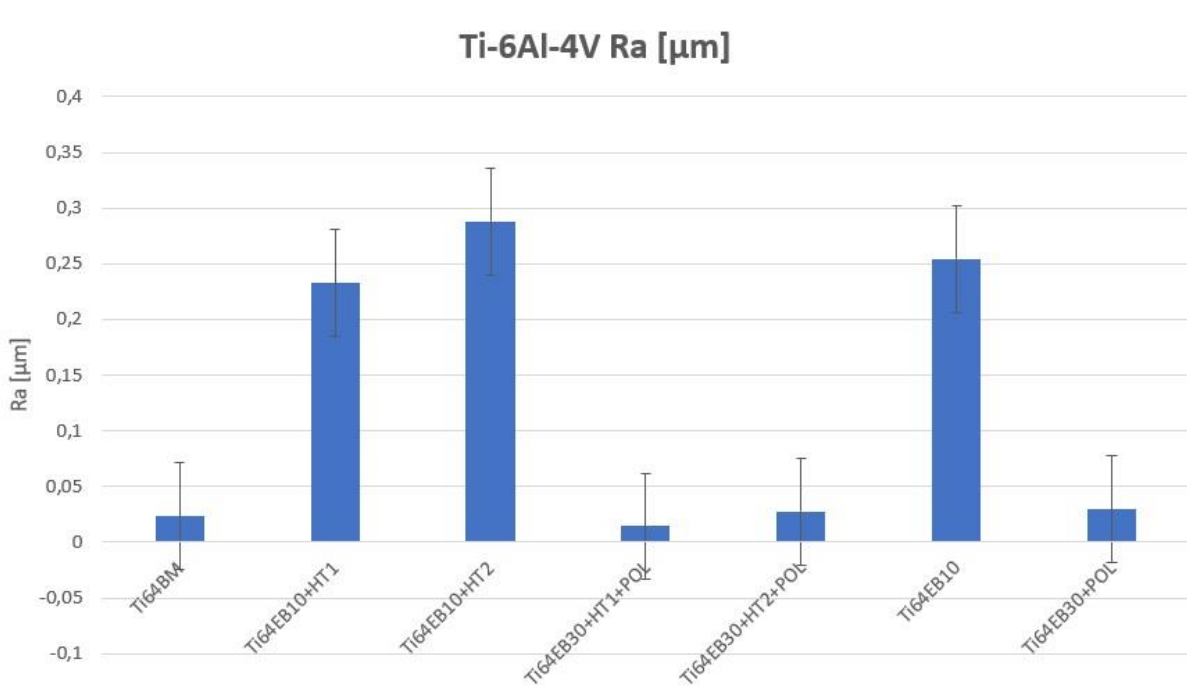


Figure 6.27 Ti-6Al-4V surface roughness values in micrometers.

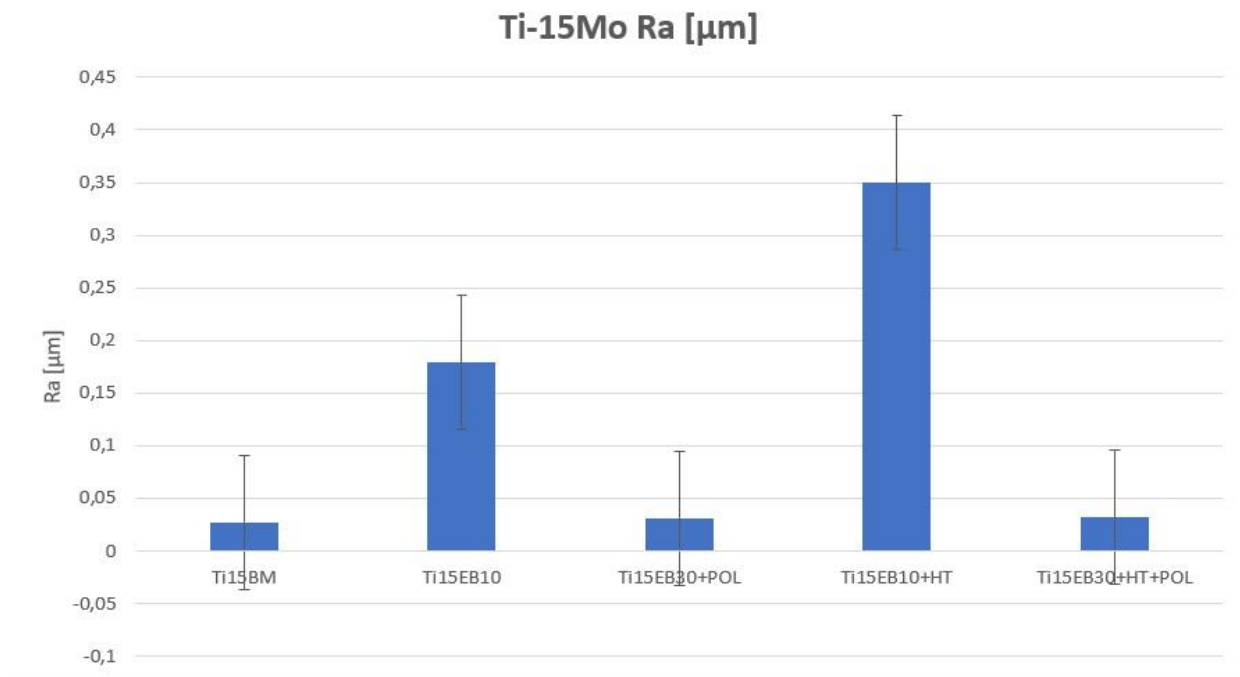


Figure 6.28 Ti-15Mo surface roughness values in micrometers.

Observing these results, it's possible to conclude that almost all the values are below the threshold value of $0.2\mu\text{m}$, above which bacterial adhesion is favored.

About Ti-6Al-4V all the values, except EB10, are below $0.2\mu\text{m}$ and are very low and this is due to the mirror polishing, which allowed to realize very smooth surfaces. As expected EB10 samples have the higher roughness because they weren't polished after structuring and they still maintaining the grooves.

About Ti-15Mo we have the same expected results as in the case of Ti-6Al-4V, in facts the graph shows how the EB10 samples have the higher roughness even in this case.

WETTABILITY TESTS

This test was carried out on the samples previously seen (Materials and methods) and there were calculated 4 contact angle values per each sample. Then it was calculated the average and the standard deviation of all the values. All the values are in degrees.

Sample Type	First value of Contact angle	Second value of Ca	Third value of Ca	Fourth value of Ca	Mean	Standard deviation
Ti64BM	75,9	75,7	84,9	88,3	81,2	6,389
Ti64EB10+HT1	80,9	87,2	76,1	76,1	80,075	5,261
Ti64EB10+HT2	90,4	86,5	87,6	88,4	88,225	1,646
Ti64EB30+HT1+POL	89,4	91,9	93,1	95	92,35	2,344
Ti64EB30+HT2+POL	90,7	88	82,2	85	86,475	3,68
Ti64EB10	85,8	90,5	82,1	82,7	85,275	3,842
Ti64EB30+POL	82,5	87,5	89,3	86,8	86,525	2,883
Ti15BM	84,6	82,2	81,6	80,9	82,325	1,607
Ti15EB10	85,1	88,4	77,9	76,7	82,025	5,641
Ti15EB30	93,6	102,3	91,6	93,9	95,35	4,744
Ti15EB10+HT	90,8	90,7	97,7	93,2	93,1	3,277
Ti15EB30+HT+POL	98	93,1	96	100,4	96,875	3,093

Tab 6.2 Contact angle values. HT1: 950°C(4h)_1K/min_850°C_200K/min;
HT2: 1030°C(5min)_300K/min; HT: 850°C (5min)_20K/min;

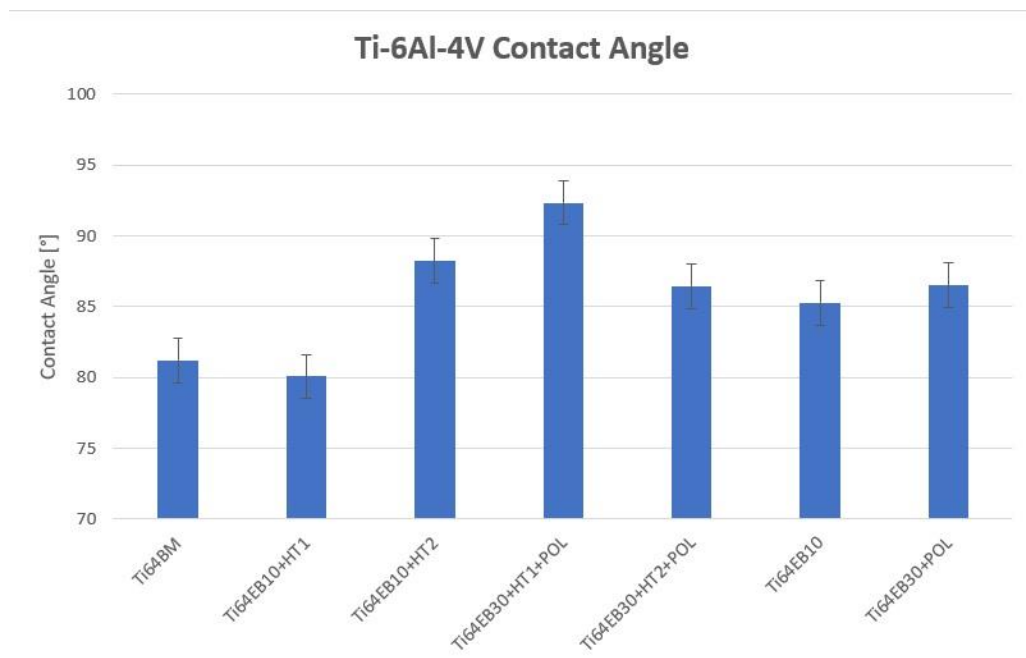


Figure 6.29 Ti-6Al-4V contact angle values in degrees.

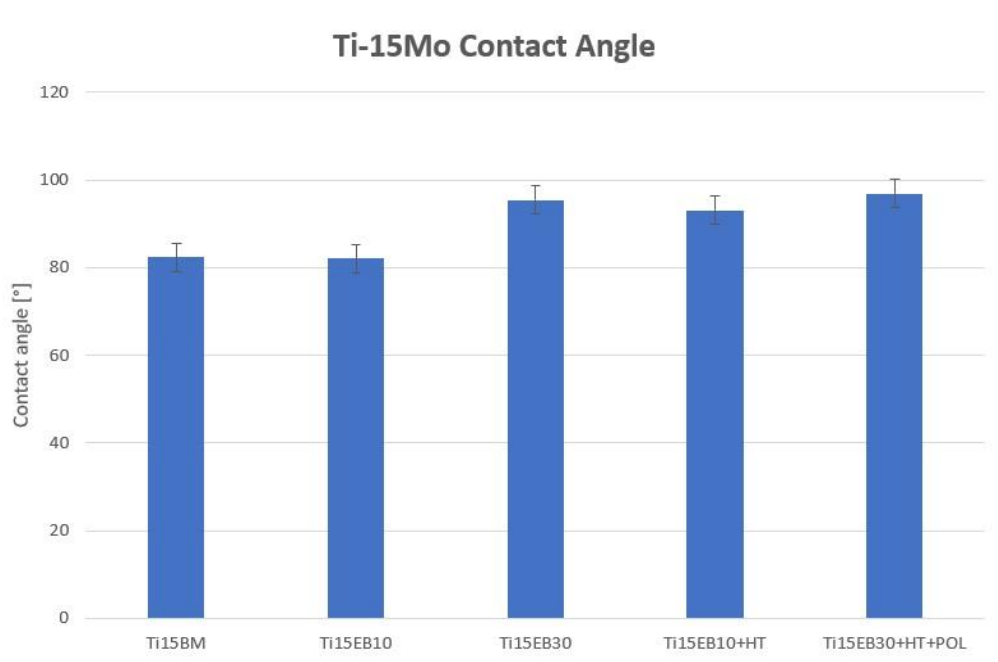


Figure 6.30 Ti-15Mo contact angle values in degrees.

It's possible to say that almost all the surfaces, for Ti-6Al-4V have low values of the contact angle, so they are mainly hydrophilic. Only Ti-6Al-4V EB30 HT1 shows a higher value of contact angle, still hydrophilic, and this is probably due to the heat treatment and the modification in the microstructure.

In case of Ti-15Mo the surfaces are slightly hydrophobic, and the contact angle values are higher. As it was possible to expect the nano topography increases the values of contact angle, in fact the air remains trapped in the nanoholes.

XRD

XRD was used to analyze and identify the crystallographic structure of the samples. The following graphs were obtained from the analysis of the diffraction spectra carried out with the XPERT High Score software in which the significant peaks were identified and then exported to an Excel file.

Each graph was normalized against the reference sample's main peak (BM) in order to compare the intensity of the other peaks.

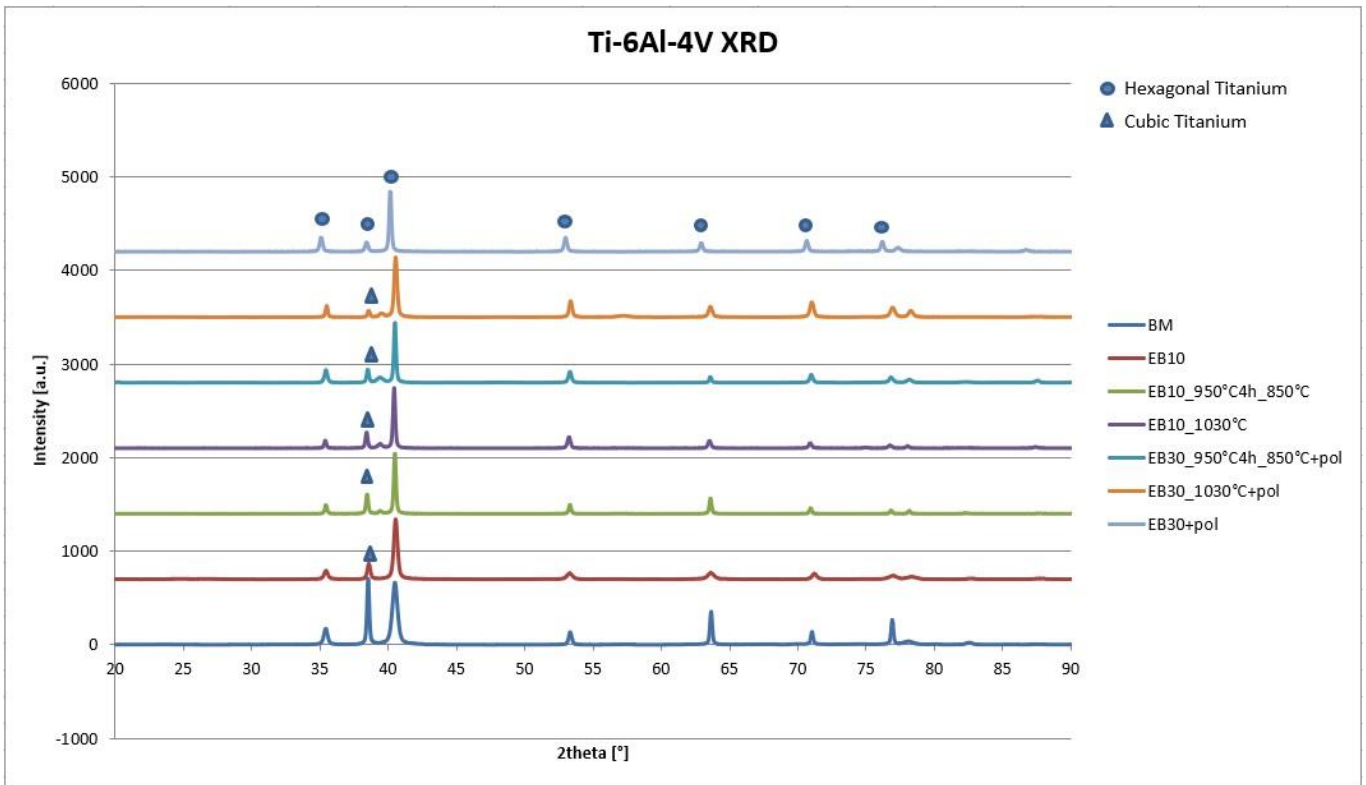


Figure 6.30 Ti-6Al-4V X-ray diffraction.

The main peaks of XRD patterns of base material sample are attributable to hexagonal titanium, but we have also cubic titanium in the base material, reported with the triangle. Only EB10 and EB30 don't present cubic titanium, but just distort hexagonal crystallographic structure, which means that the amount of cubic phase is decreased after EB structuring or has a different crystallographic orientation compared to mirror polishing

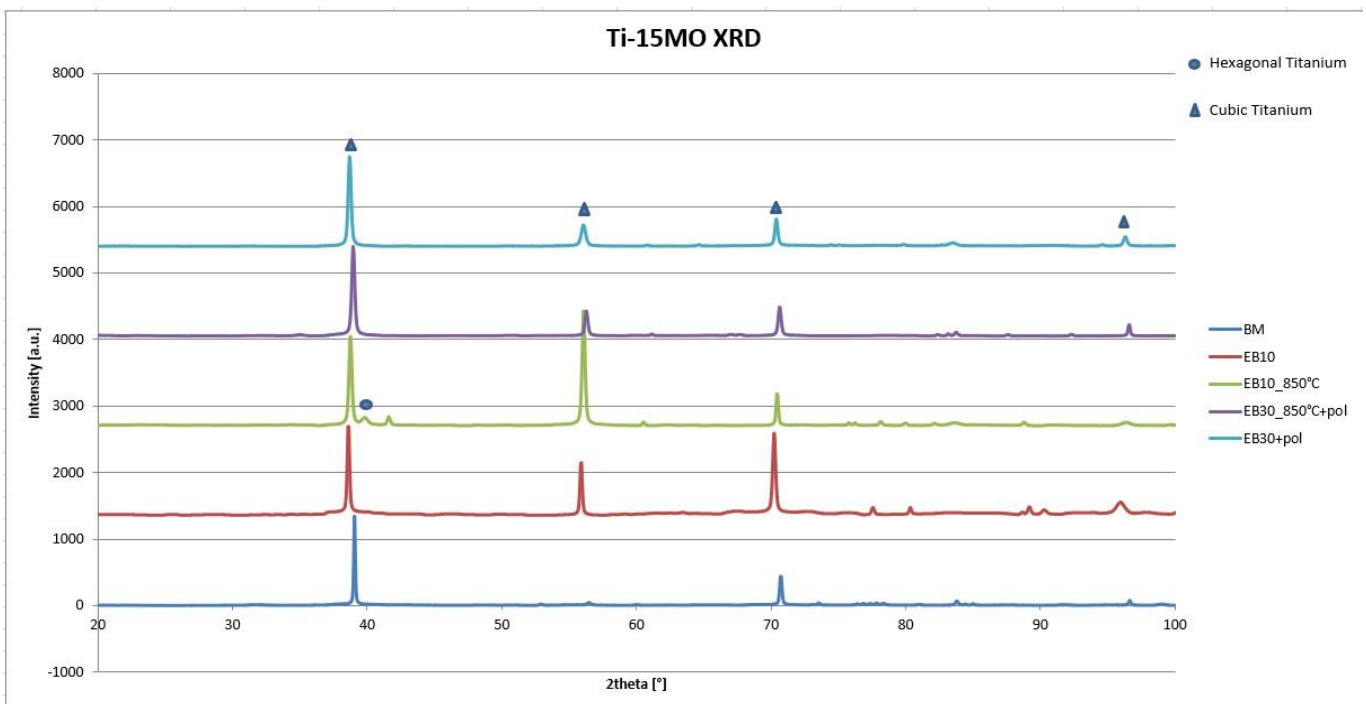


Figure 6.31 Ti-15Mo X-ray diffraction.

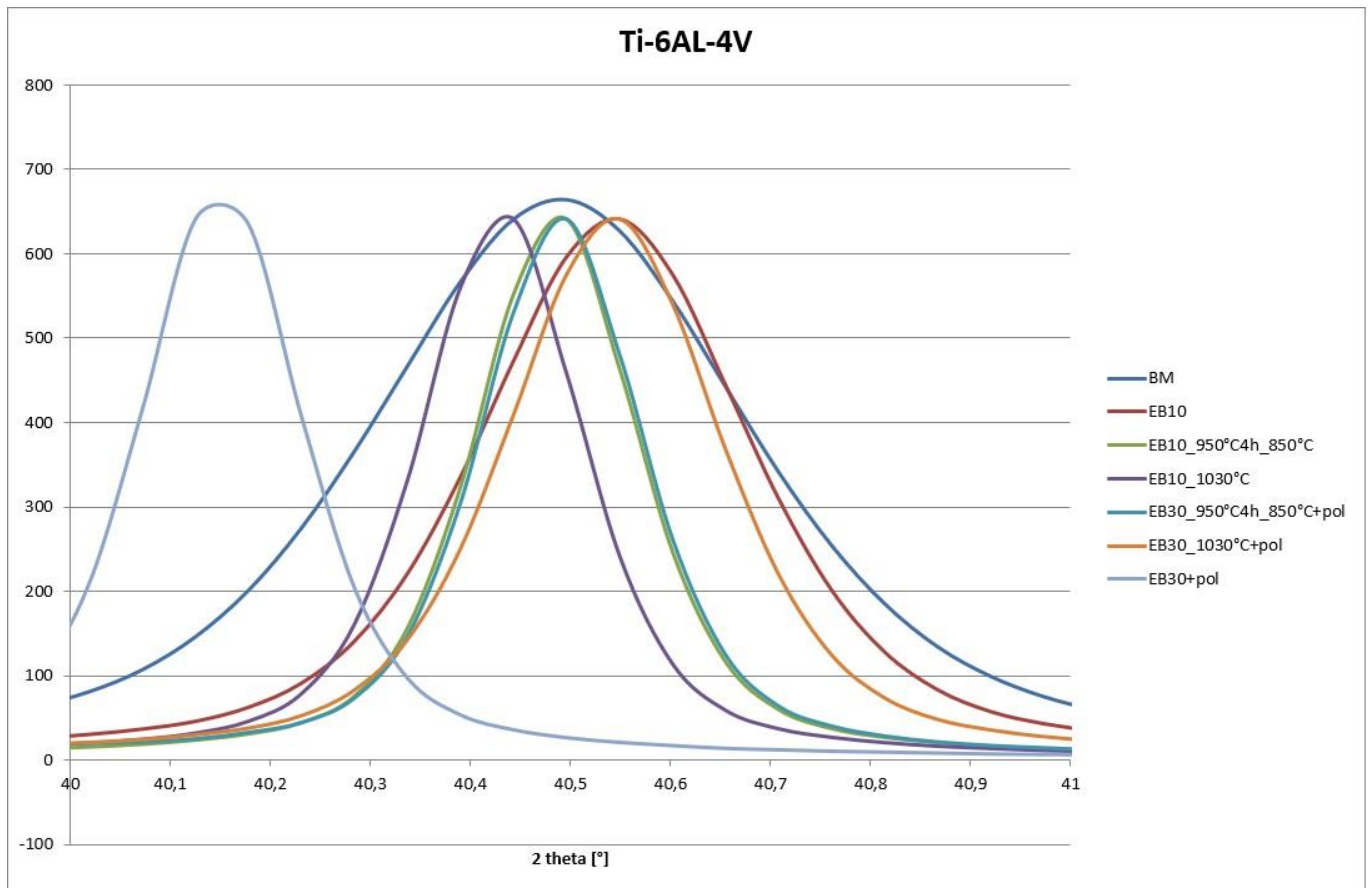


Figure 6.32 Ti-6Al-4V X-ray peaks comparison.

Observing the graph is possible to notice that Ti-6Al-4V presents smaller grains than other samples because it has the largest peak. The other samples have, all of them, narrower peaks, so they show bigger grains. We can also conclude that only EB10 and EB30 present martensite because the peak is shifted, while in the other cases the peak is aligned with the base material one. It's just anomalous the EB30+pol peak, because is shifted, but in the other direction, this could probably due to the not planarity of the sample.

In Fig.6.31 is possible to see the X-ray diffraction of Ti-15Mo, that is a metastable β alloy, so it's composed only by cubic Titanium. Only the EB10 HT and the EB30 HT have an alpha peak.

BIOLOGICAL RESULTS

Biological results were evaluated after one, two and three days after cultivation; we took the base material, mirror polished as control sample. The results are referred to the relative fluorescence units (RFU).

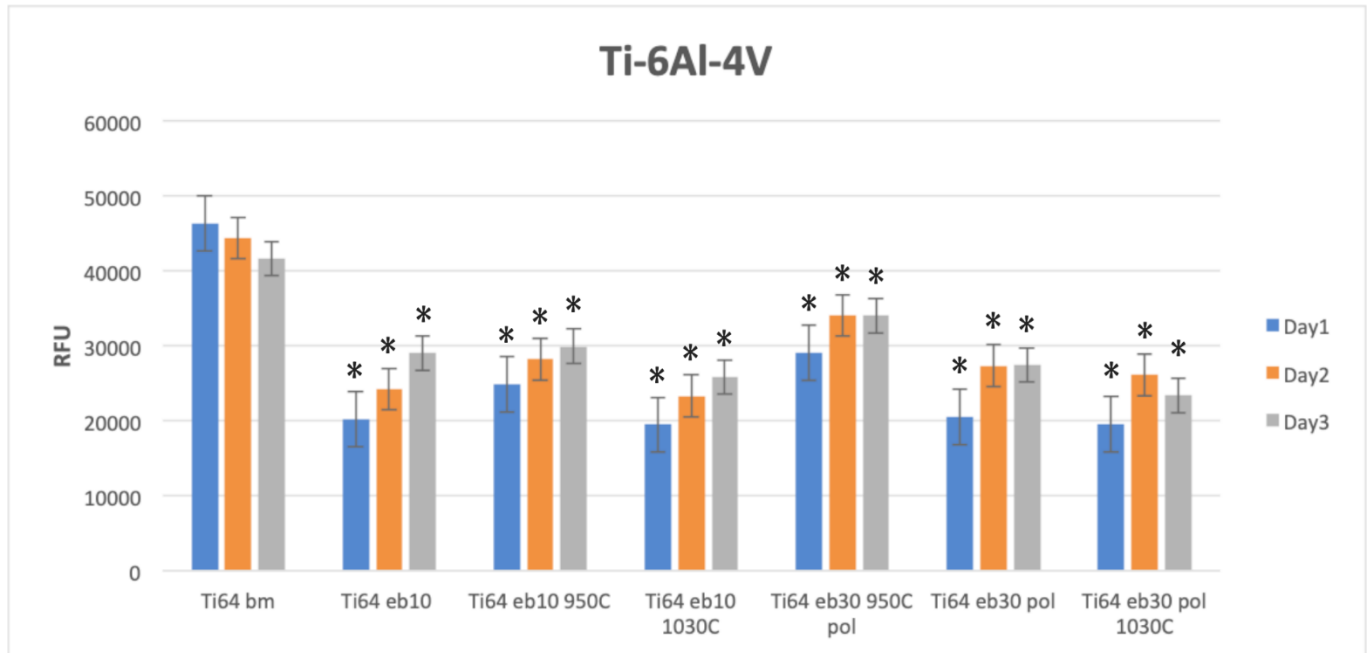


Figure 7.1 Ti-6Al-4V viability RFU.

A statistical analysis was performed to compare the different treatments carried out on the samples. As it's possible to see in the figure (Fig.7.1) every sample is statistical different from the control sample (Ti-6Al-4V BM) per each day.

Moreover, we can notice an important decreasing in bacterial adhesion at the first day for Ti-6Al-4V, as it was expected by previous results in literature. EB10 HT samples have a good behavior, avoiding bacterial adhesion at the first day. In the second day the result it's not really promising because for all the sample the value of bacterial adhesion increases consistently. In the third day the value continues to increase for each sample, except for Ti-6Al-4V EB30 HT (1030°C) POL.

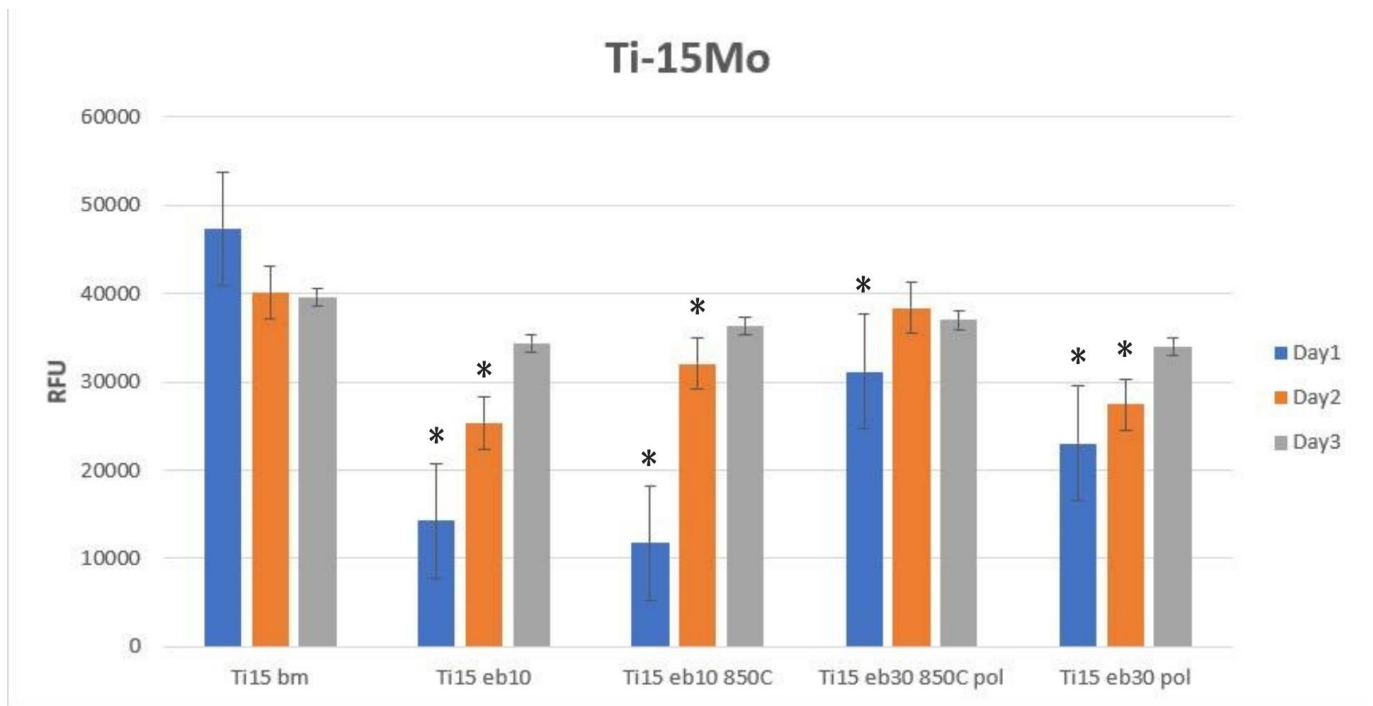


Figure 7.2 Ti-15Mo viability RFU.

Even in the case of Ti-15Mo the results are hopeful at the first day, especially for Ti-15MoEB10 and EB10 HT. The second day the results are not anymore so good, because the value of bacterial adhesion increases and continues to increase at the third day.

Tab. Ti-6Al-4V

Sample Name	Processing	Surface Topography	Crystallographic Structure	Nano topography	Microstructure	Roughness	Wettability	Bacteria Adhesion
BM	Mirror polishing	Smooth	Hcp + bcc	None	$\alpha+\beta$ bimodal condition	0.023 μm	83.81°	44101.11
EB10	Electron Beam 10 μm width	10 μm grooves	Distort hcp	Martensite shaping	Martensite	0.254 μm	85.27°	24485.78
EB30+POL	Electron Beam 30 μm width and final polishing	Smooth central square	Distort hcp	Martensite shaping	Martensite	0.030 μm	86.52°	25081.56
EB10+HT1	Electron Beam 10 μm width and heat treatment1	10 μm grooves	Hcp + bcc	Coarser α lamellae + β phase, with thicker stairs-like nanostructures	Coarser α lamellae + β phase	0.232 μm	80.07°	27660.67
EB30+HT1+POL	Electron Beam 30 μm width, heat treatment1 and final polishing	Smooth central square	Hcp + bcc	Coarser α lamellae + β phase, with thicker stairs-like nanostructures	Coarser α lamellae + β phase	0.015 μm	92.35°	32370.22
EB10+HT2	Electron Beam 10 μm width and heat treatment2	10 μm grooves	Hcp + bcc	Finer alpha lamellae with finer stairs-like nanostructures	Finer alpha lamellae + β phase	0.288 μm	88.22°	22877.44
EB30+HT2+POL	Electron Beam 30 μm width, heat treatment2 and final polishing	30 μm grooves	Hcp + bcc	Finer alpha lamellae with finer stairs-like nanostructures	Finer alpha lamellae + β phase	0.028 μm	86.47°	22983.56

Tab 7.1 Ti-6Al-4V results table.

Tab. Ti-15Mo

Sample Name	Processing	Surface Topography	Crystallographic Structure	Nano topography	Microstructure	Roughness	Wettability	Bacteria Adhesion
BM	Mirror polishing	Smooth	Bcc	None	Beta annealed condition	0.027 μ m	82.32°	42390.78
EB10	Electron Beam 10 μ m width	10 μ m grooves	Bcc	Beta grains	Beta grains	0.178 μ m	82.02°	24664.78
EB30+POL	Electron Beam 30 μ m width and final polishing	Smooth central square	Bcc	Beta grains	Beta grains	0.031 μ m	95.35°	28176
EB10+HT	Electron Beam 10 μ m width and heat treatment	10 μ m grooves	Bcc + hcp	Thicker stairs like nanostructure	Beta grains with alpha phase mostly decorating beta grain boundary	0.350 μ m	93.1°	26706.56
EB30+HT+POL	Electron Beam 30 μ m width, heat treatment and final polishing	Smooth central square	Bcc + hcp	Thicker stairs like nanostructure	Beta grains and alpha phase mostly decorating beta grain boundary	0.032 μ m	96.87°	35520.78

Tab 7.2 Ti-15o results table.

In these two table is possible to see a summary of all the treatments for each sample and the different observable structure at the nano and micro scale level. We can notice that in the case of Ti-6Al-4V we can find coarser α lamellae in the first heat treatment (950°C_1K/min_850°C) than the second heat treatment (1030°C_300K/min), according to literature, where is widely demonstrated that a slow cooling rate produces coarse laths and increasing the cooling rate we have finer alpha laths. This phenomenon is present also at the nanoscale, in facts, the nano structures (stairs-like structures) are thicker in the first heat treatment in comparison with the second one.

About Ti-15Mo it's just possible to say that the microstructure is composed by beta grains in every case, but in the heat-treated cases the samples present also alpha phase at grain boundaries.

CONCLUSION

In this master thesis were realized some Ti-6Al-4V and Ti-15Mo samples with different structuring realized by electron beam and different heat treatment carried out by dilatometer. Were obtained 10 and 30 μ m spaced groove structures for the two materials, observable by SEM and LOM and evident on the surface of the material. About heat treatments, they were performed in order to obtain different microstructures and observe the changing in the micro and nano structure of the material. After that the EB30 specimens were polished with a specific protocol in order to make the grooves disappear, maintaining the microstructure changes in the material.

All the samples were well characterized by means of several techniques, such as X-ray diffraction, wettability and surface roughness tests in Politecnico of Turin. The roughness average values were very hopeful because they were in almost all the cases below the threshold value of 0.2 μ m, widely known in literature, above which bacterial adhesion is enhanced. Also contact angle values were in accordance with those found in literature, for Ti-6Al-4V the surfaces were hydrophilic for each sample, while for Ti-15Mo the surface was slightly hydrophobic and this is due to the change in nano topography, as previously described. The XRD technique allowed to know the crystallographic structure of the samples, and even in this case, as expected we found the presence of hexagonal titanium in all the Ti-6Al-4V specimens and cubic titanium for the Ti-15Mo, being a metastable alloy.

It's possible to notice also, the presence of the martensite in the microstructure of Ti-6Al-4V EB10 and EB30, due to the electron beam structuring. The martensite is removed by heat treatments in β transus temperature (1030°C).

In conclusion biological tests were performed in order to evaluate bacterial behavior on the surface of all the different samples after 24-48 and 72 hours. It was noticed a reduced bacterial adhesion, especially for EB10 specimens (with and without heat treatments) in the case of Ti-6Al-4V and Ti-15Mo in comparison with the control sample, the base material. In the case of EB30 polished samples the bacterial adhesion decreased, even if less than EB10, and this is probably due to the microstructure in the material, because after polishing the grooves were eliminated. The decreasing of bacterial adhesion in case of EB structured sample, without any heat treatment, for Ti-6Al-4V can lead us to think that also martensite plays an important role in bacteria behavior.

BIBLIOGRAPHY

- [1] Williams, D. F. (1986). *Definitions in biomaterials: proceedings of a consensus conference of the European Society for Biomaterials*. *European cells & materials* (Vol. 25). Retrieved from <http://www.ncbi.nlm.nih.gov/pubmed/23636950>
- [2] O'Brien, F. J. (2011). *Biomaterials & scaffolds for tissue engineering* (Vol. 14)
- [3] Ratner, B. D., Hoffman, A. S., Schoen, F. J., & Lemons, J. E. (2013a). *Biomaterials Science: An Introduction to Materials: Third Edition*. *Biomaterials Science: An Introduction to Materials: Third Edition*. <https://doi.org/10.1016/B978-0-08-087780-8.00148-0>
- [4] ASM International. (2003). Overview of Biomaterials and Their Use in Medical Devices. *ASM International*. <https://doi.org/10.1361/hmmd2003p001>
- [5] Ratner, B. D., Hoffman, A. S., Schoen, F. J., & Lemons, J. E. (2013b). Introduction - Biomaterials Science: An Evolving, Multidisciplinary Endeavor. *Biomaterials Science: An Introduction to Materials: Third Edition*. <https://doi.org/10.1016/B978-0-08-087780-8.00153-4>
- [6] Geetha, M., Singh, A. K., Asokamani, R., & Gogia, A. K. (2009). Ti based biomaterials, the ultimate choice for orthopaedic implants - A review. *Progress in Materials Science*. <https://doi.org/10.1016/j.pmatsci.2008.06.004>
- [7] Posada, O. M., Tate, R. J., & Grant, M. H. (2015). *Effects of CoCr metal wear debris generated from metal-on-metal hip implants and Co ions on human monocyte-like U937 cells*. *Toxicology in Vitro*. <https://doi.org/10.1016/j.tiv.2014.11.006>
- [8] Ramskogler C. (2018). *Surface modification of titanium alloys for orthopedic implants*.
- [9] Asgharzadeh Shirazi, H., Ayatollahi, M. R., & Asnafi, A. (2017). To reduce the maximum stress and the stress shielding effect around a dental implant–bone interface using radial functionally graded biomaterials. *Computer Methods in Biomechanics and Biomedical Engineering*. <https://doi.org/10.1080/10255842.2017.1299142>
- [10] Lutjering, G., & Williams, J. C. (2007). Titanium - 2nd Edition. *Engineering*. <https://doi.org/10.1007/978-3-540-73036-1>.
- [11] Niinomi, M., & Nakai, M. (2011). Titanium-based biomaterials for preventing stress shielding between implant devices and bone. *International Journal of Biomaterials*. <https://doi.org/10.1155/2011/836587>.
- [12] Long, M., & Rack, H. J. (1998). *Titanium alloys in total joint replacement - A materials science perspective*. *Biomaterials*. [https://doi.org/10.1016/S0142-9612\(97\)00146-4](https://doi.org/10.1016/S0142-9612(97)00146-4).
- [13] Oshida Y. (2013). *Bioscience and Bioengineering of Titanium Materials*.
- [14] Ribeiro, M., Monteiro, F. J., & Ferraz, M. P. (2012). *Infection of orthopedic implants with emphasis on bacterial adhesion process and techniques used in studying bacterial-material interactions*. *Biomatter*.
- [15] Niinomi, Mitsuo. (1998). Mechanical properties of biomedical titanium alloys. *Materials Science and Engineering A*.
- [16] Mazid Md. Abdul (2012). Parametric Optimization of Machining Ti-Alloys in Respect to Surface Roughness - A Review "Titanium & its Alloys," in *Materials Science & Metallurgy*.
- [17] Peters, M., & Leyens, C. (2003). Titanium and Titanium Alloys: Fundamentals and Applications. *Titanium and Titanium Alloys Fundamentals and Applications*. <https://doi.org/10.1002/3527602119>.

- [18] Yang Yang (2015). Investigation of the martensitic transformation and the deformation mechanisms occurring in the superelastic Ti-24Nb-4Zr-8Sn alloy. *Material chemistry*.
- [19] Rack, H. J., & Qazi, J. I. (2006). Titanium alloys for biomedical applications. *Materials Science and Engineering C*. <https://doi.org/10.1016/j.msec.2005.08.032>.
- [20] Chen, Q., & Thouas, G. A. (2015). Metallic implant biomaterials. *Materials Science and Engineering R: Reports*. <https://doi.org/10.1016/j.mser.2014.10.001>
- [21] Mei, W., Sun, J., & Wen, Y. (2017). Martensitic transformation from β to α' and α'' phases in Ti-V alloys: A first-principles study. *Journal of Materials Research*.
<https://doi.org/10.1557/jmr.2017.276>
- [22] Zhang, J., Tasan, C. C., Lai, M. J., Dippel, A. C., & Raabe, D. (2017). Complexion-mediated martensitic phase transformation in Titanium. *Nature Communications*.
<https://doi.org/10.1038/ncomms14210>.
- [23] Liu, X., Chu, P. K., & Ding, C. (2004). Surface modification of titanium, titanium alloys, and related materials for biomedical applications. *Materials Science and Engineering R: Reports*.
<https://doi.org/10.1016/j.mser.2004.11.001>
- [24] Ramskogler, C., Warchomicka, F., Mostofi, S., Weinberg, A., & Sommitsch, C. (2017). Innovative surface modification of Ti6Al4V alloy by electron beam technique for biomedical application. *Materials Science and Engineering C*. <https://doi.org/10.1016/j.msec.2017.03.311>
- [25] Anselme, K. (2000). Osteoblast adhesion on biomaterials. *Biomaterials*.
[https://doi.org/10.1016/S0142-9612\(99\)00242-2](https://doi.org/10.1016/S0142-9612(99)00242-2)
- [26] Cheng, Y. T., & Rodak, D. E. (2005). Is the lotus leaf superhydrophobic? *Applied Physics Letters*.
<https://doi.org/10.1063/1.1895487>
- [27] Martines, E., Seunarine, K., Morgan, H., Gadegaard, N., Wilkinson, C. D. W., & Riehle, M. O. (2005). Superhydrophobicity and superhydrophilicity of regular nanopatterns. *Nano Letters*.
<https://doi.org/10.1021/nl051435t>
- [28] Goodman, S. L., Sims, P. A., & Albrecht, R. M. (1996). Three-dimensional extracellular matrix textured biomaterials. *Biomaterials*. [https://doi.org/10.1016/0142-9612\(96\)00016-6](https://doi.org/10.1016/0142-9612(96)00016-6)
- [29] Abrams, G. A., Goodman, S. L., Nealey, P. F., Franco, M., & Murphy, C. J. (2000). Nanoscale topography of the basement membrane underlying the corneal epithelium of the rhesus macaque. *Cell and Tissue Research*. <https://doi.org/10.1007/s004410050004>
- [30] Pamuła, E., De Cupere, V., Dufrêne, Y. F., & Rouxhet, P. G. (2004). Nanoscale organization of adsorbed collagen: Influence of substrate hydrophobicity and adsorption time. *Journal of Colloid and Interface Science*. <https://doi.org/10.1016/j.jcis.2003.11.012>
- [31] Ambrose, E. J. (1956). A surface contact microscope for the study of cell movements [32]. *Nature*. <https://doi.org/10.1038/1781194a0>
- [32] Wolf, K., Müller, R., Borgmann, S., Bröcker, E. B., & Friedl, P. (2003). Amoeboid shape change and contact guidance: T-lymphocyte crawling through fibrillar collagen is independent of matrix remodeling by MMPs and other proteases. *Blood*. <https://doi.org/10.1182/blood-2002-12-3791>
- [33] Friedl, P. (2004). Prespecification and plasticity: Shifting mechanisms of cell migration. *Current Opinion in Cell Biology*. <https://doi.org/10.1016/j.ceb.2003.11.001>
- [34] Ferraris, S., Warchomicka, F., Ramskogler, C., Tortello, M., Cochis, A., Scalia, A., ... Spriano, S. (2019). Surface structuring by Electron Beam for improved soft tissues adhesion and reduced bacterial contamination on Ti-grade 2. *Journal of Materials Processing Technology*.
<https://doi.org/10.1016/j.jmatprotec.2018.11.026>
- [35] Humphries, J. D., Wang, P., Streuli, C., Geiger, B., Humphries, M. J., & Ballestrem, C. (2007). Vinculin controls focal adhesion formation by direct interactions with talin and actin. *Journal of Cell Biology*. <https://doi.org/10.1083/jcb.200703036>

- [36] Van der Flier, A., & Sonnenberg, A. (2001). Function and interactions of integrins. *Cell and Tissue Research*. <https://doi.org/10.1007/s004410100417>
- [37] Kanchanawong, P., Shtengel, G., Pasapera, A. M., Ramko, E. B., Davidson, M. W., Hess, H. F., & Waterman, C. M. (2010). Nanoscale architecture of integrin-based cell adhesions. *Nature*. <https://doi.org/10.1038/nature09621>
- [38] Rivelino, D., Zamir, E., Balaban, N. Q., Schwarz, U. S., Ishizaki, T., Narumiya, S., ... Bershadsky, A. D. (2001). Focal contacts as mechanosensors: Externally applied local mechanical force induces growth of focal contacts by an mDia1-dependent and ROCK-independent mechanism. *Journal of Cell Biology*. <https://doi.org/10.1083/jcb.153.6.1175>
- [39] Ingber, D. E. (1997). TENSEGRITY: THE ARCHITECTURAL BASIS OF CELLULAR MECHANOTRANSDUCTION. *Annual Review of Physiology*. <https://doi.org/10.1146/annurev.physiol.59.1.575>
- [40] Rekka, N. C. I., Sathiyawathie, R. S., & Abilasha, R. (2019). Cell adhesion molecules. *Drug Invention Today*.
- [41] Ferraris, Sara, Guarino, V., Cochis, A., Varesano, A., Cruz Maya, I., Vineis, C., ... Spriano, S. (2018). Aligned keratin submicrometric-fibers for fibroblasts guidance onto nanogrooved titanium surfaces for transmucosal implants. *Materials Letters*. <https://doi.org/10.1016/j.matlet.2018.06.103>
- [42] Rajnicek, A. M., Britland, S., & McCaig, C. D. (1997). Contact guidance of CNS neurites on grooved quartz: Influence of groove dimensions, neuronal age and cell type. *Journal of Cell Science*.
- [43] Teixeira, A. I., Abrams, G. A., Bertics, P. J., Murphy, C. J., & Nealey, P. F. (2003). Epithelial contact guidance on well-defined micro- and nanostructured substrates. *Journal of Cell Science*. <https://doi.org/10.1242/jcs.00383>
- [44] Kaiser, J. P., Reinmann, A., & Bruinink, A. (2006). The effect of topographic characteristics on cell migration velocity. *EMPA Activities*.
- [45] Cavalcanti-Adam, E. A., Micoulet, A., Blümmel, J., Auernheimer, J., Kessler, H., & Spatz, J. P. (2006). Lateral spacing of integrin ligands influences cell spreading and focal adhesion assembly. *European Journal of Cell Biology*. <https://doi.org/10.1016/j.ejcb.2005.09.011>
- [46] Dalby, M. J. (2005). Topographically induced direct cell mechanotransduction. *Medical Engineering and Physics*. <https://doi.org/10.1016/j.medengphy.2005.04.005>
- [47] Dalby, M. J., Riehle, M. O., Sutherland, D. S., Agheli, H., & Curtis, A. S. G. (2004). Use of nanotopography to study mechanotransduction in fibroblasts - Methods and perspectives. *European Journal of Cell Biology*. <https://doi.org/10.1078/0171-9335-00369>
- [48] Anselme, K., Davidson, P., Popa, A. M., Giazzon, M., Liley, M., & Ploux, L. (2010). The interaction of cells and bacteria with surfaces structured at the nanometre scale. *Acta Biomaterialia*, 6(10), 3824–3846. <https://doi.org/10.1016/j.actbio.2010.04.001>
- [49] Arnold, M., Cavalcanti-Adam, E. A., Glass, R., Blümmel, J., Eck, W., Kantlehner, M., ... Spatz, J. P. (2004). Activation of integrin function by nanopatterned adhesive interfaces. *ChemPhysChem*. <https://doi.org/10.1002/cphc.200301014>
- [50] Buttiglieri, S., Pasqui, D., Migliori, M., Johnstone, H., Affrossman, S., Sereni, L., ... Camussi, G. (2003). Endothelialization and adherence of leucocytes to nanostructured surfaces. *Biomaterials*. [https://doi.org/10.1016/S0142-9612\(03\)00088-7](https://doi.org/10.1016/S0142-9612(03)00088-7)
- [51] Madigan, M., Martinko, J., Dunlap, P., & Clark, D. (2008). *Brock Biology of microorganisms* 12th edn. Int. Microbiol.
- [52] Proft, T., & Baker, E. N. (2009). Pili in Gram-negative and Gram-positive bacteria - Structure, assembly and their role in disease. *Cellular and Molecular Life Sciences*. <https://doi.org/10.1007/s00018-008-8477-4>

- [53] Srivastava, S., & Srivastava, P. S. (2003). Understanding Bacteria. Understanding Bacteria. <https://doi.org/10.1007/978-94-017-0129-7>
- [54] JW Costerton. (1999). Introduction to biofilm. Int J Antimicrob Agents.
- [55] Ploux, L., Ponche, A., & Anselme, K. (2011). Bacteria/material interfaces: Role of the material and cell wall properties. In Surface and Interfacial Aspects of Cell Adhesion.
- [56] Branda, S. S., Vik, Å., Friedman, L., & Kolter, R. (2005). Biofilms: The matrix revisited. Trends in Microbiology. <https://doi.org/10.1016/j.tim.2004.11.006>
- [57] Seyer, D., Cosette, P., Siroy, A., Dé, E., Lenz, C., Vaudry, H., ... Jouenne, T. (2005). Proteomic comparison of outer membrane protein patterns of sessile and planktonic *Pseudomonas aeruginosa* cells. Biofilms. <https://doi.org/10.1017/S1479050505001638>
- [58] Fröjd, Victoria Linderbäck, Paula Wennerberg, Ann Chávez de Paz. (2011). Effect of nanoporous TiO₂ coating and anodized Ca²⁺ modification of titanium surfaces on early microbial biofilm formation. BMC Oral Health.
- [59] Teughels, W., Van Assche, N., Sliepen, I., & Quirynen, M. (2006). Effect of material characteristics and/or surface topography on biofilm development. Clinical Oral Implants Research. <https://doi.org/10.1111/j.1600-0501.2006.01353.x>
- [60] Valle, J., Burgui, S., Langheinrich, D., Gil, C., Solano, C., Toledo-Arana, A., ... Lasa, I. (2015). Evaluation of Surface Microtopography Engineered by Direct Laser Interference for Bacterial Anti-Biofouling. Macromolecular Bioscience, 15(8), 1060–1069. <https://doi.org/10.1002/mabi.201500107>
- [61] Puckett, S. D., Taylor, E., Raimondo, T., & Webster, T. J. (2010). The relationship between the nanostructure of titanium surfaces and bacterial attachment. Biomaterials. <https://doi.org/10.1016/j.biomaterials.2009.09.081>
- [62] Del Curto, B., Brunella, M. F., Giordano, C., Pedferri, M. P., Valtulina, V., Visai, L., & Cigada, A. (2005). Decreased bacterial adhesion to surface-treated titanium. International Journal of Artificial Organs. <https://doi.org/10.1177/039139880502800711>
- [63] Yang, B., Uchida, M., Kim, H. M., Zhang, X., & Kokubo, T. (2004). Preparation of bioactive titanium metal via anodic oxidation treatment. Biomaterials. [https://doi.org/10.1016/S0142-9612\(03\)00626-4](https://doi.org/10.1016/S0142-9612(03)00626-4)
- [64] Wang, X., Lu, T., Wen, J., Xu, L., Zeng, D., Wu, Q., ... Jiang, X. (2016). Selective responses of human gingival fibroblasts and bacteria on carbon fiber reinforced polyetheretherketone with multilevel nanostructured TiO₂. Biomaterials. <https://doi.org/10.1016/j.biomaterials.2016.01.001>
- [65] Ferraris, S., Truffa Giachet, F., Miola, M., Bertone, E., Varesano, A., Vineis, C., ... Spriano, S. (2017). Nanogrooves and keratin nanofibers on titanium surfaces aimed at driving gingival fibroblasts alignment and proliferation without increasing bacterial adhesion. Materials Science and Engineering C. <https://doi.org/10.1016/j.msec.2017.02.152>
- [66] Mitik-Dineva, N., Wang, J., Truong, V. K., Stoddart, P. R., Malherbe, F., Crawford, R. J., & Ivanova, E. P. (2009). Differences in colonisation of five marine bacteria on two types of glass surfaces. Biofouling. <https://doi.org/10.1080/08927010903012773>
- [67] Truong, V. K., Lapovok, R., Estrin, Y. S., Rundell, S., Wang, J. Y., Fluke, C. J., ... Ivanova, E. P. (2010). The influence of nano-scale surface roughness on bacterial adhesion to ultrafine-grained titanium. Biomaterials. <https://doi.org/10.1016/j.biomaterials.2010.01.071>
- [68] Nightingale, K. R. (1989). Electron beam welding. Production Engineer London.
- [69] Dance B. and Buxton A. (2007). An introduction to Sur -Sculpt R technology - new opportunities, new challenges. 7th International Conference on Beam Technology.

- [70] Stokes, D. J. (2008). Principles and Practice of Variable Pressure/Environmental Scanning Electron Microscopy (VP-ESEM). Principles and Practice of Variable Pressure/Environmental Scanning Electron Microscopy (VP-ESEM). <https://doi.org/10.1002/9780470758731>.
- [71] <http://emicroscope.blogspot.com/2011/03/scanning-electron-microscope-sem-how-it.html?view=snapshot>.
- [72] http://www.vcbio.science.ru.nl/public/pdf/fesem_info_eng.pdf.
- [73] https://en.wikipedia.org/wiki/Optical_microscope#Lighting_techniques.
- [74] https://en.wikipedia.org/wiki/Contact_angle.
- [75] <https://www.biolinscientific.com/measurements/contact-angle>.
- [76] <http://www.rubert.co.uk/faqs/roughness-parameters/>.
- [77] <https://www.stresstech.com/en-fi/products/x-ray-diffraction-equipment/x-ray-diffraction/>.